Multiple Antenna Systems in a Mobile-to-Mobile Environment

A Thesis
Presented to
The Academic Faculty

by

Heewon Kang

In Partial Fulfillment
of the Requirements for the Degree
Doctor of Philosophy

School of Electrical and Computer Engineering
Georgia Institute of Technology
December 2006

Multiple Antenna Systems in a Mobile-to-Mobile Environment

Approved by:

Professor Gordon L. Stüber, Adviser
School of Electrical and Computer Engineering
Georgia Institute of Technology

Professor John R. Barry
School of Electrical and Computer Engineering
Georgia Institute of Technology

Professor Mary Ann Ingram
School of Electrical and Computer Engineering
Georgia Institute of Technology

Professor Gregory David Durgin
School of Electrical and Computer Engineering
Georgia Institute of Technology

Professor Guillermo Goldsztein
School of Mathematics
Georgia Institute of Technology

Date Approved: Nov. 15, 2006

To,

My wife, Jiyeon and our parents

for their love and support for all these years.

ACKNOWLEDGEMENTS

First and foremost, I would like to express my sincere gratitude to my advisor, Professor Gordon L. Stüber, for guiding and inspiring me in all respects of education and research through five and a half years of my Ph. D. work at Georgia Tech. It has been an honor to have him as my thesis advisor. This dissertation would not have been possible without his guidance.

I would like to thank Professor John R. Barry who served as my Ph. D. Proposal committee chair and provides valuable comments and feedback. I would like to extend my sincere thanks to Professor May Ann Ingram who served as reading committee member, and is co-author of some of my papers. I would also like to thank Professor Gregory D. Durgin and Professor Guillermo Goldsztein for their efforts and supports.

I would like to express my appreciation to Dr. Jinsam Kwak for his invaluable contribution to collaborative efforts, much of which is partly presented in this dissertation. I also like to express sincere thanks to Dr. Thomas G. Pratt for his guidance as a project leader throughout my doctoral research.

I am lucky to have worked with wonderful members of Wireless Systems Laboratory (WSL), past and present. Chirag Patel has always been a great partner for numerous discussions, and I am indebted to Joonbeom Kim, Kihong Kim, Hasung Kim, Apruva Mody, Qing Zhao, Galib Asadullah, Alenka Zajic for always being willing to help and their friendship.

Finally, I would like to thank my family. I could not be at this point without their love and support. I would like to thank my mother and late father for their love and dedication. I believe he must have been very happy with my achievement. I also would like to thank my mother-in-law for her continuous encouragement and patience. I would like to express my gratitude to my children, Minkyu and Yeonkyu, for their encouragement and understanding. Last, but not least, I would like to express my deepest appreciation to my wife, Jiyeon, for her love, support, patience, encouragement and sacrifice.

TABLE OF CONTENTS

LIST OF TABLES

LIST OF FIGURES

LIST OF ABBREVIATION

AD	Antenna diversity
AWGN	Additive white Gaussian noise
BER	Bit error rate
BPSK	Binary phase-shift-keying
cdf	cumulative distribution function
i.i.d.	Independently and identically distributed
CSI	Channel state information
INR	Interference-to-noise ratio
MB	Multi-mode-beamforming
MDPSK	M-ary differential phase-shift-keying
MGF	Moment generating function
MIMO	Multiple input multiple output
MISO	Multiple input single output
MMSE	minimum mean square error
MPSK	M-ary phase-shift-keying
MQAM	M-ary quadrature amplitude modulation
MRC	Maximum ratio combining
MRT	Maximum ratio transmission
MUD	Multi-user diversity
NLOS	Non-line-of-sight
OC	Optimal combining
pdf	Probability density function

QOS	Quality of service
RF	Radio frequency
SB	Single-mode-beamforming
SDB	Single-mode-beamforming with diversity antennas
SER	Symbol error rate
SNDB	Single-mode-beamforming with non-diversity antennas
SNR	Signal-to-noise ratio
SIMO	Single input multiple output
SINR	Signal-to-interference-plus-noise ratio
SIR	Signal-to-interference ratio
SISO	Single input single output
SOOC	Select outputs of optimal combining

SUMMARY

The objective of this dissertation is to design new architectures for multiple antenna wireless communication systems operating in a mobile-to-mobile environment and to develop a theoretical framework according to which these systems can be analyzed. Recent information theory has demonstrated that the wireless channel can support enormous capacity if the multipath is properly exploited by using multiple antennas. Future communication systems will likely evolve into a variety of combinations encompassing mobile-to-mobile and mobile-to-fixed-station communications. Therefore, we explore the use of multiple antennas for mobile-to-mobile communications.

Based on the characteristics of mobile-to-mobile radio channels, we propose new architectures that deploy directional antennas for multiple antenna systems operating in a mobile-to-mobile environment. The first architecture consists of multiple input and multiple output (MIMO) systems with directional antennas, which have good spatial correlation properties, and provides higher capacities than conventional systems without requiring a rich scattering environment. The second one consists of single input and multiple output (SIMO) systems with directional antennas, which improve signal-to-interference-plus-noise ratio (SINR) over conventional systems. We also propose a new combining scheme to select the outputs of optimal combing (SOOC) in this architecture.

Optimal combining (OC) is the key technique for multiple antenna systems to suppress interference and mitigate the fading effects. Based on the complex random matrix theory, we develop an analytical framework for the performance analysis of

OC. We derive several important closed-form solutions such as the moment generating function (MGF) and the joint eigenvalue distributions of SINR with arbitrary-power interferers and thermal noise. We also analyze the effects of spatial correlations on MIMO OC systems with arbitrary-power interferers in an interference environment.

Multi-user diversity (MUD), inherent in wireless communications, is a source of increasing sum capacity of systems. We study the capacity of broadcast channels for a single transmitter with multiple antennas and multiple receivers with a single antenna, which is a typical scenario for cellular systems. We investigate the relation between MUD and antenna diversity (AD), and propose an efficient algorithm for selecting users, which is as good as optimal with significantly reduced complexity.

Our novel multiple antenna architectures and the theoretical framework according to which they can be analyzed would provide other researchers with useful tools to analyze and develop future MIMO systems.

CHAPTER I

INTRODUCTION

1.1 Multiple Antenna Systems in a Mobile-to-Mobile Environment

Wireless communications are among the most significant technologies that have changed our daily life. Advances in semiconductor, digital communication, and signal processing technologies have led to a wide range of wireless services and enabled people to communicate anywhere at anytime. Due to the huge success of cellular systems, consumers are demanding better quality of service (QOS) and higher speed broadband access with increased mobility support. New wireless communication architectures are envisioned to improve current services and meet future needs. These architectures include multiple input and multiple output (MIMO) systems with deploying multiple antennas.

The use of multiple antennas is a promising technique for increasing the capacity of wireless communication systems. Information theory has shown that wireless channels can support enormous theoretical capacities if the multipath is properly exploited using MIMO [3, 4]. Capacity increases linearly with the number of antennas without requiring extra bandwidth and power. Considering the demand for high-speed wireless broadband services, multiple antenna systems are leading candidates for future communication systems.

The principle concept of MIMO systems is space-time processing, in which time is complemented by the spatial dimension inherent in the use of multiple spatially-distributed antennas. A key feature of MIMO systems is the ability to turn multipath fading, traditionally a drawback of wireless communications, into a benefit for the user with higher capacities [1]. MIMO effectively takes advantage of the multipath fading and delay spread [28].

Future communication systems will likely evolve into a variety of combinations encompassing mobile-to-mobile and mobile-to-fixed communications [21, 22]. Mobile-to-mobile channels are characteristically different from cellular channels. One important distinction is that both ends of mobile-to-mobile channels can experience multipath with large angular spread as a result of local scatterers in the vicinity of antennas since the antennas are typically a few feet above ground level. This can impact the antenna correlation in multi-antenna architectures and contribute to Doppler spread.

Although few research topics in wireless communications have captured as much attention as multiple antenna systems in recent years, investigating multiple antenna systems in a mobile-to-mobile environment is relatively new and poses numerous research problems. Therefore, our research focuses on the study of multiple antenna systems in a mobile-to-mobile environment.

Enormous capacities are promised only when channels between different transmit and receive antenna pairs are statistically independent [3, 4]. If there is a correlation, the capacity is reduced [23] since the correlation between different transmitting and receiving antenna pairs has a direct connection to the capacity of MIMO systems. Previous research has mainly considered the correlation of antennas at the base station [24, 25, 26], where cost and size are much less an issue than at the mobile station.

It is well known that the first null crossing in the correlation between antenna elements at the mobile station occurs when spatial separation is 0.382 times the wavelength for an isotropic scattering environment [2], and an antenna separation of one-half wavelength gives relatively low correlation in traditional mobile-to-fixed-station communications [26]. However, depending on the carrier frequency, mobile stations might have difficulty accommodating multiple antennas, particulary more than two, because of the size of the mobile station. Therefore, the spatial correlation might be an issue for multiple antenna systems in a mobile-to-mobile environment.

Another important factor that determines the capacity of MIMO systems is multipath richness. The capacity of MIMO systems is significantly degraded if the number of scatterers is not sufficient [27]. In a scarce multipath environment, elements in the channel matrix are not sufficiently de-correlated, leading capacity degradation.

Previous research has not focused on using directional antennas in MIMO systems because it is believed that a rich scattering environment is required to maximize the capacity, and directional antennas might degrade the capacity as a result of a reduction of the richness of the scattering environment [33]. Hence, it has been assumed that MIMO systems with omni-directional antennas fare better than MIMO systems with directional antennas. Our study shows that this is only partially true in a mobile-to-mobile environment. Results reveal that rich scattering is required to maximize the capacity for omni-directional antennas, but not for MIMO systems with directional antennas. A MIMO system with directional antennas provides a better alternative when mobile stations have insufficient separation between antenna elements, and/or when the number of scatterers is insufficient.

To explore the mobile-to-mobile environment, we utilize a “two ring” propagation model [32] which is a simple extension of the previous “one ring” model [23, 25, 26]. While scatterers encircle only one mobile station in the “one ring” model, both mobile stations are encircled by scatterers in the “two ring” model. We use this model to derive the spatial correlation of MIMO systems in a mobile-to-mobile environment. We also use the finite scatterers model, which accounts each distinct multipath signal [28] to identify the capacity trade-off, depending on multipath richness.

We develop new architectures of multiple antenna systems in a mobile-to-mobile environment to enhance the capacity and the performance over conventional systems. We design novel MIMO and single input and multiple output (SIMO) systems, which take advantage of mobile-to-mobile channels, and investigate the performance of these systems in terms of various performance measures such as capacity, outage probability, and output signal-to-interference-plus-noise ratio (SINR).

1.2 Performance Analysis on Optimal Combining

One of the most challenging problems for wireless communication systems is to achieve the maximum spectral efficiency and to accommodate an increasing number of users while maintaining minimum QOS. Unfortunately, it is difficult to accommodate an increasing number of users in a limited spectrum. Spectrum sharing among the users results in co-channel interference, which limits the radio link performance [2].

Adaptive antenna arrays significantly improve the performance of wireless communication systems by suppressing interference and mitigating fading effects. With optimum combining (OC), the received signals are weighted and combined to maximize the output SINR. In the presence of interference, OC yields substantial performance improvement over maximal ratio combining (MRC) [2] and maximum ratio transmission (MRT) [66], both of which maximize only the signal-to-noise ratio (SNR) [44]. A large volume of research has been actively conducted on evaluating the performance of OC [40] - [55].

Earlier work applied OC to SIMO systems that have a single antenna at the transmitter and multiple antennas at the receiver. Initial publications considered the performance of the OC of SIMO (SIMO-OC) either with simplified assumptions such as an interference-limited environment [43, 44] or with simplified analysis based on various approximations [45] -[47]. Later on, the exact distribution of the maximum output SINR and the error performance of OC were provided in [52, 55]. A closed-form expression for the bit error rate (BER) of OC with coherent binary-phase-shift-keying (BPSK) for a single-channel interferer is provided in [40]. In the presence of multiple interferers, upper bounds have been proposed [41], and the BER expression for BPSK systems has been derived in the presence of equal-power interferers and no thermal noise [43]. Recently, Chiani *et al.* [55] derived the moment-generating function (MGF) and analyzed the average symbol error rate (SER) of OC for coherent M-ary phase-shift-keying (MPSK) with unequal-power interferers and thermal noise. However, the analysis in [55] cannot be used for equal-power interferers. More importantly, the analysis is limited to the cases in which the number of interferers is less than the number of receive antennas.

MIMO systems are natural extensions of antenna array systems. MRT has been proposed to exploit the full transmit-receive diversity of MIMO systems [66], [67, 68]. In the presence of multiple co-channel interferers, MIMO optimum combining (MIMO-OC), which maximizes the output SINR, outperforms MRT. The joint optimal antenna weights at the transmitter and receiver have been derived for MIMO-OC, and the average SER performance has been evaluated by Monte-Carlo simulation [69, 70]. Recently, the outage probability of MIMO-OC has been studied in an interference-limited environment, *i.e.*, where thermal noise is ignored [71], and in the presence of interference and noise with all distinct interfering powers [72].

We develop a new analytical framework that provides a simple and accurate way to assess the effects of arbitrary-power interferers and thermal noise. Using some new results of joint eigenvalue distributions of complex random matrices, we derive several closed-form formulas to analyze the performance of OC in MIMO and SIMO systems.

Although the spatial correlation among receive antennas was considered in an interference limited environment in [71] [1], to the best of our knowledge, there has been no analytical results on the outage probability of MIMO-OC systems with the spatial fading correlation at the transmitter or receiver over a Rayleigh fading channel.

[1] Since the effects of spatial correlation vanish in the interference-limited environment when the desired user and interferer are subject to a fading channel with the same correlation matrix, the theoretical approach in [71] is applicable to MIMO-OC systems over the independent and identically distributed fading channels.

We analyze the effects of spatial correlation of MIMO-OC systems in an interference limited environment, and derive closed-form solutions for the pdf and the outage probability of output SINR for MIMO-OC systems.

1.3 Multi-user MIMO Systems

Traditionally, fading is considered as a serious hindrance in wireless communications as a source of unreliability that must be mitigated. As a result, numerous researchers have developed many useful diversity techniques in time, frequency, and space [2]. However, it can be exploited to increase the capacity as we consider multi-user and multi-antenna communications. High capacity gain is achieved simply by scheduling transmissions to the best user when each user among multiple users experiences independent fading [100]. It should be also noted that the huge capacity gain promised by MIMO is realizable only if independent fading between each transmit and receive antenna pair occurs providing unique signatures of spatial modes. Therefore, fading can be considered as a beneficial source of randomization that increases capacity instead of a source of hindrance. [97].

In this dissertation, we study the broadcast channel with multi-user and multi-antennas, focusing on the case in which only the transmitter has multiple antennas, and each receiver has a single antenna, a typical downlink scenario in the current commercial cellular environment. Another important aspect of this study is that this model forms a MIMO arrangement without requiring multiple antennas at the receiver, and it can achieve the MIMO capacity. In addition, this model can be extended easily to cases for receivers with multiple antennas.

Antenna diversity (AD) is one of the techniques for mitigating fading for reliable communications in the cases of multiple antennas at the transmitter and/or receiver [2]. Multi-user diversity (MUD), inherent in wireless communication, is the source to increase the capacity [97]. Though both diversity techniques can increase system capacity, the combined advantages or trade-offs are not clear. We study their relationship by investigating the capacity of single-mode-beamforming (SB) broadcast channels.

We show that there is a conflict between MUD and AD as reported as channel hardening [98]. Since AD mitigates fading, the diversity gain by MUD decreases as the gain of AD increases. We also show that single-mode-beamforming with non-diversity antennas (SNDB) provides higher capacity than single-mode-beamforming with diversity antennas (SDB) at all SNRs.

Although correlation is always considered a serious hindrance that reduces the capacity of systems [26, 23, 30], we observe that capacity can be enhanced by an introduction of intentional correlation in SB. According to [97], correlation is beneficial by assigning random phase in each antenna, but the proposed scheme achieves only a single user beamforming bound without requiring channel state information (CSI). In [99], multi-user diversity gain in MIMO has been observed for correlated channels, but did not reach our conclusion. We believe that no previous work has addressed the relationship between AD and MUD as explicitly as we have.

With a single transmit antenna at each user and a single receive antenna at the base-station (uplink in a single cell), Knopp and Humblet showed that the optimal strategy to maximize capacity is to schedule only one user with the best instantaneous channel among all the users [100]. Such a scheduling algorithm with fairness [101] is implemented in the downlink of the IS-856 commercial system [102]. Multi-user diversity is achieved by scheduling the user whose channel is at near peak. With a large number of users, it is likely that the channel of one user is near peak.

Borst and Whiting studied multi-user diversity for various systems with multiple diversity antennas at the transmit side and/or the receive side in [103]. An interesting observation in [103] is that multi-user diversity does not buy a considerable gain compared with a single-user case particulary at high SNR. However, we showed that multi-user diversity is more efficient in a system with multiple antennas than in a system with a single antenna by properly exploiting multi-user diversity with multiple-mode-beamforming (MB).

The main problem with exploiting the multi-user diversity is the complexity for choosing users that achieve the best sum capacity [104]. Thus, we propose an efficient algorithm for selecting users to exploit multi-user diversity. The proposed algorithm is nearly optimal, with significantly reduced complexity.

1.4 Thesis Outline

The remainder of the thesis is organized as follows. Chapter II presents background information, including a brief review of the capacity of MIMO systems, characteristics of mobile-to-mobile channels, and adaptive antenna techniques. It will also briefly introduce the theory of the eigenvalue distribution of the functions of complex Gaussian matrices, which play an important role in the analysis of OC in later chapters. Chapter III presents a design and an analysis of new MIMO architectures in a mobile-to-mobile environment and effects of the spatial correlation and mutipath richness on MIMO capacity. Chapter IV proposes new SIMO architectures in a mobile-to-mobile environment and a new combining scheme as a consequence of the architecture, and then investigates the performance on the proposed combining scheme. Chapter V presents an analytical framework for the analysis of OC in MIMO and SIMO systems in a Rayleigh fading environment with arbitrary-power co-channel interferers and thermal noise, and several important closed-form solutions dervied using the framework. In Chapter VI investigates the effects of the spatial correlation on MIMO-OC systems in an interference-limited environment with unequal-power co-channel interferers. Closed-form formulas for pdf and the outage probability of output SINR are derived. In Chapter VI, we analyze the capacity of multi-user muti-antenna broadcast channels and the relation between AD and MUD, and propose an efficient suboptimal algorithm for selecting users to exploit MUD. Chapter VIII summarizes the research contributions and proposes ideas for future research.

CHAPTER II

BACKGROUND

Although the promised capacity using multiple antennas is theoretically huge, the full realization of this capacity has not been achieved yet [1]. There is significant ongoing research to realize the full potential of multiple antenna systems. Our goal is to contribute to this effort by designing new architectures and developing an analytical framework for wireless systems with multiple antennas.

The wireless channel encountered in mobile communications is harsh. Radio signals suffer severe path loss, and undergo reflection, diffraction, and scattering as a result of obstacles between the transmitter and the receiver. These effects result in severe distortion of the signal, which is called fading [2]. The desired receiver must also combat the co-channel interference inherited from the frequency reuse to improve the spectral efficiency. The signals transmitted from the different transmitter antennas also interfere with one another. To realize the promised capacity, we must understand the fundamental issues related to these different kinds of impairments to develop wireless systems with multiple antennas in a mobile-to-mobile environment. The following is a brief background summary on these topics.

2.1 MIMO Capacity

While the available radio spectrum is limited, demands for capacity in wireless communications have been increasing rapidly. Significant advances in spectral efficiency are available by increasing the number of antennas in MIMO systems [3, 4]. In this subsection, we briefly discuss MIMO capacity.

Consider a communication link whose transmitter has L antennas, and the receiver has M antennas. We designate the configuration as an (M,L) MIMO system. The bandwidth of the signal is narrow enough for the channel to be frequency flat. We also assume that the channel is "quasi-static." The channel may change from burst to burst, but remains constant during a burst. It is also assumed that the channel is not known at the transmitter, while perfect channel knowledge is available at the receiver.

The transmitted signal $\mathbf{s}$ is an $L \times 1$ vector, and the received signal $\mathbf{r}$ is an $M \times 1$ vector. Then, the channel is represented by an $M \times L$ channel matrix $\mathbf{H}$. H_{ij}, the element of the ith row and jth column of the channel matrix $\mathbf{H}$, represents the complex channel gain between the jth transmitting antenna and the ith receiving antenna. The noise $\mathbf{n}$ is an $M \times 1$ zero mean complex AWGN vector whose real and imaginary parts are independently and identically distributed (i.i.d.) $N(0, \sigma^2/2)$, so its covariance matrix is equal to an $M \times M$ identity matrix multiplied by σ^2.

To investigate the spatial correlation, it is appropriate to normalize the channel matrix $\mathbf{H}$, so that the variance of each component of $\mathbf{H}$ is unity. We assume that the total transmit power is unity, regardless of the number of antennas used in the transmitter. If the average power at each receiving antenna is P, then the average signal-to-noise ratio (SNR) ρ in each receiving antenna is P/σ^2. The received signal associated with an (M,L) MIMO system can be expressed as

$$\mathbf{r} = (P/L)^{1/2}\mathbf{H}\mathbf{s} + \mathbf{n} \tag{1}$$

The MIMO channel capacity is [3, 4]

$$C = \log_2 \det[I_M + (\rho/L)\mathbf{H}\mathbf{H}^\dagger] \quad \text{bps/Hz} \tag{2}$$

where $\mathbf{H}^\dagger$ is the conjugate transpose of $\mathbf{H}$.

More insight can be obtained by the singular value decomposition (SVD) [5] of $\mathbf{H}$. It is easy to see that after SVD operation on $\mathbf{H}$, (29) is converted to

$$C = \sum_{i=1}^{m} \log_2(1 + (\rho/L)\,\sigma_i), \quad \text{bps/Hz} \tag{3}$$

where $m = \min(M, L)$, and σ_i's are the eigenvalues of $\mathbf{H}\mathbf{H}^{\dagger}$. Thus, MIMO capacity keeps increasing without limit as we increase the number of antennas. This promising capacity gain has attracted the attention of many researchers. Further capacity improvement can be made by properly allocating power at the transmitter according to the "water-filling" [4].

2.2 Mobile-to-Mobile Channels

While there is extensive research in cellular channels [2], a much smaller body of work exists in the mobile-to-mobile channel. This subsection briefly discuss the characteristics of mobile-to-mobile channels.

Consider transmission from a mobile transmitter to a mobile receiver. Each communication end is surrounded by scatterers, such as buildings and trees, resulting in non-line-of-sight (NLOS) propagation conditions. The transmitted signal undergoes reflection, diffuse scattering, and diffraction on the obstacles. As a result, the received signal is a sum of several different scattered or reflected paths [6]. One interesting characteristic of the mobile-to-mobile channel is the Doppler shift resulting from the motion of both the transmitter and the receiver. The Doppler shift of mobile-to-mobile channel is

$$f_n = f_t \cos(\alpha_n) + f_r \cos(\beta_n), \tag{4}$$

where f_n is the Doppler shift of the nth path, f_t, f_r are the maximum Doppler shift resulting from the motion of the transmitter and the receiver, respectively, and α_n and β_n are the angle of departure and the angle of arrival of the nth path, respectively. This increased Doppler shift makes the signal fluctuate more rapidly. In certain environments, the double mobility introduced in mobile-to-mobile channels improves the performance of systems [7].

Assuming omni-directional transmit and receive antennas and an isotropic scattering environment, α_n and β_n are uniformly distributed over $[-\pi, \pi)$. The time auto-correlation of the complex channel envelope is given by [6]

$$\phi_{\alpha\alpha}(\tau) = J_o(2\pi f_t \tau) J_o(2\pi f_r \tau) \tag{5}$$

The auto-correlation for mobile-to-mobile channels is a product of two Bessel functions rather than a single Bessel function that characterizes cellular channels [2]. Taking the Fourier transform of the auto-correlation, we obtain the Doppler spectrum. Figure 6 in [8] shows the Doppler spectrum encountered in mobile-to-mobile channels, which clearly differs from the traditional U-shaped spectrum of cellular channels [9]. The higher-order statistics such as the level crossing rates and average fade durations are also different [8].

2.3 Adaptive Antenna Techniques

Antenna arrays can combat multipath fading of the desired signal and suppress the co-channel interference, thereby increasing the capacity of wireless systems. A generally accepted definition of an adaptive antenna system is the combination of antennas with signal processing algorithms to yield an antenna system with dynamic adjustment of the radiation beam pattern. The major aim of adaptive antenna techniques is to improve the signal quality for mobile communications in terms of reducing the probability of making an error at the receiver or maximizing SINR at the antenna output. Since this pattern adjustment is the optimum way for reception and/or transmission, an adaptive antenna is also called a *smart antenna* [10, 11].

The most important benefit of using the adaptive antenna techniques is to separate signals collocated in frequency, but separated in space domain. In this concept, there are well-known adaptive antenna techniques, namely, sectorization, switched-beam adaptive antennas, and adaptive antennas.

Sectorization is a technique that makes use of several directional antennas collocated in the same cell, each radiating within a specified sector, to provide coverage of an entire cell and to reduce the effects of co-channel interference. The improvement of the relative signal-to-interference ratio (SIR) resulting from the high directivity of the antennas leads to an increase in the system capacity by allowing the reuse of the same set of frequency bands more frequently. However, there are several penalties for the improved capacity, such as an increase in the system hardware to make the required radio channel units at each sector, the reduction in trunking efficiency resulting from channel sectoring at the base station, and additional handoff from sector to sector [12].

A switched-beam adaptive antenna system, which is an alternative adaptive antenna strategy besides the basic sectorization system, forms a number of narrow beams pointing to many different pre-determined directions and controls the antenna switch to select the beam maximizing the output SINR. In addition to the antenna directivity that greatly improves the SINR, switched-beam adaptive antenna systems achieve a higher trunking efficiency compared to sectorized systems, which is obtained by allowing all the channels available to a cell to be assigned to every subscriber in the cell [11].

In contrast to the above techniques for adaptive antenna systems, which are considered as a fixed beam pattern or selection of a finite number of pre-defined beams, fully adaptive antenna systems form a radiation pattern that focuses on the direction of the target mobile user and adjust the radiation pattern dynamically. To form the desired radiation pattern, the antenna-weighting vectors should be determined by minimizing a cost function to maximize the signal quality at the output of the beamformer. In the sense of minimum mean square error (MMSE), it is well-known that the fully adaptive antenna system, which is called *optimum combining* [40], optimizes the system performance by maximizing the SINR at the antenna output with optimal weighting vectors. The weight vectors can be tracked by using weight control techniques, such as the least mean square (LMS) technique [13], the recursive least-squares (RLS) technique [14], and the sample matrix inverse (SMI) technique [15, 16], etc.

2.4 Complex Hypergeometric Functions

The probability distributions of random matrices are often derived in terms of the hypergeometric functions of matrix arguments. To understand hypergeometric functions with matrix arguments, we need to know the zonal polynomials of a matrix. The zonal polynomials of a matrix are defined in terms of partitions of positive integers. Let $\kappa = (k_1, k_2, \cdots, k_m)$ be a partition of the integer k with $k_1 \geq k_2 \geq \cdots \geq k_m$ and $k = k_1 + k_2 + \cdots + k_m$. Then, the complex zonal polynomial of a complex matrix $\mathbf{X} \in \mathrm{C}^{m \times m}$ is defined by [17, 18]

$$\tilde{C}_\kappa(\mathbf{X}) = \chi_{[\kappa]}(1)\, \chi_{[\kappa]}(\mathbf{X}) \tag{6}$$

where $\chi_{[\kappa]}(1)$ is the dimension of the representation $[\kappa]$ of the symmetric group given by

$$\chi_{[\kappa]}(1) = k! \frac{\prod_{i<j}^{m} (k_i - k_j - i + j)}{\prod_{i=1}^{m} (k_i + m - i)!} \tag{7}$$

and $\chi_{[\kappa]}(\mathbf{X})$ is the character of the representation $[\kappa]$ of the linear group given as a symmetric function of the eigenvalues $\lambda_1, \lambda_2, \cdots, \lambda_m$ of $\mathbf{X}$ by

$$\chi_{[\kappa]}(\mathbf{X}) = \frac{\det\left[\left(\lambda_i^{k_j+m-j}\right)\right]}{\det\left[\left(\lambda_i^{m-j}\right)\right]} \quad . \tag{8}$$

Now, we consider hypergeometric functions of matrix arguments. First, we define the complex multivariate hypergeometric coefficient $[a]_\kappa$ as

$$[a]_\kappa = \prod_{i=1}^{m} (a-i+1)_{k_i} = \frac{\tilde{\Gamma}_m(a,\kappa)}{\tilde{\Gamma}_m(a)} \tag{9}$$

where $(a)_k = a(a+1)\cdots(a+k-1)$ is the Pochhammer symbol and

$$\tilde{\Gamma}_m(a,\kappa) = \pi^{m(m-1)/2} \prod_{i=1}^{m} \Gamma\left(a+k_i-i+1\right),\ Re(a) > (m-1). \tag{10}$$

The complex hypergeometric functions with matrix arguments are defined as

$${}_p\tilde{F}_q\left(a_1, a_2, \cdots, a_p; b_1, b_2, \cdots, b_q; \mathbf{X}\right) = \sum_{k=0}^{\infty} \sum_{\kappa} \frac{[a_1]_\kappa \cdots [a_p]_\kappa}{[b_1]_\kappa \cdots [b_q]_\kappa} \frac{\tilde{C}_\kappa(\mathbf{X})}{k!} \tag{11}$$

and

$${}_p\tilde{F}_q^{(m)}\left(a_1, a_2, \cdots, a_p; b_1, b_2, \cdots, b_q; \mathbf{X}, \mathbf{Y}\right) = \sum_{k=0}^{\infty} \sum_{\kappa} \frac{[a_1]_\kappa \cdots [a_p]_\kappa}{[b_1]_\kappa \cdots [b_q]_\kappa} \frac{\tilde{C}_\kappa(\mathbf{X})\tilde{C}_\kappa(\mathbf{Y})}{k!\tilde{C}_\kappa(\mathbf{I}_m)} \tag{12}$$

where $\mathbf{X}$, $\mathbf{Y} \in \mathrm{C}^{m\times m}$ and Σ_κ denotes summation over all partitions κ of k.

Special cases for complex hypergeometric function with one matrix argument are ${}_0\tilde{F}_0(\mathbf{X}) = \mathrm{etr}(\mathbf{X})$ and ${}_1\tilde{F}_0(a;\mathbf{X}) = \det(\mathbf{I}-\mathbf{X})^{-a}$. For the complex hypergeometric function with two matrix arguments, however, an infinite sum of zonal polynomials involving an inner summation over partitions is completely impractical for numerical work.

Gross and Richards derived an alternative formulation, in which the complex hypergeometric function with two matrix arguments is related to the classical hypergeometric function [19]. If the eigenvalues of $\mathbf{X}$ and $\mathbf{Y}$ are denoted by $x_1, x_2, \cdots, \quad x_m$ and $y_1, y_2, \cdots, y_m$ with $x_1 > x_2 > \cdots > x_m$ and $y_1 > y_2 > \cdots > y_m$, respectively, then

$$\begin{aligned} & {}_p\tilde{F}_q^{(m)}\left(a_1, a_2, \cdots, a_p; b_1, b_2, \cdots, b_q; \mathbf{X}, \mathbf{Y}\right) \\ & \quad = c_{p,q} \frac{\det\left[\left({}_pF_q\left(a_1 - m + 1, \cdots, a_p - m + 1; b_1 - m + 1, \cdots, b_q - m + 1; x_i y_j\right)\right)\right]}{\det\left[\mathbf{V}(\mathbf{X})\right] \det\left[\mathbf{V}(\mathbf{Y})\right]} \end{aligned} \tag{13}$$

where $\mathbf{V}(\mathbf{X})$ denotes the Vandermonde matrix of the ordered eigenvalues of $\mathbf{X}$, *i.e.*,

$$\mathbf{V}(\mathbf{X}) = \begin{bmatrix} 1 & 1 & \cdots & 1 \\ x_1 & x_2 & \cdots & x_m \\ \vdots & \vdots & \ddots & \vdots \\ x_1^{m-1} & x_2^{m-1} & \cdots & x_m^{m-1} \end{bmatrix}, \tag{14}$$

and the coefficient $c_{p,q}$ is

$$c_{p,q} = \prod_{i=1}^{m} (i-1)! \frac{\prod_{j=1}^{q} \left(b_j - m + 1\right)_{m-i}}{\prod_{j=1}^{p} \left(a_j - m + 1\right)_{m-i}}. \tag{15}$$

2.5 Probability Distributions of Complex Random Matrices

Let an $r \times s$ complex random matrix $\mathbf{Y} \sim \tilde{N}_{r,s}(\mathbf{M}, \Sigma, \Psi)$ be normally distributed, where $\mathbf{M}$, Σ, and Ψ are $r \times s$, $r \times r$, and $s \times s$ positive definite matrices, respectively. This means that the vector $\mathbf{y} = \operatorname{vec}\left[\mathbf{Y}^H\right] \in \mathrm{C}^{rs \times 1}$ has the distribution $\mathbf{y} \sim \tilde{N}_{rs \times 1}(\mathbf{m}, \Sigma^T \otimes \Psi)$, where $\otimes$ denotes the Kronecker product $\mathbf{m} = \operatorname{vec}(\mathbf{M}^H)$ and

$\Sigma^T \otimes \Psi$ is the covariance matrix of $\mathbf{y}$. Consider the $r \times s$ matrix $\mathbf{Y} \sim \tilde{N}_{r,s}(\mathbf{M}, \Sigma, \Psi)$, where Σ and Ψ are $r \times r$ and $s \times s$ Hermitian positive definite matrices, respectively. Then, the density of $\mathbf{Y}$ is given by [58]

$$f_{\mathbf{Y}}(\mathbf{Y}) = \pi^{-rs} (\det \Sigma)^{-s} (\det \Psi)^{-r} \operatorname{etr}\left[-\Sigma^{-1}(\mathbf{Y}-\mathbf{M})\Psi^{-1}(\mathbf{Y}-\mathbf{M})^H\right]. \quad (16)$$

From the complex Gaussian distribution, some distributions of functions of the positive definite matrix in quadratic forms are derived. These distributions are useful in deriving the joint distributions of ordered eigenvalues of complex random matrices. Consider the $m \times n$ matrix $\mathbf{Y} \sim \tilde{N}_{m,n}(\mathbf{0}, \Sigma, \Psi)$, where Σ and Ψ are $m \times m$ and $n \times n$ Hermitian positive definite matrices, respectively. Then, the density function of $\mathbf{Z} = \mathbf{Y}\mathbf{B}\mathbf{Y}^H$, where $m \leq n$ and $\mathbf{B}$ is $n \times n$ Hermitian positive definite matrix, is given by [58]

$$f_{\mathbf{Z}}(\mathbf{Z}) = \frac{(\det \Sigma)^{-n} (\det (\mathbf{B}\Psi))^{-m}}{\tilde{\Gamma}_m(n)} (\det \mathbf{Z})^{n-m} \, {}_0\tilde{F}_0^{(n)} \left(\text{-}\mathbf{B}^{-1/2}\Psi\mathbf{B}^{-1/2}, \Sigma^{-1}\mathbf{Z}\right). \quad (17)$$

If $\mathbf{B}\Psi = \mathbf{I}_n$ in the above theorem, then the density function of $\mathbf{Z}$ is given by

$$f_{\mathbf{Z}}(\mathbf{Z}) = \frac{(\det \Sigma)^{-n}}{\tilde{\Gamma}_m(n)} (\det \mathbf{Z})^{n-m} \operatorname{etr}\left(-\Sigma^{-1}\mathbf{Z}\right). \quad (18)$$

Note that the distribution in (18) is the complex central Wishart distribution with n degrees of freedom and covariance matrix Σ, denoted as $\mathbf{Z} \sim \tilde{W}_m(n, \mathbf{0}, \Sigma)$. In general, the complex non-central Wishart distribution is given by [17].

From the distribution functions of quadratic forms in a complex Gaussian matrix, the joint distribution of ordered eigenvalues of the complex random matrix can be derived. The distribution of eigenvalues facilitates theoretical performance evaluation for adaptive antenna systems in the presence of multiple co-channel interferers.

Consider the $m \times n$ matrix $\mathbf{Y} \sim \tilde{N}_{m,n}(\mathbf{0}, \Sigma, \mathbf{I}_n)$, where Σ is the $m \times m$ Hermitian positive definite matrix with distinct eigenvalues $\sigma_1 > \sigma_2 > \cdots > \sigma_m$. Then, the joint density function of the ordered eigenvalues $\lambda_1, \lambda_2, \cdots, \lambda_m$ *of* $\mathbf{Z} = \mathbf{Y}\mathbf{Y}^H$, *i.e.*, $\mathbf{Z} \sim \tilde{W}_m(n, \mathbf{0}, \Sigma)$, is given by [55]

$$f_\Lambda(\lambda_1, \lambda_2, \cdots, \lambda_m) = K_0(m, n, \Sigma)(\det \Lambda)^{n-m} \det(\mathbf{V}(\Lambda)) \det(\mathbf{F}_0(\Sigma, \Lambda)) \tag{19}$$

where

$$K_0(m, n, \Sigma) = \frac{\pi^{m(m-1)} \prod_{i=1}^{m} \Gamma(i)}{\tilde{\Gamma}_m(n)\tilde{\Gamma}_m(m)} \frac{(\det \Sigma)^{-n}}{\det(\mathbf{V}(-\Sigma^{-1}))}$$

and

$$\{\mathbf{F}_0(\Sigma, \Lambda)\}_{i,j} = \exp(-\lambda_j/\sigma_i).$$

2.6 Generalized Binet-Cauchy Formula

The Generalized Binet-Cauchy Formula is used to give a simple analytic expression converting multiple integral equation to a single integral equation. The following theorem for the generalized integral version of Binet-Cauchy formula is an extended result of the classical Binet-Cauchy formula in [20].

Theorem 1. *Let* $\mathbf{F}(\mathbf{x})$ *be an* $m \times m$ *matrix function of* $\mathbf{x} = (x_1, x_2, \cdots, x_m)^T$ *with* $\{\mathbf{F}(\mathbf{x})\}_{i,j} = f_i(x_j)$, $\mathbf{G}(\mathbf{x})$ *be an* $n \times n$ $(n \geq m)$ *matrix function of* $\mathbf{x}$ *with*

$$\{\mathbf{G}(\mathbf{x})\}_{i,j} = \begin{cases} g_i(x_j), & j = 1, 2, \cdots, m \\ \hat{g}_{i,j}, & j = m+1, m+2, \cdots, n, \end{cases} \tag{20}$$

and $S(\mathbf{x}) = \prod_{i=1}^{m} s(x_i)$, *where* $S(\mathbf{x})$ *be the arbitrary symmetric function of* $\mathbf{x}$. *Then,*

$$\int_D S(\mathbf{x}) \det(\mathbf{F}(\mathbf{x})) \det(\mathbf{G}(\mathbf{x}))\,(d\mathbf{x}) = \det \mathbf{H} \tag{21}$$

where $D = \{a \le x_m \le x_{m-1} \le \cdots \le x_1 \le b\}$ *and* $\mathbf{H}$ *is an* $n \times n$ *matrix whose entries are given by*

$$\{\mathbf{H}\}_{i,j} = \begin{cases} \int_a^b s(x) f_j(x) g_i(x)\,dx, \;\; j = 1, 2, \cdots, m \\ \hat{g}_{i,j}, \;\; j = m+1, m+2, \cdots, n. \end{cases} \tag{22}$$

Proof. . Since the integrand on the left side of (48) is a symmetric function of $x_1, x_2, \cdots, x_m$, which can be attributed for the scaling of a factor $m!$, we get

$$\int_D S(\mathbf{x}) \det(\mathbf{F}(\mathbf{x})) \det(\mathbf{G}(\mathbf{x}))\,(d\mathbf{x}) = \frac{1}{m!} \int_{D'} S(\mathbf{x}) \det(\mathbf{F}(\mathbf{x})) \det(\mathbf{G}(\mathbf{x}))\,(d\mathbf{x})$$

$$\begin{aligned}
&= \frac{1}{m!} \int_{D'} \prod_{k=1}^{m} s(x_k) \left\{ \sum_{\sigma} sgn(\sigma) \prod_{i=1}^{m} f_{\sigma_i}(x_i) \right\} \left\{ \sum_{\mu} sgn(\mu) \prod_{j=1}^{m} g_{\mu_j}(x_j) \prod_{j=m+1}^{n} \hat{g}_{\mu_j,j} \right\} (d\mathbf{x}) \\
&= \frac{1}{m!} \int_{D'} \sum_{\sigma} sgn(\sigma) \sum_{\mu} sgn(\mu) \prod_{k=1}^{m} s(x_k) f_{\sigma_k}(x_k) g_{\mu_k}(x_k) \prod_{j=m+1}^{n} \hat{g}_{\mu_j,j}\,(d\mathbf{x}) \\
&= \frac{1}{m!} \sum_{\sigma} sgn(\sigma) \sum_{\mu} sgn(\mu) \left\{ \int_a^b \prod_{k=1}^{m} s(x_k) f_{\sigma_k}(x_k) g_{\mu_k}(x_k)\,dx_k \right\} \prod_{j=m+1}^{n} \hat{g}_{\mu_j,j}
\end{aligned} \tag{24}$$

where $D' = \{a \le x_k \le b, \;\; k = 1, 2, \cdots, m\}$, $\sigma = (\sigma_1, \sigma_2, \cdots, \sigma_m)$ is the permutation of $\{1, 2, \cdots, m\}$, $\mu = (\mu_1, \mu_2, \cdots, \mu_n)$ is the permutation of $\{1, 2, \cdots, n\}$, the sum runs over all possible permutations, and $sgn(\,\cdot\,)$ denotes the sign of permutation. Letting $\sigma_k = k$, $k = 1, 2, \cdots, m$, and changing the order of μ_k corresponding σ_k, we get

$$\int_D S(\mathbf{x}) \det(\mathbf{F}(\mathbf{x})) \det(\mathbf{G}(\mathbf{x}))\,(d\mathbf{x})$$

$$= \frac{1}{m!} \sum_{\sigma} (sgn(\sigma))^2 \sum_{\mu} sgn(\mu) \left\{ \prod_{k=1}^{m} \int_a^b s(x) f_k(x) g_{\mu_k}(x)\, dx \right\} \prod_{j=m+1}^{n} \hat{g}_{\mu_j,j} \quad (26)$$

$$= \sum_{\mu} sgn(\mu) \left\{ \prod_{k=1}^{m} \int_a^b s(x) f_k(x) g_{\mu_k}(x)\, dx \right\} \prod_{j=m+1}^{n} \hat{g}_{\mu_j,j} = \det \mathbf{H}. \quad (27)$$

□

CHAPTER III

MIMO SYSTEMS IN MOBILE-TO-MOBILE ENVIRONMENT

3.1 Overview

The use of MIMO antennas is a promising technique for increasing the capacity of wireless communication systems. Huge capacities are guaranteed only when channels between different transmitting and receiving antenna pairs are statistically independent. In this chapter, we investigate capacities of MIMO systems in a mobile-to-mobile environment by employing a "two ring" model which is simple extension of previous "one ring" model. With this model, we investigate the spatial correlation and information theoretic channel capacity of MIMO systems with omni-directional antennas as well as MIMO systems with directional antennas. We show that MIMO systems with directional antennas yield good spatial de-correlation between antenna pairs even in a scarce scattering environment, while MIMO systems with omni-directional antennas suffer capacity degradation either when antennas are located closely, or when there is not enough multipath richness. Directional antennas guarantee the independence between different antenna pairs by not sharing scatterers, and the capacity is maximized by exploiting the independence between antenna pairs.

The remainder of this chapter is organized as follows. In Section 3.2, we define the MIMO system model. The theoretical model and analysis of the spatial correlation in a mobile-to-mobile environment is presented in Section 3.3. We present the "two ring" model and derive the spatial correlation for both omni-directional and directional antennas in MIMO systems. Section 3.4 presents simulation results and compares

MIMO capacity using omni-directional antennas as well as directional antennas. In the section, capacities depending on spatial correlation and multipath richness are studied. We use uniform array antennas for a MIMO system with omni-directional antenna up to this section. Finally, summary and conclusions are presented in Section 3.5.

3.2 System Model

Our focus is on a single point-to-point communications. One end of communication link is a transmitter with L antennas, and the other end is the receiver with M antennas. We designate the configuration as an (M,L) MIMO system. The bandwidth of signal is narrow enough for the channel to be frequency flat. We also assume that the channel is "quasi-static". The channel may change from burst to burst, but remains constant during a burst. It is also assumed that channel is not known at the transmitter, while perfect channel knowledge is available at the receiver.

The transmitted signal $\mathbf{s}$ is an $L \times 1$ vector, and the received signal $\mathbf{r}$ is an $M \times 1$ vector. Then channel is represented by an $M \times L$ channel matrix $\mathbf{H}$. H_{ij}, the element of ith row and jth column of channel matrix $\mathbf{H}$, represents the complex channel gain between the jth transmitting antenna and the ith receiving antenna. The noise $\mathbf{n}$ is $M \times 1$ zero mean complex AWGN vector whose real and imaginary parts are i.i.d. $N(0, \sigma^2/2)$, so its covariance matrix is equal to an $M \times M$ identity matrix multiplied by σ^2.

It is appropriate for an investigation of correlation, to normalize the channel matrix $\mathbf{H}$, so that the variance of each component of $\mathbf{H}$ is 1. We assume that the total transmit power is unity regardless of number of antennas used in the transmitter. If the average power at each receiving antenna is P, then the average SNR ρ in each receiving antenna is P/σ^2. The received signal associated with an (M,L) MIMO system can be expressed as

$$\mathbf{r} = (P/L)^{1/2} \cdot \mathbf{Hs} + \mathbf{n} \tag{28}$$

The MIMO channel capacity is [3, 4]

$$C = \log_2 \det[I_M + (\rho/L) \cdot \mathbf{HH}^\dagger] \quad \text{bps/Hz} \tag{29}$$

3.3 Theoretical Model and Spatial Correlation Analysis

In this section, "two ring" model is introduced, and the spatial correlation of a MIMO system is investigated based on the model. The channel characteristics of the same model is investigated in [31, 32].

Figure 1 shows the abstract view of the "two ring" model. Each mobile station is surrounded by scatterers as classical "one ring" model [23, 25, 26]. The transmitter is travelling with speed of v_2 km/h, and the receiver is moving with speed of v_1 km/h. We assume that transmitter and receiver are moving in uniform scattering areas, and the statistical properties of scatterers remain unchanged while both mobile stations are moving. Of particular interest in this chapter is the correlation between each transmitting and receiving antenna pair, which is the correlation of every element in channel matrix $\mathbf{H}$. Correlations between antenna pairs degrade the capacity of MIMO systems [23].

We consider a MIMO system with omni-directional antennas as shown in Fig. 1. A similar figure for a mobile-to-fixed scenario can be found in [25]. We focus on a (4,4) MIMO system for the purpose of illustration. Extension to other dimensions is straightforward. First, consider the channel between one transmitter-receiver antenna pair, i.e., H_{11} from antenna 1 in the transmitter to antenna 1 in the receiver. If the distance between mobile stations is large enough not to significantly change the angle

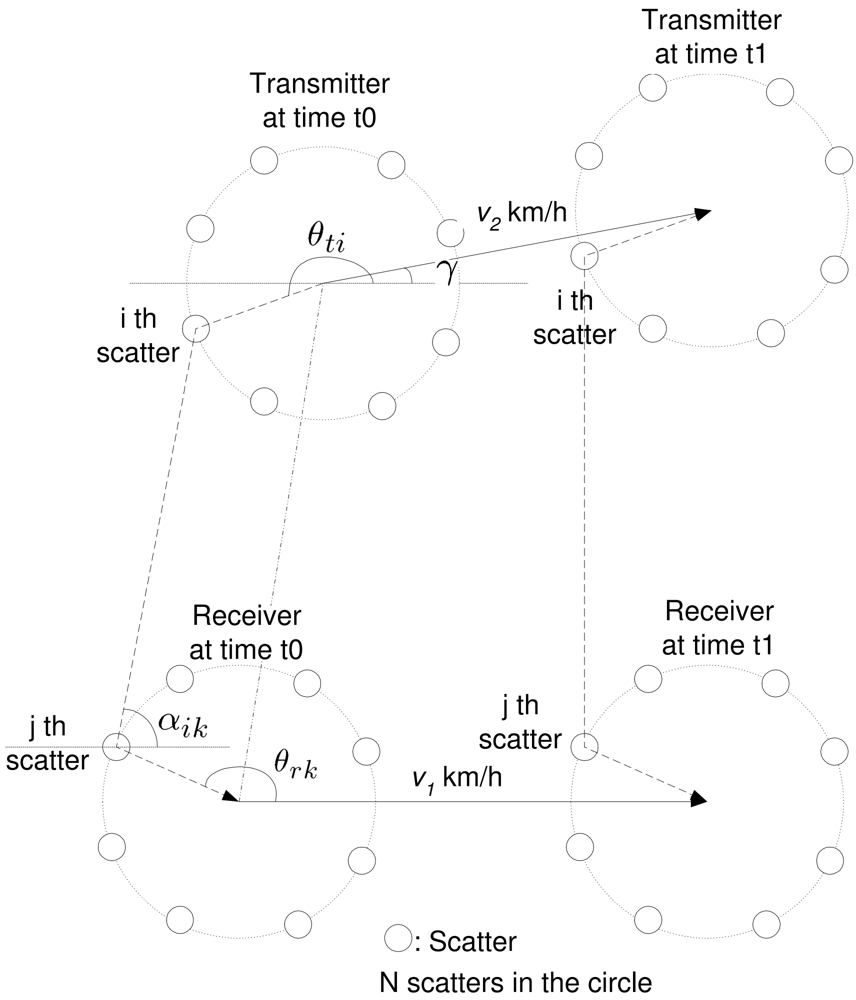

Figure 1: A schematic diagram of "two ring" model

between each pair of scatterers during a burst, α_{ik}, then [34],

$$H_{11} = 1/N \sum_{i=1}^{N} \sum_{k=1}^{N} A_{ik} \exp(j\phi_{ik}), \tag{30}$$

where

$\phi_{ik} = w_c(t - \tau_{ik}) - \beta v_2(t - \tau_{ik})\cos(\theta_{ti} - \gamma) - \beta v_1(t - \tau_{ik})\cos(\theta_{rk})$

A_{ik} : Amplitude of the ikth wave path with unit variance

w_c : Angular carrier frequency

β : Wave number equal to $2\pi/\lambda$

τ_{ik} : Time delay of ikth path

γ : Angle between horizontal line and direction of transmitter

v_1 : Velocity of the transmitter

v_2 : Velocity of the receiver

θ_{ti} : Angle of departure of wave to ith scatter at the transmitter antenna

θ_{rk} : Angle to incidence of wave from kth scatter at the receiver antenna

N : Number of scatterers in each ring

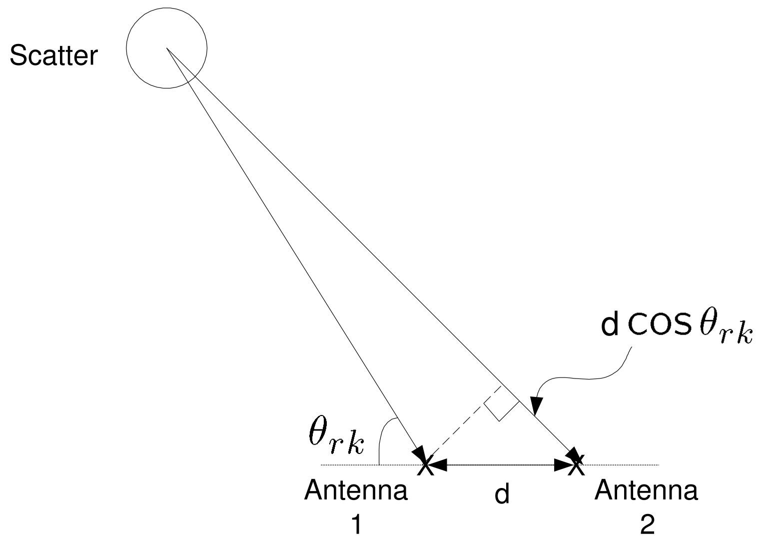

Figure 2: Signal received at two antennas from the scatterer

The ϕ_{ik}'s are assumed independent with uniformly distributed random phase.

It is assumed that antennas are deployed in a uniform linear array with d being the antenna element spacing between two closest antenna elements for both transmitter and receiver (Fig. 2). Then, H_{21} from antenna 1 in the transmitter to antenna 2 in the receiver is

$$H_{21} = 1/N \sum_{i=1}^{N} \sum_{k=1}^{N} A_{ik} \exp[j\phi_{ik} + \beta d(2-1)\cos(\theta_{rk})] \tag{31}$$

It is assumed that the separation between antenna elements is relatively small in comparison to the distance between antennas and scatterers, and hence, the angles from the scatterer to two antenna elements are equal.

Then, other elements in the channel matrix **H** can be similarly calculated. For example, H_{22} from Antenna 2 in the transmitter to Antenna 2 in the receiver with separation d is,

$$H_{22} = 1/N \sum_{i=1}^{N} \sum_{k=1}^{N} A_{ik} \exp[j\phi_{ik} + \beta d(2-1)\cos(\theta_{rk}) + \beta d(2-1)\cos(\theta_{tk})] \quad (32)$$

The correlation between H_{11} and H_{21} is

$$C_{11,21} = E[H_{11}^{*} H_{21}], \quad (33)$$

where $*$ is complex conjugate. By substituting (30) and (31) into (33),

$$\begin{aligned} C_{11,21} &= E[1/N^2 \sum_{i=1}^{N} \sum_{k=1}^{N} \sum_{l=1}^{N} \sum_{m=1}^{N} A_{ik}^{*} \exp(-j\phi_{ik}) A_{lm} \exp(j\phi_{l}m + \beta d\cos(\theta_{rm}))] \\ &= 1/N^2 \sum_{i=1}^{N} \sum_{k=1}^{N} \sum_{l=1}^{N} \sum_{m=1}^{N} E[A_{ik}^{*} \exp(-j\phi_{ik}) A_{lm} \exp(j\phi_{lm} + \beta d\cos(\theta_{rm}))] \end{aligned}$$

Since the A_{ij}'s, ϕ_{ij}'s, and θ_{rj}'s are assumed mutually independent,

$$C_{11,21} = 1/N^2 \sum_{i=1}^{N} \sum_{k=1}^{N} \sum_{l=1}^{N} \sum_{m=1}^{N} E[A_{ik}^{*} A_{lm}] E[\exp(j(\phi_{lm} - \phi_{ik}))] E[\exp(j\beta d\cos(\theta_{rm}))] \quad (34)$$

$$= 1/N^2 \sum_{i=1}^{N} \sum_{k=1}^{N} E[A_{ik}^{2}] E[\exp(j\beta d\cos(\theta_{rk}))] \quad (35)$$

$$= 1/N \sum_{k=1}^{N} E[\exp(j\beta d\cos(\theta_{rk}))] \quad (36)$$

$$= \int_{-\pi}^{\pi} p(\theta_{rk})\, E[\exp(j\beta d\cos(\theta_{rk}))]\, d\theta_{rk}, \quad (37)$$

where $p(\theta_{rk})$ is probability density function of θ_{rk}.

In the last equality, we assume that N is large. If the probability density is uniform,

$$p(\theta_{rk}) = \frac{1}{2\pi}, \qquad -\pi \le \theta_{rk} \le \pi \quad (38)$$

then,

$$C_{11,21} = J_0(\beta d), \quad (39)$$

where $J_0(\cdot)$ is zero order Bessel function. This is the same result obtained in [26, 6]. Similarly, the correlation between H_{11} in (30) and H_{22} in (32) can be easily calculated as

$$C_{11,22} \quad = \quad J_0^2(\beta d). \tag{40}$$

Now, we consider a MIIMO system with directional antennas (Fig. 3). The MIMO system with directional antennas also has 4 elements at each end of the link, and is assumed to be ideal in the sense that the beams provide full angle coverage, but are non-overlapping. Extending to other dimensions is straightforward like a MIMO system with omni-directional antennas.

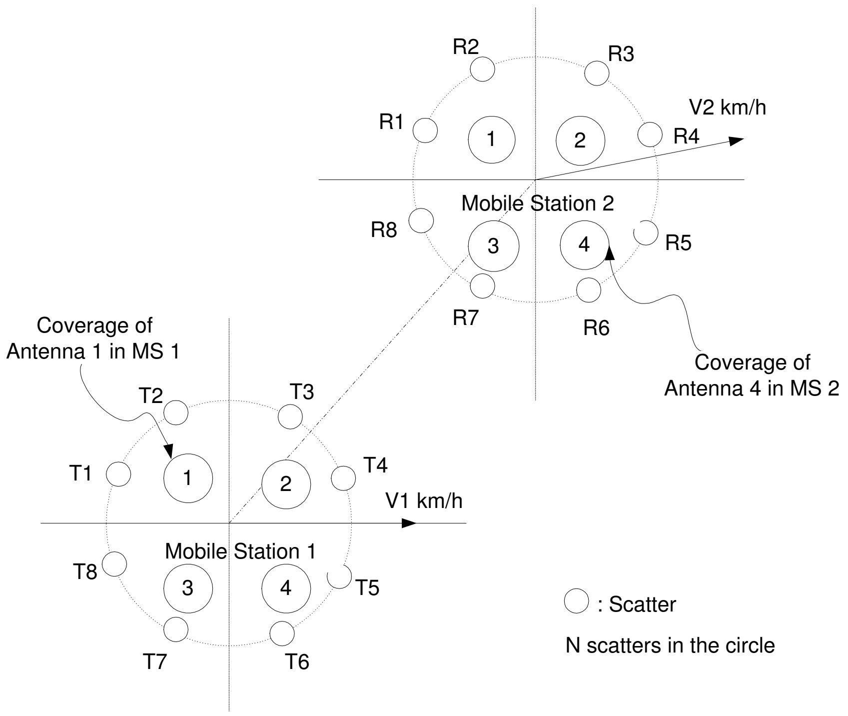

Figure 3: Example of using directional antennas in a MIMO system when number of antennas is 4

We define the following scatter sets from the scatterers enumerated based upon the transmit or receive side as in Fig. 3. Here, the number of scatterers is chosen to be divided by number of antennas, i.e., 8.

TS1: T1, T2; TS2: T3, T4; TS3: T5, T6; TS4 : T7, T8,

RS1: R1, R2; RS2: R3, R4; RS3: R5, R6; RS4: R7, R8,

where T stands for the transmitter, and R for the receiver. For a MIMO system with omni-directional antennas, all antenna pairs share scatterers, but for the MIMO with directional antennas, the antenna pairs do not share scatterers (Table 1). In other words, the antenna pairs have disjoint scatterers sets, so the channel response in the channel matrix is random. Thus, the channel responses between different antenna pairs are independent. Therefore,

$$C_{11,12} = 0 \tag{41}$$

$$C_{11,22} = 0 \tag{42}$$

for a MIMO system with directional antennas.

Table 1: Example of involved scatter sets for both MIMO with omni-directional and directional, where A: antenna pairs(T,R), B: directional antennas, and C: omni-directional antennas.

A	B	C
(1,1)	TS1, RS1	TS1, TS2, TS3, TS4, RS1, RS2, RS3, RS4
(1,2)	TS1, RS2	TS1, TS2, TS3, TS4, RS1, RS2, RS3, RS4
(2,2)	TS2, RS2	TS1, TS2, TS3, TS4, RS1, RS2, RS3, RS4

It is not surprising to have (39) and (40) for the correlations with omni-directional antennas in a mobile-to-mobile environment, which implies that $\lambda/2$ antenna spacing will sufficiently decorrelate elements in the channel matrix $\mathbf{H}$.

However, it is quite surprising, but obvious to have (41) and (42) as the results of the correlation of the MIMO with directional antennas in a mobile-to-mobile environment, which implies that arbitrarily small spacing between antenna elements can be used while still achieving channel de-correlation between the different antenna pairs.

One question might arise as how MIMO systems with directional antennas overcome the reduced richness of multi-path environment due to spatial filtering. The effects of both correlation and richness in the scattering environment are evaluated in the following section.

3.4 Capacity Comparison

In this section, capacities between a MIMO system with omni-directional antennas and a MIMO system with directional antennas is studied over the spatial correlation and the multipath richness.

Based on the model developed in the previous sections, the channel matrix $\mathbf{H}$ is randomly generated. Based on the realization, information theoretic capacity is calculated by (29). The number of realizations of $\mathbf{H}$ in the simulations is 10000. In the simulation, 4 antennas at each end are used. The validation of the model can also be found in [30].

3.4.1 Capacity comparison by spatial correlation

In this subsection, capacity comparison between a MIMO system with omni-directional antennas and a MIMO system with directional antennas is performed over the spatial correlation.

We can easily see that average capacity is bounded using Jensen's inequality [35].

$$\begin{aligned} C_E &= E\{\log_2 \det[I_M + (\rho/L) \cdot \mathbf{H}\mathbf{H}^\dagger]\} && (43) \\ &\leq \log_2 \det[I_M + (\rho/L) \cdot E\{\mathbf{H}\mathbf{H}^\dagger\}] && (44) \end{aligned}$$

Interesting observation in (44) is that the bounded average capacity is effected by the correlation of one side, not of both [35]. When we let $\mathbf{R}$ be $E\{\mathbf{H}\mathbf{H}^\dagger\}$,

$$\begin{aligned} R_{ij} &= \sum_{k=1}^{n} E\{H_{ik} {H_{jk}}^\dagger\} && (45) \\ &= n J_0(\beta(i-j)d) && (46) \end{aligned}$$

In (45), it is noticed that only the correlation in the receiver side is considered. If there is large correlation in the transmitter side, the bound (44) is going to be very loose because it does not capture the correlation of transmitter side. Then, instead of (44),

$$C_E \leq \log_2 \det[I_L + (\rho/L) \cdot E\{\mathbf{H}^{\dagger}\mathbf{H}\}] \tag{47}$$

should be used using $\det[I + AB] = \det[I + AB]$.

Figure 4 shows simulation results for capacities of MIMO systems by changing antenna separation with SNR = 10 dB. As expected, the capacity of MIMO systems with omni-directional antennas is a function of antenna element separation. As antenna element spacing is reduced, there is a corresponding capacity loss. In contrast, the capacity of MIMO systems with directional antennas is independent on the antenna element separation. The bounded average capacity analysis (44) follows the characteristics of the real simulation well, but give slightly higher values.

3.4.2 Capacity comparison by multipath richness

In this subsection, capacity comparison between MIMO systems with omni-directional antennas and MIMO systems with directional antennas is performed over the multipath richness.

Figure 5 shows the simulation results of MIMO capacities by changing the number of scatterers in each ring. It should be noted that total effective number of scatterers is squared because of squared number of multipaths due to scatterers of each ring.

We first consider the capacity of MIMO systems with omni-directional antennas. One interesting observation is the number of scatterers required to achieve the considerable level of the theoretical capacity. The capacity begin to deviate from the theoretical capacity as the number of scatterers is reduced. We see that the capacity is pretty low when the number of scatterers is less than 16, supporting the notion that rich scattering is required to maximize the capacity of MIMO systems.

As we see in [27], the capacity of MIMO systems is significantly reduced when there is not enough number of scatterers. By random matrix theory [29], asymptotic

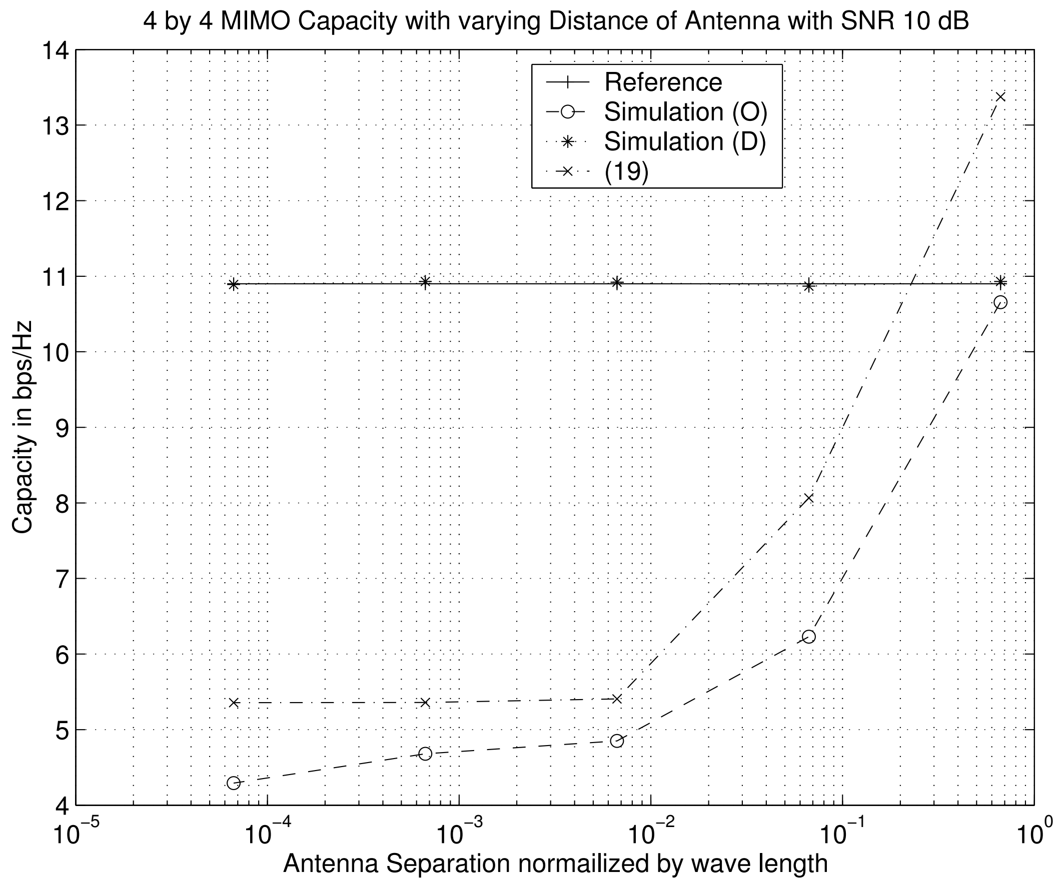

Figure 4: Capacities w.r.t. antenna separation of (4,4) MIMO system with omnidirectional antennas and SNR =10 dB, where O:omnidirectional antennas, and D:directional antennas.

average capacity with limited number of scatterers becomes [27]

$$C_E = \frac{n_s}{\ln 2} \exp(\frac{n_s}{\rho}) \, \Gamma(0, \frac{n_s}{\rho}), \tag{48}$$

where n_s is the number of scatterers, and $\Gamma(0, x)$ is the incomplete Gamma function, denoted as

$$\Gamma(0, x) = \int_x^\infty \frac{\exp(-t)}{t} dt. \tag{49}$$

For $n_s = 16$, SNR 10 dB gives 9.6878 bps/Hz. It should be also noted that with fixed number of antennas, this limit is not applicable because the rank of channel matrix is also bounded by minimum of M, L, or n_s.

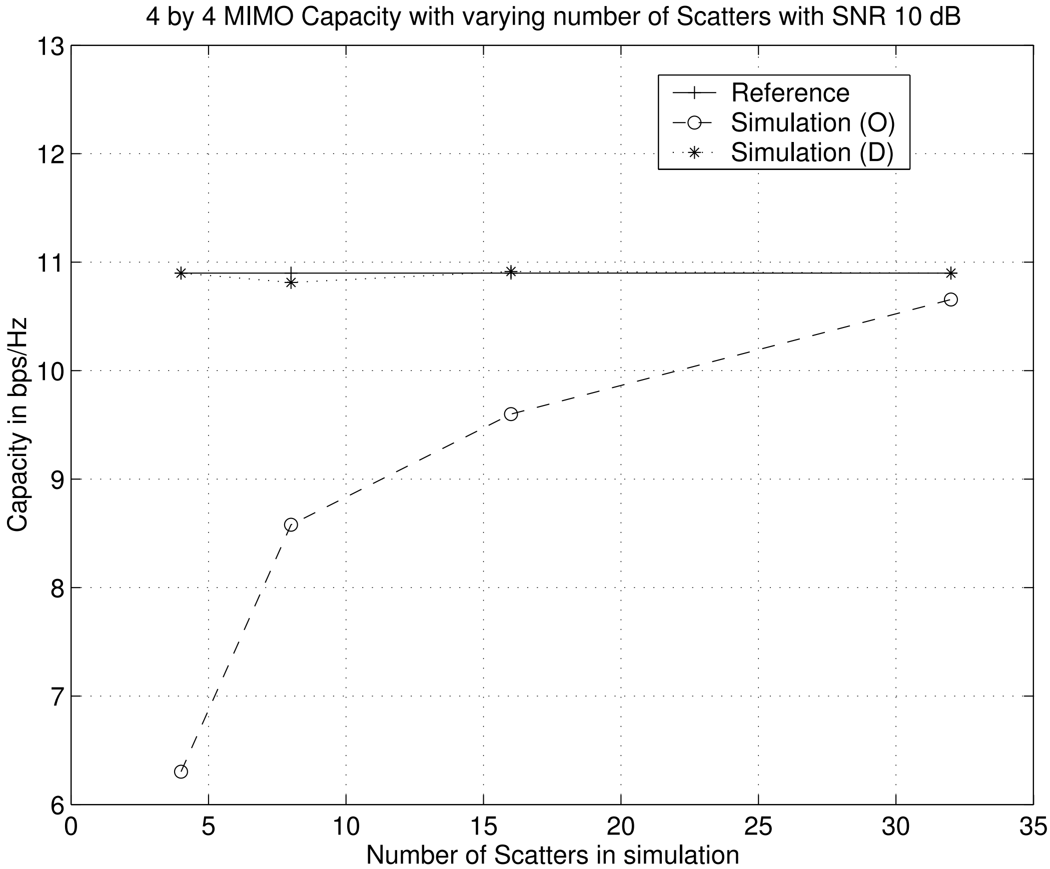

Figure 5: Capacities w.r.t. number of scatterers of (4,4) MIMO systems with SNR =10 dB, where O:omnidirectional antennas, and D:directional antennas.

We now consider the capacity of MIMO systems with directional antennas. Surprisingly, the capacity of MIMO systems with directional antennas does not depend on the number of scatterers. Even with very small number of scatterers like 1, the capacity of MIMO systems with directional antennas is not affected due to inherent independence of each element of channel matrix. While omni-directional antennas are sharing all scatterers in every pair of transmitter and receiver antennas, directional antennas have disjoint sets of scatterers. The result is that each element of channel matrix, $\mathbf{H}$, is independent, and the capacity is maximized. In this sense, directional antennas are found to enhance capacity of MIMO systems.

Simulation results for more realistic experiments which accounts the various level of side-lobes are shown in Fig. 6. It shows that MIMO systems with directional antennas with up to 20 dB side-lobe work perfectly. There is almost no degradation observed in the figure when side-lobe level is less than 20 dB. However, we see bigger degradation as side-lobe level gets higher. As side-lobe level gets higher, the capacity of MIMO systems wit directional antennas gets closer to one of a MIMO system with omni-directional antennas. It confirms our previous results shown in Fig. 5. We think that a MIMO system with directional antennas with 20 dB side-lobe is pretty standard, so its capacity advantage may be achievable.

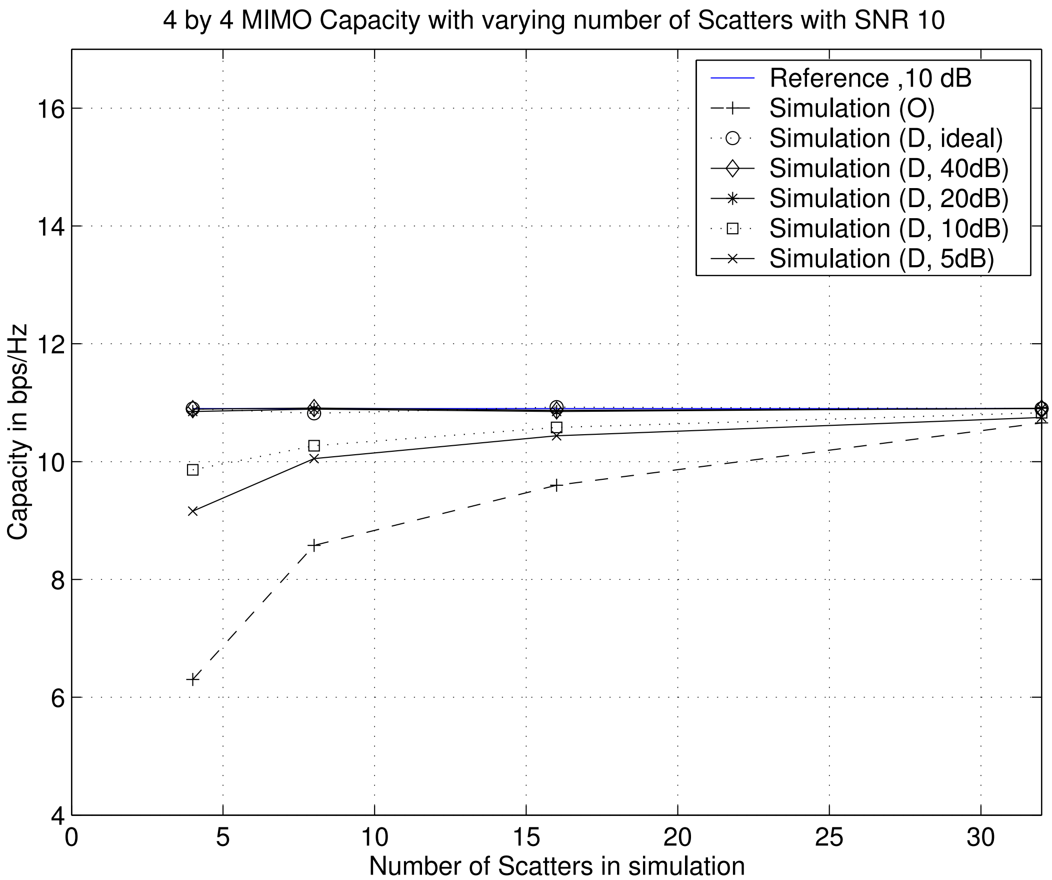

Figure 6: Capacities for various level of sidelobes w.r.t. number of scatterers of (4,4) MIMO systems with SNR =10 dB, where O: omni-directional antennas, and (D, xdB): directional antennas with sidelobe level of x dB.

MIMO systems with directional antennas can be viewed as MIMO systems with omni-directional antennas with pre-fixed beam-forming in the sense of adaptive arrays. Simply fixing the beam pattern as in Fig. 3 instead of doing complicated adaptive beam formation, we can achieve high capacity in a mobile-to-mobile environment. The risk is that we might suffer rank deficiency of the channel matrix **H**, when the number of scatterers is very small, and scatterers are not distributed uniformly.

3.5 Conclusion

In this chapter, we derived the spatial correlations for the elements of channel matrix **H** utilizing a "two ring" model to investigate MIMO systems in a mobile-to-mobile communications. Correlations are generally indicative of the MIMO capacity. Analysis indicates that MIMO systems with directional antennas is superior than MIMO systems with omni-directional antennas. Simulation results confirm that higher capacities are achieved for MIMO systems with directional antennas relative to MIMO systems with omni-directional antennas when antenna spacing is less than $\lambda/2$, or when number of scatterers is small. Simulation results also verify that richness of multi-path is required to maximize the capacity of MIMO systems with omni-directional antennas, but not for MIMO systems with directional antennas. With these results, we might conclude that multi-path richness is required to guarantee the independence of different antenna pairs, which is an inherent nature of MIMO systems with directional antennas. MIMO systems with directional antennas seem to be very attractive in a mobile-to-mobile environment.

CHAPTER IV

SIMO SYSTEMS IN A MOBILE-TO-MOBIE ENVIRONMENT

4.1 Overview

Multi-antenna implementations for wireless communications remain an active research area receiving wide interest. In cellular applications, multi-antenna architectures typically have been considered for use at the base station on up-links from a mobile stations [37]. The need for multiple antennas at the user terminal has been suggested in [38], and further studied in [39].

Mobile-to-mobile communication systems, where both the transmitter and the receiver are in motion, have different scattering environments compared to the conventional cellular systems. Both ends of the communication link are surrounded by scatterers as a result of their relative low antenna elevation. A new architecture to deploy directional antennas to the adaptive antenna array systems in mobile-to-mobile environment is introduced showing superior performance than systems with omni-directional antennas. In the architecture, a new combining scheme to select the outputs of optimal combining (SOOC) is also developed and shows huge performance gain over the conventional optimal combining (OC) scheme.

OC has attracted great interest as a space-time processing of adaptive antenna arrays to suppress the interference and mitigate the fading effect with reception diversity in wireless communication environment. Antennas are weighted and combined to maximize the output signal-to-interference-plus-noise ratio (SINR). A large volume of research has been actively conducted on evaluating the performance of OC [40] -

[55].

This chapter analyze the performance of SOOC with multiple equal-power interferers in an interference limited environment. We derive several important closed-form solutions for SOOC such as the pdf, the outage probability, and the average output SIR. We also derive a closed-form solution for the SER of BPSK systems.

The remainder of this chapter is organized as follows. Section 4.2 introduces a new multiple-antenna architecture and a new combining scheme of a SIMO system. In Section 4.3, we define the system model and a brief overview of OC is given. Section 4.4 provides the derivation for the pdf of OC and SOOC. Based on the distribution of OC and SOOC, analysis on the performance of SOOC are presented in Section 4.5. The average SIR, the outage probability, and the SER for MPSK systems of SOOC are derived. Finally, summary and conclusions are provided in Section 4.6.

4.2 A New SIMO system in Mobile-to-Mobile communications with co-channel interference

We develop a new architecture that employs directional antennas in a multiple-antenna SIMO configuration in a mobile-to-mobile environment. Figure 7 shows an example of the proposed SIMO system with a single antenna at one end and multiple antennas at the other end.

We investigate the performance of the developed SIMO system in a non-line-of-sight (NLOS) mobile-to-mobile channel. Channel impairments include Doppler spread and angular spread originating from scatterers in the vicinity of both the transmitter and the receiver. We employ the "two ring" scattering model and compare the performance of the proposed system to the performance of adaptive arrays implemented with omni-directional antennas. Interested reader may see the details of performance analysis depending on such impairments in [56]. Several practical suboptimal algorithms for the selection are proposed and analyzed in [57].

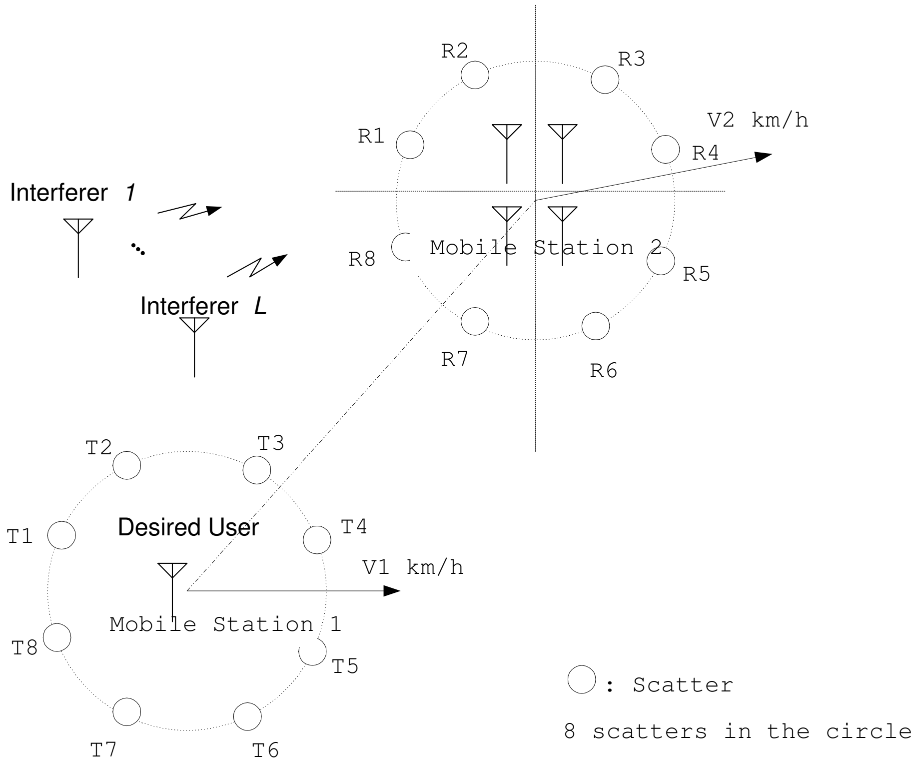

Figure 7: Example of a SIMO system with directional antennas. Four directional antennas are deployed in a multiple antenna system, and each antenna covers each quadrant of the area.

In the developed architecture, a new combining scheme, SOOC, is also developed. A schematic view of the SOOC is shown in Fig. 8. In the figure, the central controller selects the best output from outputs of two independent adaptive antenna array systems. This may arise in different situations. It is possible to communicate the outputs of receivers when they are physically separated and deployed with adaptive arrays. A good example is a cellular system in which each base station is deployed with adaptive array antennas and communicates with the base station controller, which is the typical scenario for the soft handoff. The other situation may arise when there are only a limited number of radio frequency (RF) chains, which can not support more antennas. RF chains are switched to adaptive array antennas with a better SINR. RF chains are generally considered expensive resources.

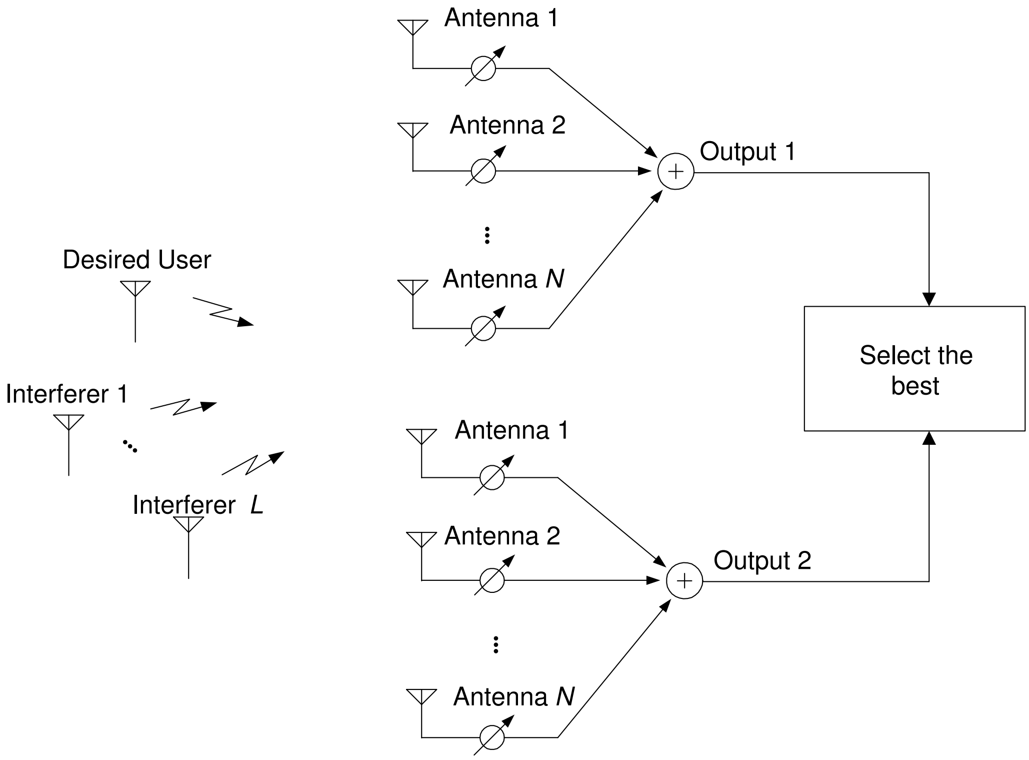

Figure 8: A schematic view of SOOC.

4.3 System Model

Consider M independent adaptive array systems with N antennas. There are L interferers with a single antenna in the system. We assume that the channel is frequency flat faded and perfect channel knowledge is available at the receiver. Then, the array response of each antenna system is given by,

$$\mathbf{r}_i = \sqrt{P_S}\mathbf{c}_i b_0 + \sqrt{P_I}\sum_{k=1}^{L}\mathbf{c}_{k,i}b_k, \qquad i = 1, 2, \ldots, M, \tag{50}$$

where $\mathbf{c}_i$ and $\mathbf{c}_{k,i}$ are $N \times 1$ complex channel response vectors of desired user and the kth interferer for the ith system, respectively. We consider the interference limited case $(L > N)$ in which we can ignore the background noise. P_s and P_I are the average powers of desired user and interfering signals, and b_0 and b_k represent MPSK modulated transmit symbol of desired and the kth interferer with unit variance, respectively. We omit the time index for brevity. We also model each element of

$\mathbf{c}_i, \mathbf{c}_{k,i}$ as independent and identical (i.i.d.) random variables with unit variance.

Let $\mathbf{C}_{I,i}$ be the aggregated $N \times L$ channel gain matrix for the cochannel interferers of system i, which is given by

$$\mathbf{C}_{I,i} = (\mathbf{c}_{1,i}, \mathbf{c}_{2,i}, \cdots, \mathbf{c}_{L,i}), \qquad i = 1, 2, \ldots, M. \tag{51}$$

Then, the received vector can be rewritten as

$$\mathbf{r}_i = \sqrt{P_S}\mathbf{c}_i b_0 + \sqrt{\mathrm{P_I}}\ \mathbf{C}_{I,i}\mathbf{b}_I, \qquad i = 1, 2, \ldots, M, \tag{52}$$

where $\mathbf{b}_I = (b_1, b_2, \cdots, b_L)^T$, and $(\mathbf{X})^{\mathbf{T}}$ is the transpose of $\mathbf{X}$.

The weight vector to maximize the output signal-to-interference ratio (SIR) is

$$\mathbf{w}_i = \mathbf{R}_i^{-1}\mathbf{c}_i, \qquad i = 1, 2, \ldots, M, \tag{53}$$

$$\mathbf{R}_i = P_I \mathbf{C}_{I,i}\mathbf{C}_{I,i}^{\dagger}, \qquad i = 1, 2, \ldots, M, \tag{54}$$

where $(\cdot)^{\dagger}$ is the conjugate transpose of the matrix. Then, the maximum SIR at each of the OC combiner output is

$$\gamma_i = \mathbf{c}_i^{\dagger}\mathbf{R}_i^{-1}\mathbf{c}_i, \qquad i = 1, 2, \ldots, M. \tag{55}$$

4.4 pdf of SOOC

It is well known that $\mathbf{R}_i$ has the Wishart distribution and γ_i is a quadratic form of multi-variate Gaussian random matrices, which is extensively studied at 1960's [58, 17]. The pdf, $f_{\gamma_i}(\gamma)$, and the cumulative distribution function (cdf), $F_{\gamma_i}(\gamma)$, are [58, 43]

$$f_{\gamma_i}(\gamma) = \frac{\Gamma(L+1)}{\Gamma(N)\Gamma(L+1-N)} (\Lambda)^{L+1-N} \frac{\gamma^{N-1}}{(\gamma+\Lambda)^{L+1}}, \tag{56}$$

$$F_{\gamma_i}(\gamma) = \frac{\Gamma(L+1)}{\Gamma(N+1)\Gamma(L+1-N)} \left(\frac{\gamma}{\Lambda}\right)^N {}_2F_1\left(L+1, N; N+1; -\frac{\gamma}{\Lambda}\right), \tag{57}$$

where $\Lambda = P_s/P_I$, $\Gamma(\cdot)$ is the gamma function and ${}_pF_q\left(a_1, \ldots, a_p; b_1, \ldots, b_q; x\right)$ is the generalized hypergeometric function defined as [59]

$$ {}_pF_q\left(a_1, \ldots, a_p; b_1, \ldots, b_q; x\right) = \sum_{n=0}^{\infty} \frac{(a_1)_n \ldots (a_p)_n}{(b_1)_n \ldots (b_q)_n} \frac{x^n}{n!}, \tag{58} $$

where $(a)_n$ is the Pochhammer symbol equal to $\Gamma(a+n)/\Gamma(a)$. It is worth noting that the outage probability has direct relation with cdf given by

$$ \tag{59} $$

$$ \begin{aligned} P_O &= \text{Probability}\{\gamma \geq \gamma_O\}. & (60) \\ &= F_\gamma(\gamma_O). & (61) \end{aligned} $$

Selecting the best branch implies selecting the branch with the best SIR amongst the M outputs of the OC combiner. Hence, the pdf of the output SIR of SOOC is [2]

$$ f_{\widehat{\gamma}}(\widehat{\gamma}) = M f_\gamma(\widehat{\gamma}) F_\gamma^{M-1}(\widehat{\gamma}). \tag{62} $$

We focus on the case where $M = 2$ throughout the paper. However, results can be extended for higher values of M. Figure 9 shows the pdf's of SIR of OC and SOOC with different number of antennas when $M = 2$ and $L = 6$. They show the pdf of SOOC is shifted to the right compared to the pdf of OC, which indicates that the mean SIR of SOOC is greater than the mean of SIR of OC.

4.5 Performance Analysis of SOOC

In this section, we analyze the performance of SOOC systems. The closed-form expression of the average SIR and the outage probability are derived. SER of MPSK systems is also derived as the sum of single integral formulas and the closed-form expression for BPSK systems as a special case.

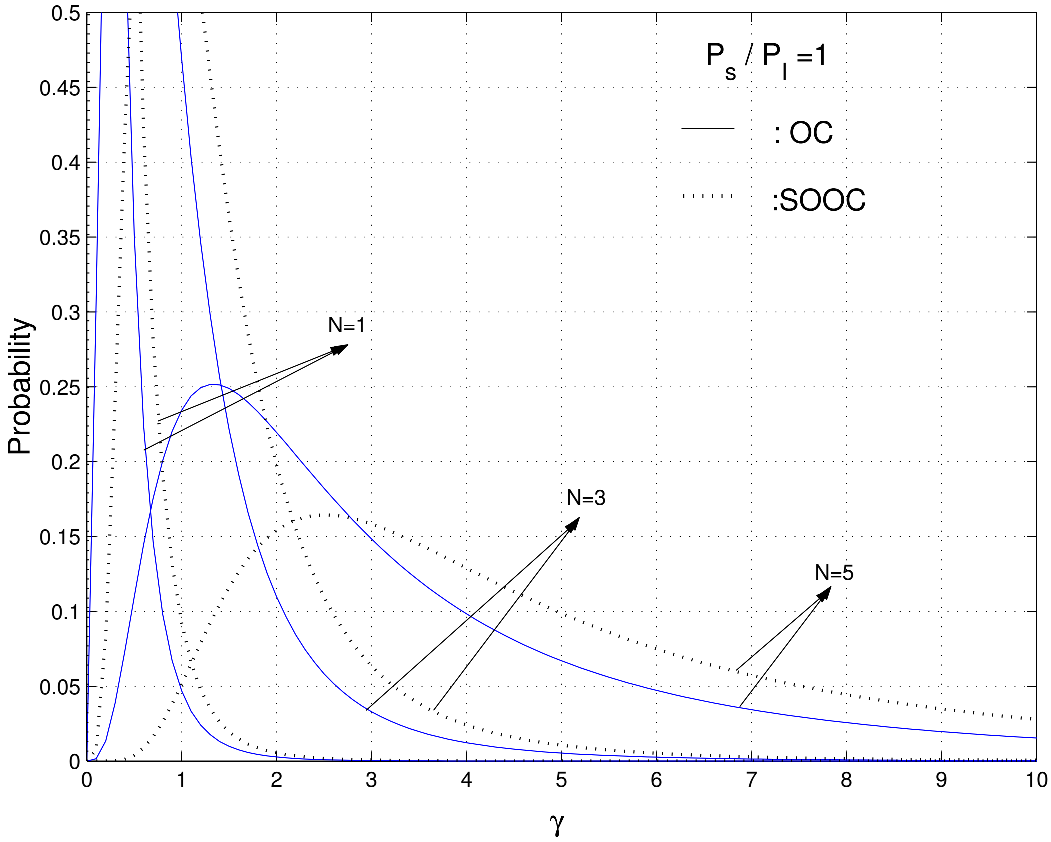

Figure 9: Pdf of OC and SOCC with varing number of antennas when L = 6.

4.5.1 Average SIR

The average SIR of SOOC is derived using (56), (95), and (62).

$$\widetilde{\widehat{\gamma}} = \int_0^\infty \widehat{\gamma} f_{\widehat{\gamma}}(\widehat{\gamma}) d\widehat{\gamma}. \tag{63}$$

$$= K_1 \Lambda^{L+1-2N} \int_0^\infty \frac{\widehat{\gamma}^{2N}}{(\widehat{\gamma}+\Lambda)^{L+1}} {}_2F_1\left(L+1, N; N+1; -\frac{\widehat{\gamma}}{\Lambda}\right) d\widehat{\gamma}, \tag{64}$$

where

$$K_1 = \frac{2\Gamma^2(L+1)}{\Gamma^2(L+1-N)\Gamma(N)\Gamma(N+1)}. \tag{65}$$

Using the identity in [60], the hypergeometric function in (64) can be expressed as

$$ {}_2F_1\left(L+1, N; N+1; -\frac{\widehat{\gamma}}{\Lambda}\right) = \frac{\Gamma(N+1)}{\Gamma(L+1)\Gamma(N)} G_{22}^{12}\left(\frac{\widehat{\gamma}}{\Lambda}\middle| \begin{array}{cc} -L & 1-N \\ 0 & -N \end{array}\right), \tag{66} $$

where G_{pq}^{mn} is the Meijer G function defined as

$$ G_{pq}^{mn}\left(x \middle| \begin{array}{ccc} a_1, & \dots, & a_p \\ b_1 & \dots, & b_q \end{array}\right) = \frac{1}{2\pi i}\int \frac{\prod_{j=1}^{m}\Gamma(b_j - s)\prod_{j=1}^{n}\Gamma(1-a_j+s)}{\prod_{j=m+1}^{q}\Gamma(1-b_j+s)\prod_{j=n+1}^{p}\Gamma(a_j - s)} x^s ds. \tag{67} $$

See [60] for more details. Using the integral transform [61, p418], we have the closed-form solution for average SIR of $\widehat{\gamma}$

$$ \widetilde{\widehat{\gamma}} = \frac{2\Gamma(L+1)}{\Gamma^2(L+1-N)\Gamma^2(N)} \Lambda G_{33}^{23}\left(\frac{\widehat{\gamma}}{\Lambda}\middle| \begin{array}{ccc} -2N, & -L, & 1-N \\ L-2N & 0, & -N \end{array}\right). \tag{68} $$

Unfortunately, we found that this expression is simple, but not numerically stable when we evaluate with the current software package. We derive alternative expression by transforming the hypergeometic function in (64) to the sum of finite analytic functions using the identity in [62],

$$ {}_2F_1\left(L+1, N; N+1; -\frac{\widehat{\gamma}}{\Lambda}\right) = \frac{1}{\left(1+\frac{\widehat{\gamma}}{\Lambda}\right)^L} {}_2F_1\left(N-L, 1; N+1; -\frac{\widehat{\gamma}}{\Lambda}\right). \tag{69} $$

$$ = \frac{1}{\left(1+\frac{\widehat{\gamma}}{\Lambda}\right)^L} \sum_{i=0}^{L-N} c_i \frac{(-1)^i}{\Lambda^i}\widehat{\gamma}^i, \tag{70} $$

$$ c_i = \frac{(N-L)_i (1)_i}{(N+1)_i \, i!}. \tag{71} $$

This identity is useful to evaluate the performance of SOOC. Now, the average SIR of $\widehat{\gamma}$ is expressed as [60]

$$\widetilde{\widehat{\gamma}} = K_1 \sum_{i=0}^{L-N} (-1)^i \Lambda^{-2N-i} c_i \int_0^{\infty} \frac{\widehat{\gamma}^{2N+i}}{\left(1+\frac{\widehat{\gamma}}{\Lambda}\right)^{2L+1}} d\widehat{\gamma}. \tag{72}$$

$$= K_1 \Lambda \sum_{i=0}^{L-N} (-1)^i \, c_i \, B(2N+i+1, 2L-2N-i), \tag{73}$$

where $B(a,b)$ is the beta function defined as

$$B(a,b) = \frac{\Gamma(a)\Gamma(b)}{\Gamma(a+b)}. \tag{74}$$

The average SIR of OC is known as [43]

$$\widehat{\gamma} = \frac{N}{L-N} \Lambda. \tag{75}$$

Figure 10 plots the average SIR of OC and SOOC with varying number of antennas when L = 10 and Λ = 10 dB, and shows a good match between analysis and the simulation results. We observe that there is considerable gain of SOOC over OC in terms of average SIR, and the gain becomes larger as the number of antennas increases.

4.5.2 Outage Probability

The outage probability can be derived using the identity (70) as follows

$$P_o(\gamma_o) = \int_0^{\gamma_o} f_{\widehat{\gamma}}(\widehat{\gamma}) d\widehat{\gamma}. \tag{76}$$

$$= K_1 \sum_{i=0}^{L-N} (-1)^i \Lambda^{-2N-i} \, c_i \int_0^{\gamma_o} \frac{\widehat{\gamma}^{2N+i-1}}{\left(1+\frac{\widehat{\gamma}}{\Lambda}\right)^{2L+1}} d\widehat{\gamma}. \tag{77}$$

$$= K_1 \sum_{i=0}^{L-N} (-1)^i \Lambda^{-2N-i} \, c_i \, \frac{\gamma_o^{2N+i}}{2N+i} \, {}_2F_1 \left(2L+1, 2N+i; 2N+i+1; -\frac{\gamma_o}{\Lambda}\right) \tag{78}$$

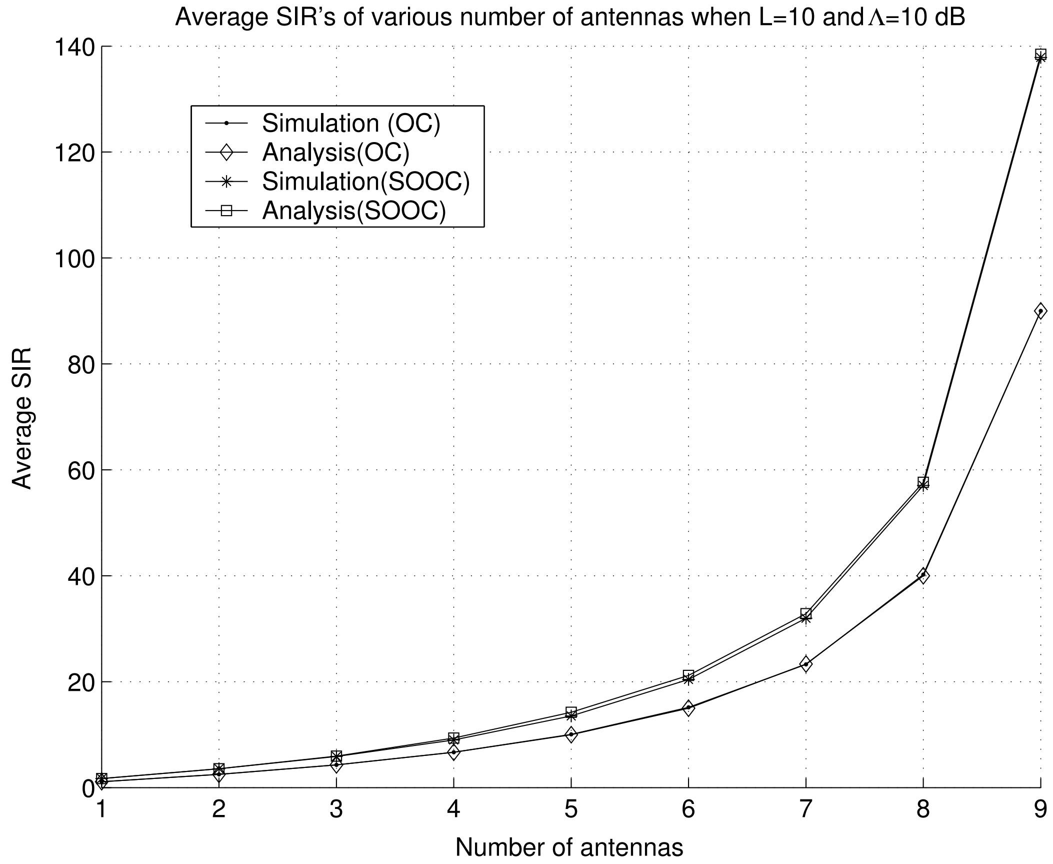

Figure 10: Average SIR of OC and SOOC of various of number of antennas with L = 10 and Λ = 10 dB.

where K_1 and c_i are defined in (65) and (71), respectively. The outage probability of OC and SOOC is plotted in Fig. 11 with L=7 and N=3 with various values of Λ. The effective input SIR's are -8.5 dB, 1.5 dB and 11.5 dB when Λ equals to 0 dB, 10 dB, and 20 dB, respectively since there are seven interfers. It shows that Both OC and SOOC suppress the interference efficiently, but SOOC has the superior performance than OC.

4.5.3 Average SER

Based on the distribution of SIR derived in the previous section, we can have a single integral expression for the SER of MPSK system. The SER of MPSK system is given by [63]

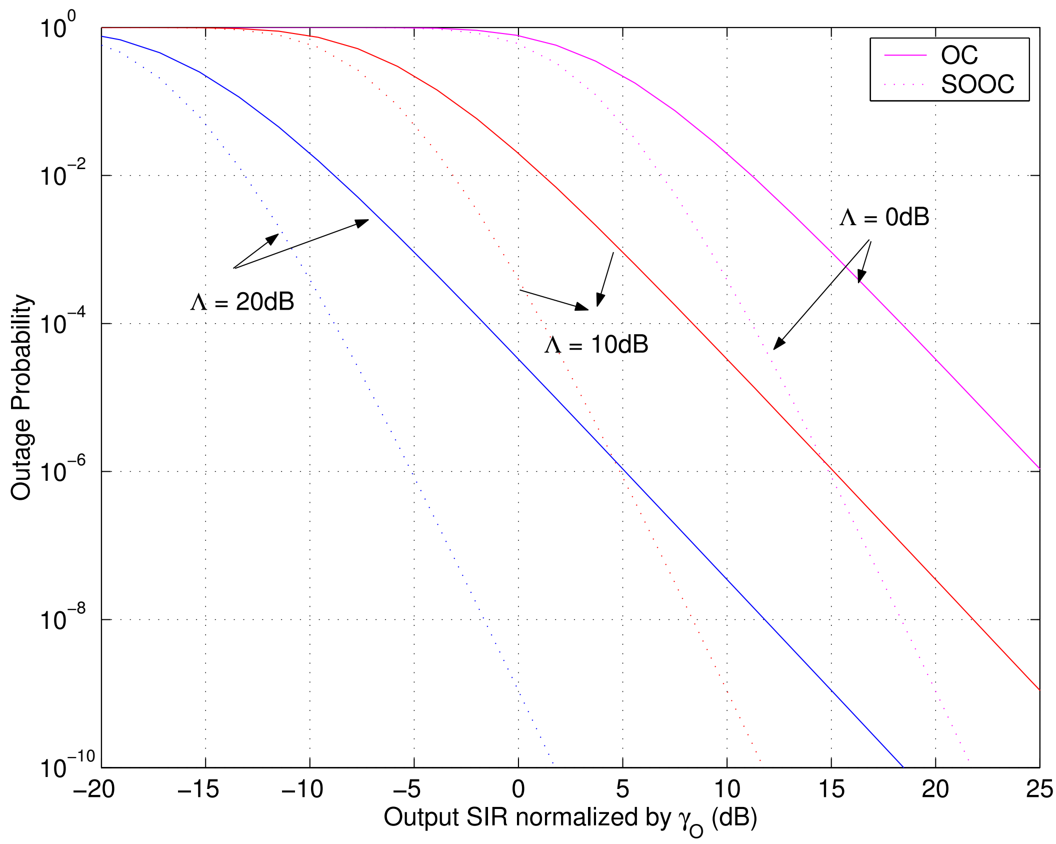

Figure 11: Outage probability of OC and SOOC with various values of Λ, L=7 and N=3.

$$\bar{P}_s = \frac{1}{\pi}\int_0^{\pi-\pi/M}\int_0^{\infty} \exp\left(-\frac{g_{\text{PSK}}}{\sin^2\theta}\gamma\right) f_\gamma(\gamma) d\gamma\, d\theta, \tag{79}$$

where $g_{\text{PSK}} = \sin^2(\pi/M)$. Using the integration by parts and the change of variable, the SER of above equation can be expressed as

$$\bar{P}_s = \sqrt{\frac{g_{\text{psk}}}{\pi}} \int_0^{\infty} \frac{e^{-g_{\text{PSK}}\gamma}}{2\sqrt{\gamma}} \left(1 + \text{erf}\left(\sqrt{(1\text{-g}_{\text{PSK}})\gamma}\right)\right) P_{\text{out}}(\gamma)\, d\gamma, \tag{80}$$

Finally, the SER of MPSK systems is expressed as

$$\bar{P}_s = K_1 \sum_{i=0}^{L-N} (-1)^i \Lambda^{-2N-i} \frac{c_i}{2(2N+i)} \sqrt{\frac{g_{\text{psk}}}{\pi}} \sum_{j=0}^{2L-2N} (-1)^j \Lambda^{-j} d_j$$

$$\cdot \int_0^\infty \frac{\gamma^{2N+i-j} e^{-g_{\text{PSK}}\gamma}}{\sqrt{\gamma}} \left(1+\frac{\gamma}{\Lambda}\right)^{-2L} \left(1+\text{erf}\left(\sqrt{(\text{1-g}_{\text{PSK}})\gamma}\right)\right) d\gamma, \quad (81)$$

where

$$d_j = \frac{(2N+i-2L)_j (1)_j}{(2N+i+1)_j \, j!}. \quad (82)$$

We derive the closed-form expression for the SER of BPSK systems as a special case. We only include the final result for the brevity.

$$P_e = K_2 \sum_{i=0}^{L-N} P_{e,i}. \quad (83)$$

$$K_2 = \frac{\Gamma^2(L+1)}{\sqrt{\pi}\, \Gamma^2(L+1)\Gamma(2L+1-N)\Gamma(N+1)\Gamma(N)}. \quad (84)$$

$$\begin{aligned} P_{e,i} = {} & (-1)^i c_i \left[\frac{\Gamma(2N+i-2L-\frac{1}{2})\Gamma(2N+i-2L-1)\Gamma(2L+1)}{\Gamma(2N-2L+i)} \Lambda^{2L+1-2N-i} \right. \\ & \cdot {}_2F_2\left(2L+1, 2L+1-2N-i; 2L+\frac{3}{2}-2N-i, 2L+2-2N-i; \Lambda\right) \\ & -0.5\Gamma(2L+\frac{1}{2}-2N-i)\Gamma(2N+i+\frac{1}{2})\Lambda^{\frac{1}{2}} \\ & \left. \cdot {}_2F_2\left(2N+i+\frac{1}{2}, \frac{1}{2}; 2N+i+\frac{1}{2}-2L, \frac{3}{2}; \Lambda\right) + \sqrt{\pi}\Gamma(2L+1-2N-i)\Gamma(2N+i) \right]. \end{aligned} \quad (85)$$

The average SER's of MPSK systems with four modulation symbols are plotted in Fig. 12. It shows a good match between analysis and simulation results. As we see in the outage probability in Fig. 11, the performance difference of OC and SOOC is increased as we approach to the high SIR region. It is due to the characteristic of outage probability of OC and SOOC. The outage probability of SOOC is superior at the low outage probability region. When SER= 0.01 and N=2, more than 4 dB performance difference is observed between OC and SOOC.

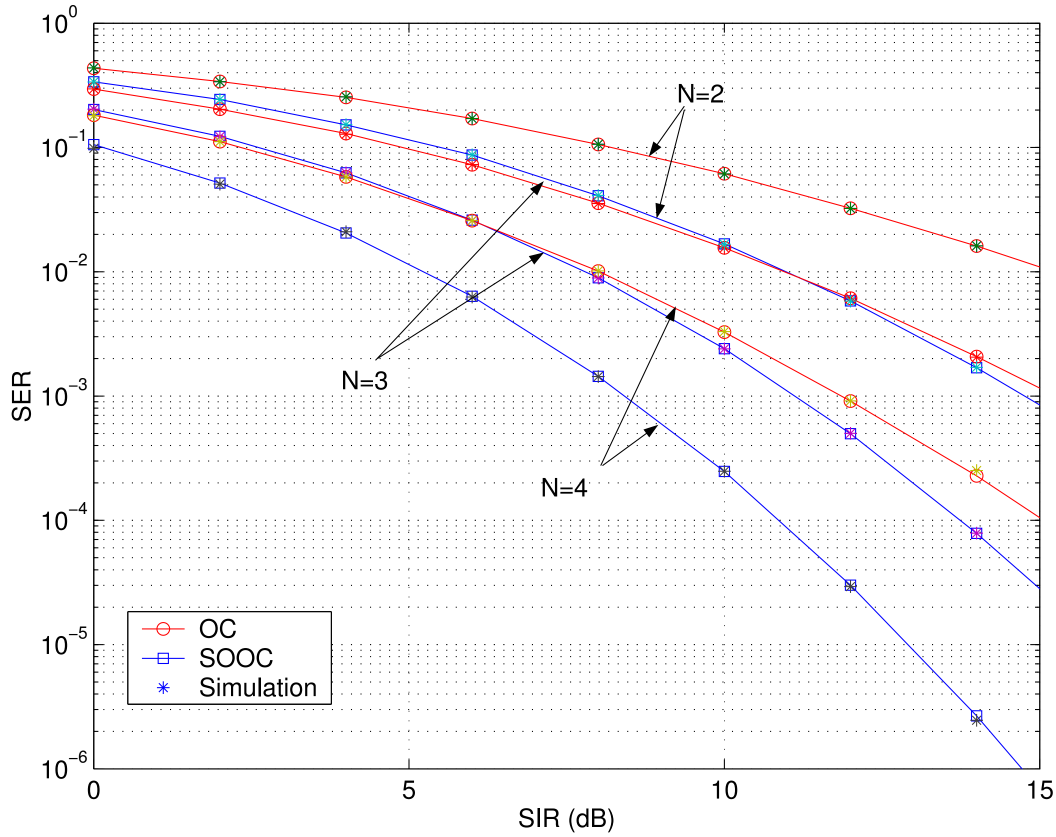

Figure 12: Average SER of MPSK of OC and SOOC with four modulation sysmbols, L=7 and various number of N.

4.6 Conclusion

An interesting configuration of multiple antenna systems using directional antennas arise in the mobile-to-mobile environment. As a result, the selection combining of outputs of optimal combing (SOOC) were introduced. This chapter studies the performance of SOOC with multiple co-channel interferences. We derive the pdf of SOOC and the average SIR of SOOC. We also derive the expressions for the outage probability and the SER for MPSK systems of SOOC. We evaluate the performance of SOOC by comparing with the performance of OC. SOOC is especially beneficial over OC when the required SER is low.

CHAPTER V

PERFORMANCE ANALYSIS ON OPTIMAL COMBINING IN THE PRESENCE OF INTERFERERS AND THERMAL NOISE

5.1 Overview

The performance of MIMO systems with optimum combining (OC) is studied in a Rayleigh fading environment with arbitrary-power co-channel interference and thermal noise. Based on the joint eigenvalue distributions of quadratic forms in complex Gaussian matrices, a closed-form expression for the exact distribution of the output SINR is derived. A closed-form expression for exact MGF of the output SINR of SIMO systems is also derived. From the exact MGF, the moments of the output SINR and the symbol error rate of various M-ary modulation schemes are obtained. We verify the accuracy of our analytical results by the numerical examples. The new analytical framework provides a simple and accurate way to assess the effects of equal and unequal-power co-channel interferers and thermal noise on the performance of optimum combining.

The remainder of this chapter is organized as follows. Section 5.2 provides some new results on the joint eigenvalue distributions of quadratic forms in complex Gaussian matrices, which play a major role in the derivation of the performance of OC. In Section 5.3, we define the system model and briefly review OC systems. Section 5.4 presents the outage probability, pdf of output SINR, and SER of MPSK for MIMO-OC system with cochannel interference and thermal noise. Section 5.5 presents the derivation of the MGF, the moments of output SINR of SIMO-OC, and average SERs for MPSK, MQAM, and MDPSK in the presence of interference and thermal noise on a Rayleigh fading channel. In Section 5.6, we show some numerical examples to confirm our analysis by comparing with simulation results. Finally, the main results of this paper are summarized in Section 5.7.

5.2 Joint Eigenvalue Distributions of Quadratic Forms in Complex Gaussian Matrices

Based on the distribution functions of the ordered eigenvalues of certain quadratic forms in complex Gaussian matrices reviewed in Chapter II, we develop two important theorems, which is useful to analyze the performance of optimal combing in the presence of arbitrary-powered interferers and thermal noise.

Theorem 2. *Consider the* $m \times n$ *matrix* $\mathbf{Y} \sim \tilde{N}_{m,n}(\mathbf{0}, \mathbf{I}_m, \mathbf{\Psi})$ *with* $m \leq n$*, where* $\mathbf{\Psi}$ *is the* $n \times n$ *Hermitian positive definite matrix with* n *eigenvalues* $\psi_1 \geq \psi_2 \geq \cdots \geq \psi_n$*, and* ρ *distinct ordered eigenvalues* $\psi_{<1>} > \psi_{<2>} > \cdots > \psi_{<\rho>}$ *, and* $\boldsymbol{I}_m$ *is the* $m \times m$ *identity matrix. Then, the joint density function of the ordered eigenvalues* $\lambda_1, \lambda_2, \cdots, \lambda_m$ *of* $\mathbf{Z} = \mathbf{Y}\mathbf{Y}^H$ *is given by*

$$f_{\mathbf{\Lambda}}(\lambda_1, \lambda_2, \cdots, \lambda_m) = K_1(m, n, \Psi) \det(\mathbf{V}(\mathbf{\Lambda})) \frac{\det\left(\begin{bmatrix} \boldsymbol{Y}_1 & \boldsymbol{Y}_2 & \cdots & \boldsymbol{Y}_\rho \\ \boldsymbol{Z}_{(n-m),1} & \boldsymbol{Z}_{(n-m),2} & \cdots & \boldsymbol{Z}_{(n-m),\rho} \end{bmatrix}\right)}{\det\left(\begin{bmatrix} \boldsymbol{Z}_{(n),1} & \boldsymbol{Z}_{(n),2} & \cdots & \boldsymbol{Z}_{(n)\rho} \end{bmatrix}\right)}, \tag{86}$$

where $\mathbf{V}(\mathbf{X})$ *denotes the Vandermonde matrix of the ordered eigenvalues of* $\mathbf{X}$*,* ρ *is the number of distinct eigenvalues of* $\mathbf{\Psi}$*,* l_k *is the number of same value eigenvalues for* $k = 1, \cdots, \rho : \sum_{k=1}^{\rho} l_k = n$*,* $\boldsymbol{Y}_k$ *and* $\boldsymbol{Z}_{(l),k}$ *are* $m \times l_k$ *and* $l \times l_k$ *matrices respectively, and*

$$K_1(m, n, \mathbf{\Psi}) = (-1)^{m(n-m)} \frac{\pi^{m(m-1)} \prod_{i=n-m+1}^{n} \Gamma(i) \left(\det(\mathbf{\Psi})\right)^{-m}}{\tilde{\Gamma}_m(n) \tilde{\Gamma}_m(m)}, \tag{87}$$

$$\{\boldsymbol{Y}_k\}_{i,j} = (-\lambda_i)^{(j-1)}\exp(-\lambda_i/\psi_{<k>}), \tag{88}$$

$$\left\{\boldsymbol{Z}_{(l),k}\right\}_{i,j} = (-1)^{(j-1)}(i-j+1)_{(j-1)}(-\psi_{<k>})^{(j-i)} \ , \tag{89}$$

$$\tilde{\Gamma}_m(n) = \pi^{m(m-1)/2}\prod\nolimits_{k=1}^{m}\Gamma(n-k+1) \tag{90}$$

Proof. By putting $\mathbf{B} = \mathbf{I}_n$ and $\boldsymbol{\Sigma} = \mathbf{I}_m$ in the distribution of the quadratic forms in complex matrices in Chapter II, the density function of ordered eigenvalues of $\mathbf{Z}$ is given by [79]

$$f_{\boldsymbol{\Lambda}}(\lambda_1, \lambda_2, \cdots, \lambda_m) = \frac{\pi^{m(m-1)}(\det\boldsymbol{\Psi})^{-m}}{\tilde{\Gamma}_m(n)\tilde{\Gamma}_m(m)}\prod_{i=1}^{m}\lambda_i^{n-m}\prod_{i<j}^{m}(\lambda_i-\lambda_j)^2{}_0\tilde{F}_0^{(n)}\left(-\boldsymbol{\Psi}^{-1}, \boldsymbol{\Lambda}\right). \tag{91}$$

The complex hypergeometric function ${}_0\tilde{F}_0^{(n)}(-\boldsymbol{\Psi}^{-1}, \boldsymbol{\Lambda})$ can be represented in terms of determinants with classical hypergeometric functions using the formulation of Gross and Richards. Unfortunately, the formulation requires the number of eigenvalues for each matrix argument to be equal and all the eigenvalues of the matrix arguments to be unequal. Thus, we add the $n-m$ eigenvalues $\varepsilon_1^0 > \varepsilon_2^0 > \cdots > \varepsilon_{n-m}^0 > 0$ in $\boldsymbol{\Lambda}$ and take the limit $\{\varepsilon_i^0\} \to 0$ for $i = 1, 2, \cdots, n-m$. Adding zero eigenvalues does not change the original zonal polynomials [80]. We also introduce $\varepsilon_1^1 > \varepsilon_2^1 > \cdots > \varepsilon_{l_1}^1 > 0$, $\varepsilon_1^2 > \varepsilon_2^2 > \cdots > \varepsilon_{l_2}^2 > 0, \cdots$, and $\varepsilon_1^\rho > \varepsilon_2^\rho > \cdots > \varepsilon_{l_\rho}^\rho > 0$ to take the limit $\{\varepsilon_k^j\} \to 0$ for $j = 1, 2, \cdots, \rho$, and $k = 1, 2, \cdots, l_j$.

${}_0\tilde{F}_0^{(n)}(-\boldsymbol{\Psi}^{-1}, \boldsymbol{\Lambda})$ can be expressed as

$${}_0\tilde{F}_0^{(n)}\left(-\boldsymbol{\Psi}^{-1}, \boldsymbol{\Lambda}\right) = \lim_{\{\varepsilon_k^j\}\to 0}\lim_{\{\varepsilon_i^0\}\to 0}{}_0\tilde{F}_0^{(n)}\left(-\tilde{\boldsymbol{\Psi}}^{-1}, \tilde{\boldsymbol{\Lambda}}\right) \tag{92}$$

where $\tilde{\mathbf{\Lambda}}$ is an $n \times n$ diagonal matrix $\tilde{\mathbf{\Lambda}} = diag\{\lambda_1, \cdots, \lambda_m, \varepsilon_1^0, \cdots, \varepsilon_{n-m}^0\}$, and $\tilde{\mathbf{\Psi}}$ is an $n \times n$ diagonal matrix $\tilde{\mathbf{\Psi}}^{-1} = diag\{\tilde{\psi}_1^{-1}, \cdots, \tilde{\psi}_n^{-1}\} = diag\{\psi_{<1>}^{-1} + \varepsilon_1^1, \psi_{<1>}^{-1} + \varepsilon_2^1, \cdots, \psi_{<1>}^{-1} + \varepsilon_{l_1}^1, \psi_{<2>}^{-1} + \varepsilon_1^2, \psi_{<2>}^{-1} + \varepsilon_2^2, \cdots, \psi_{<2>}^{-1} + \varepsilon_{l_2}^2, \cdots, \psi_{<\rho>}^{-1} + \varepsilon_1^\rho, \psi_{<\rho>}^{-1} + \varepsilon_2^\rho, \cdots, \psi_{<\rho>}^{-1} + \varepsilon_{l_\rho}^\rho\}$. The determinant representation of the complex hypergeometric function ${}_0\tilde{F}_0^{(n)}(-\tilde{\mathbf{\Psi}}^{-1}, \tilde{\mathbf{\Lambda}})$ is given by

$$
\begin{aligned}
{}_0\tilde{F}_0^{(n)}\left(-\tilde{\mathbf{\Psi}}^{-1}, \tilde{\mathbf{\Lambda}}\right) &= \prod_{k=1}^{n} \Gamma(k) \frac{\det\left(\mathbf{F}_0\left(\tilde{\mathbf{\Psi}}, \tilde{\mathbf{\Lambda}}\right)\right)}{\det\left(\mathbf{V}\left(-\tilde{\mathbf{\Psi}}^{-1}\right)\right) \det\left(\mathbf{V}\left(\tilde{\mathbf{\Lambda}}\right)\right)} \\
&= \tilde{K} \frac{\det\left(\left[\mathbf{h}\left(\lambda_1\right) \ \cdots \mathbf{h}\left(\lambda_m\right) \mathbf{h}\left(\varepsilon_1\right) \ \cdots \mathbf{h}\left(\varepsilon_{n-m-1}\right) \mathbf{h}\left(\varepsilon_{n-m}\right)\right]\right)}{\det\left(\left[\mathbf{g}\left(\lambda_1\right) \ \cdots \mathbf{g}\left(\lambda_m\right) \mathbf{g}\left(\varepsilon_1\right) \ \cdots \mathbf{g}\left(\varepsilon_{n-m-1}\right) \mathbf{g}\left(\varepsilon_{n-m}\right)\right]\right)}
\end{aligned} \tag{93}
$$

where $\tilde{K} = (\prod_{k=1}^n \Gamma(k)) / \det(\mathbf{V}(-\tilde{\mathbf{\Psi}}^{-1}))$, $\mathbf{h}(x) = [e^{-x/\tilde{\psi}_1} \ e^{-x/\tilde{\psi}_2} \cdots \ e^{-x/\tilde{\psi}_n}]^T$, and $\mathbf{g}(x) = [1 \ x \ x^2 \cdots \ x^{n-1}]^T$. The ratio of $\det(\mathbf{F}_0(\tilde{\mathbf{\Psi}}, \tilde{\mathbf{\Lambda}}))$ to $\det(\mathbf{V}(\tilde{\mathbf{\Lambda}}))$ in (93) is troublesome since both vanish as $\{\varepsilon_i^0\} \to 0$. By applying the Cauchy's mean value theorem or l'Hôpital rule, ${}_0\tilde{F}_0^{(n)}(-\tilde{\mathbf{\Psi}}^{-1}, \tilde{\mathbf{\Lambda}})$ becomes [81, 82]

$$
{}_0\tilde{F}_0^{(n)}\left(-\tilde{\mathbf{\Psi}}^{-1}, \tilde{\mathbf{\Lambda}}\right) = \tilde{K} \frac{\det\left(\left[\mathbf{h}\left(\lambda_1\right) \ \cdots \mathbf{h}\left(\lambda_m\right) \mathbf{h}^{(0)}\left(\varepsilon_1\right) \ \cdots \mathbf{h}^{(n-m-2)}\left(\varepsilon_{n-m-1}\right) \mathbf{h}^{(n-m-1)}\left(\varepsilon_{n-m}\right)\right]\right)}{\det\left(\left[\mathbf{g}\left(\lambda_1\right) \ \cdots \mathbf{g}\left(\lambda_m\right) \mathbf{g}^{(0)}\left(\varepsilon_1\right) \ \cdots \mathbf{g}^{(n-m-2)}\left(\varepsilon_{n-m-1}\right) \mathbf{g}^{(n-m-1)}\left(\varepsilon_{n-m}\right)\right]\right)} \tag{94}
$$

where $\mathbf{h}^{(k)}(x)$ and $\mathbf{g}^{(k)}(x)$ denote the k-th derivatives of $\mathbf{h}(x)$ and $\mathbf{g}(x)$, respectively. Since the effect of interchanging operation between two rows upon the determinant is to multiply it by -1, ${}_0\tilde{F}_0^{(n)}(-\tilde{\mathbf{\Psi}}^{-1}, \mathbf{\Lambda})$ can be rewritten as

$$
{}_0\tilde{F}_0^{(n)}\left(-\tilde{\mathbf{\Psi}}^{-1}, \mathbf{\Lambda}\right) = (-1)^{m(n-m)} \frac{\prod_{i=1}^m \Gamma(n-i+1)}{\det\left(\mathbf{V}\left(-\tilde{\mathbf{\Psi}}^{-1}\right)\right)} \frac{\det\left(\mathbf{F}_1\left(\tilde{\mathbf{\Psi}}, \mathbf{\Lambda}\right)\right)}{\left(\det \mathbf{\Lambda}\right)^{n-m} \det\left(\mathbf{V}\left(\mathbf{\Lambda}\right)\right)}. \tag{95}
$$

and

$$\left\{\mathbf{F}_1\left(\tilde{\mathbf{\Psi}},\mathbf{\Lambda}\right)\right\}_{i,j}=\begin{cases}\exp\left(-\lambda_j/\tilde{\psi}_i\right), & j=1,\cdots,m\\ \left(-\tilde{\psi}_i\right)^{m+1-j}, & j=m+1,\cdots,n.\end{cases}$$

Similarly, we take the limit for $\{\varepsilon_k^j\}\to 0$ for $j=1,2,\cdots,\rho$, and $k=1,2,\cdots,l_j$, then ${}_0\tilde{F}_0^{(n)}(-\mathbf{\Psi}^{-1},\mathbf{\Lambda})$ is

$$ {}_0\tilde{F}_0^{(n)}\left(-\mathbf{\Psi}^{-1},\mathbf{\Lambda}\right) = \lim_{\{\varepsilon_k^j\}\to 0} {}_0\tilde{F}_0^{(n)}\left(-\tilde{\mathbf{\Psi}}^{-1},\mathbf{\Lambda}\right). \tag{96}$$

$$= (-1)^{m(n-m)}\frac{\prod_{i=1}^m\Gamma(n-i+1)}{(\det\mathbf{\Lambda})^{n-m}\det\left(\mathbf{V}\left(\mathbf{\Lambda}\right)\right)} \cdot\frac{\det\left(\begin{bmatrix}\boldsymbol{Y}_1 & \boldsymbol{Y}_2 & \cdots & \boldsymbol{Y}_\rho\\ \boldsymbol{Z}_{(n-m),1} & \boldsymbol{Z}_{(n-m),2} & \cdots & \boldsymbol{Z}_{(n-m),\rho}\end{bmatrix}\right)}{\det\left(\begin{bmatrix}\boldsymbol{Z}_{(n),1} & \boldsymbol{Z}_{(n),2} & \cdots & \boldsymbol{Z}_{(n)\rho}\end{bmatrix}\right)}. \tag{97}$$

Finally, substituting (97) into (91) yields the distribution of ordered eigenvalues of $\mathbf{Z}$.

$\square$

Theorem 3. *Consider the $m\times n$ matrix $\mathbf{Y}\sim\tilde{N}_{m,n}(\mathbf{0},\mathbf{\Sigma},\mathbf{I}_n)$, where $\mathbf{\Sigma}$ is the $m\times m$ Hermitian positive definite matrix with m eigenvalues $\sigma_1\geq\sigma_2\geq\cdots\geq\sigma_m$ and ρ distinct ordered eigenvalues $\sigma_{<1>}>\sigma_{<2>}>\cdots>\sigma_{<\rho>}$. Then, the joint density function of the ordered eigenvalues $\lambda_1,\lambda_2,\cdots,\lambda_m$ of $\mathbf{Z}=\mathbf{Y}\mathbf{Y}^H$ is given by*

$$f_{\mathbf{\Lambda}}\left(\lambda_1,\lambda_2,\cdots,\lambda_m\right) = K_2\left(m,n,\mathbf{\Sigma}\right)\left(\det\mathbf{\Lambda}\right)^{n-m}\det\left(\mathbf{V}\left(\mathbf{\Lambda}\right)\right) \cdot\frac{\det\left(\begin{bmatrix}\boldsymbol{Y}_1 & \boldsymbol{Y}_2 & \cdots & \boldsymbol{Y}_\rho\end{bmatrix}\right)}{\det\left(\begin{bmatrix}\boldsymbol{Z}_{(m),1} & \boldsymbol{Z}_{(m),2} & \cdots & \boldsymbol{Z}_{(m)\rho}\end{bmatrix}\right)}, \tag{98}$$

where ρ is the number of distinct eigenvalues of $\mathbf{\Sigma}$, l_k is the number of the same eigenvalues for k=1, $\cdots, \rho$: $\sum_{k=1}^{\rho} l_k = m$, $\boldsymbol{Y}_k$ and $\boldsymbol{Z}_{(l),k}$ are $m \times l_k$ and $l \times l_k$ matrices respectively, and

$$K_2(m, n, \mathbf{\Sigma}) = \frac{\pi^{m(m-1)} \prod_{i=1}^{m} \Gamma(i) \left(\det(\mathbf{\Sigma})\right)^{-n}}{\tilde{\Gamma}_m(n)\tilde{\Gamma}_m(m)}, \tag{99}$$

$$\{\boldsymbol{Y}_k\}_{i,j} = (-\lambda_i)^{(j-1)} \exp(-\lambda_i/\sigma_{<k>}), \tag{100}$$

$$\left\{\boldsymbol{Z}_{(l),k}\right\}_{i,j} = (-1)^{(j-1)}(i-j+1)_{(j-1)}(-\sigma_{<k>})^{(j-i)} \tag{101}$$

Proof. As seen [55, Section III.B], the joint density function of ordered eigenvalues $\lambda_1, \lambda_2, \cdots, \lambda_m$ is

$$f_{\mathbf{\Lambda}}(\lambda_1, \lambda_2, \cdots, \lambda_m) = \frac{\pi^{m(m-1)} \prod_{i=1}^{m} \Gamma(i)}{\tilde{\Gamma}_m(n)\tilde{\Gamma}_m(m)} (\det \mathbf{\Sigma})^{-n} (\det \mathbf{\Lambda})^{n-m} \det(\mathbf{V}(\mathbf{\Lambda})) \frac{\det(\mathbf{F}_0(\mathbf{\Sigma}, \mathbf{\Lambda}))}{\det\left(\mathbf{V}\left(-\mathbf{\Sigma}^{-1}\right)\right)}, \tag{102}$$

where

$$\{\mathbf{F}_0(\mathbf{\Sigma}, \mathbf{\Lambda})\}_{i,j} = \exp(-\lambda_j/\sigma_i).$$

With the same eigenvalues of $\mathbf{\Sigma}$, we also have the same problem to evaluate the density since the numerator and denominator vanishes at the same time. Applying the technique used in the the previous proof, we can reach to the final result.

$\square$

5.3 *MIMO-OC System Model*

Consider a MIMO system employing T antennas at the transmitter and R antennas at the receiver with L interferers denoted as an (T, R, L) MIMO system. SIMO is the special case of MIMO with T =1. We assume that the channel is flat faded and perfect channel knowledge is available at both the transmitter and receiver. Then, the $R \times 1$ vector at the receiver is

$$\mathbf{r} = \sqrt{P_D}\mathbf{H}_D \mathbf{w}_T s_D + \sum_{k=1}^{L} \sqrt{P_k}\mathbf{h}_k s_k + \mathbf{n} \tag{103}$$

where s_D and s_k are the unit-variance modulation symbols of the desired and the k-th interfering user, and P_D and P_k are the average powers of the desired user and the k-th interfering user, respectively; $\mathbf{w}_T$ is the $T \times 1$ weighting vector at the transmitter with $\|\mathbf{w}_T\|^2 = 1$; $\mathbf{n}$ is the additive complex Gaussian noise vector with zero mean and covariance matrix $\sigma^2\mathbf{I}_R$, where $\mathbf{I}_R$ is the $R \times R$ identity matrix; $\mathbf{H}_D$ is the $R \times T$ channel gain matrix for the desired user and $\mathbf{h}_k$ is the $R \times 1$ channel gain vector for the k-th interfering user. Each entry of $\mathbf{H}_D$ and $\mathbf{h}_k$ is an independent complex Gaussian random variable with unit-variance.

Let $\mathbf{H}_I = (\mathbf{h}_1, \mathbf{h}_2, \cdots, \mathbf{h}_L)$ be the aggregated $R \times L$ channel gain matrix for the cochannel interferers. Then, the received vector in (103) can be rewritten as

$$\mathbf{r} = \sqrt{P_D}\mathbf{H}_D \mathbf{w}_T s_D + \mathbf{H}_I \mathbf{P}_I^{1/2} \mathbf{s}_I + \mathbf{n}, \tag{104}$$

where $\mathbf{P}_I = \mathrm{diag}\{P_1, P_2, \cdots, P_L\}$ and $\mathbf{s}_I = (s_1, s_2, \cdots, s_L)^T$. The optimum weighting vector at the receiver for a given $\mathbf{w}_T$ that maximizes the output SINR is [70], [71]

$$\mathbf{w}_R = \alpha \mathbf{R}^{-1} \mathbf{H}_D \mathbf{w}_T, \tag{105}$$

where α is arbitrary constant which does not affect the output SNR, and $\mathbf{R} = \mathbf{H}_I \mathbf{P}_I \mathbf{H}_I^H + \sigma^2 \mathbf{I}_R$ is the interference-plus-noise covariance matrix. Using the optimum weighting vector $\mathbf{w}_R$ in (105) and applying the Raleigh-Ritz theorem in [5, p.176], the optimum weighting vector $\mathbf{w}_T$ at the transmitter is the eigenvector corresponding to the largest eigenvalue of $\mathbf{Z} = \mathbf{H}_D^H\mathbf{R}^{-1}\mathbf{H}_D$. Finally, the maximum output SINR per symbol becomes

$$\begin{aligned}\gamma &= P_D\mathbf{w}_T^H\mathbf{H}_D^H\mathbf{R}^{-1}\mathbf{H}_D\mathbf{w}_T, \\ &= P_D\lambda_{\max}. \end{aligned} \tag{106}$$

where $\lambda_{\max}$ is the largest eigenvalue of $\mathbf{Z}$.

5.4 Performance Analysis of MIMO-OC System With Interference and Thermal Noise

Now, we consider a MIMO adaptive antenna system in the presence of arbitrary-power interference and thermal noise. For the brevity, we assume that the number of co-channel interferers is larger than or equal to the number of receive antennas (overload case). The same method can be applied where the number of cochannel interferers exceeds the number of antennas (underload case).

Based on the joint eigenvalue distributions in Theorem 1 and 2, we derive closed-form expressions for the exact pdf and the outage probability of the maximum SINR. Then, we present the error probability of MPSK in MIMO-OC systems as a single integral formula.

5.4.1 Outage Probability

To derive the outage probability of MIMO-OC systems, we need to find the distribution function of the largest eigenvalue of $\mathbf{Z} = \mathbf{H}_D^H\mathbf{R}^{-1}\mathbf{H}_D$. Since the covariance matrix $\mathbf{R}$ is a positive definite Hermitian matrix, it can be unitarily diagonalized as $\mathbf{R} = \mathbf{E}^H\mathbf{\Sigma}\mathbf{E}$, where $\mathbf{E}$ is a unitary matrix and $\mathbf{\Sigma} = \mathrm{diag}\{\sigma_1, \sigma_2, \cdots, \sigma_R\}$ is a diagonal matrix of the ordered eigenvalues of $\mathbf{R}$ with $\sigma_1 \geq \sigma_2 \geq \cdots \geq \sigma_R$. Then, using the invariant statistical properties of unitary transformation, the random matrix $\mathbf{Z}$ is equivalent to a quadratic-form of complex Gaussian matrix with one-sided covariance matrix $\mathbf{\Sigma}$ and can be expressed as

$$\mathbf{Z} = \tilde{\mathbf{H}}_D^H \tilde{\mathbf{H}}_D, \tag{107}$$

where $\tilde{\mathbf{H}}_D \sim \tilde{\mathbf{N}}_{R,T}(0, \mathbf{\Sigma^{-1}}, \mathbf{I_T})$. Since the largest eigenvalue of $\mathbf{Z}$ has different distribution functions depending on the numbers of transmit and receive antennas, let us derive the outage probability of MIMO-OC system in two cases, i.e., $R \geq T$ and $R \leq T$.

5.4.1.1 MIMO-OC systems with $R \geq T$ and $R \geq L$

When the number of receiver antennas is greater than the number of transmit antennas, $\mathbf{Z} = \mathbf{Y_1}\mathbf{Y_1}^H$, where $\mathbf{Y_1} \sim \tilde{N}_{T,R}(\mathbf{0}, \mathbf{I}_T, \mathbf{\Sigma^{-1}})$. With distinct eigenvalues of $\mathbf{\Sigma}$, the joint density function of eigenvalues of $\mathbf{Z}$ conditioned on covariance matrix $\mathbf{\Sigma^{-1}}$ can be simplified using (91) and (95) as

$$\begin{aligned} f_{\mathbf{\Lambda}|\mathbf{\Sigma}}\left(\lambda_1, \lambda_2, \cdots, \lambda_T\right) &= (-1)^{T(R-T)} \frac{\pi^{T(T-1)} \prod_{i=R-T+1}^{R} \Gamma(i)}{\tilde{\Gamma}_T(R)\tilde{\Gamma}_T(T)} \frac{\left(\det\left(\mathbf{\Sigma}\right)\right)^T}{\det\left(\mathbf{V}\left(-\mathbf{\Sigma}\right)\right)} \\ &\quad \cdot \det\left(\mathbf{V}\left(\mathbf{\Lambda}\right)\right) \det\left(\mathbf{F}_1\left(\mathbf{\Sigma}^{-1}, \mathbf{\Lambda}\right)\right), \end{aligned} \tag{108}$$

where $\mathbf{\Lambda} = \text{diag}\{\lambda_1, \cdots, \lambda_T\}$ is a diagonal matrix of the ordered eigenvalues of $\mathbf{Z}$ with $\lambda_1 \geq \cdots \geq \lambda_T$,

$$\left\{\mathbf{F}_1\left(\mathbf{\Sigma}^{-1}, \mathbf{\Lambda}\right)\right\}_{i,j} = \begin{cases} \exp\left(-\lambda_j \sigma_i\right), & j = 1, \cdots, T \\ \left(-\sigma_i\right)^{T+1-j}, & j = T+1, \cdots, R. \end{cases}$$

Then, the cdf of the largest eigenvalue $\lambda_{\max}$ can be obtained as

$$\begin{aligned} F_{\lambda_{\max|\mathbf{\Sigma}}}(x) &= \Pr\left[\lambda_{\max} \leq x \mid \mathbf{\Sigma}\right] \\ &= \Pr\left[0 \leq \lambda_T \leq \lambda_{T-1} \leq \cdots \leq \lambda_1 \leq x \mid \mathbf{\Sigma}\right] \\ &= \int_0^x \int_{\lambda_T}^x \cdots \int_{\lambda_2}^x f_{\mathbf{\Lambda}|\mathbf{\Sigma}}\left(\lambda_1, \lambda_2, \cdots, \lambda_T\right) d\lambda_1 d\lambda_2 \cdots d\lambda_T. \end{aligned} \tag{109}$$

Since the integrand of (109) is a symmetric function of $\lambda_1, \lambda_2, \cdots, \lambda_T$, we can simplify the multi-dimensional integration in (109) into a single integral formula from the generalized Binet-Cauchy formula in Chapter II. The conditional cdf of $\lambda_{\max|\mathbf{\Sigma}}$ becomes

$$F_{\lambda_{\max|\mathbf{\Sigma}}}(x) = (-1)^{T(R-T)} \frac{\pi^{T(T-1)} \prod_{i=R-T+1}^{R} \Gamma(i)}{\tilde{\Gamma}_T(R)\tilde{\Gamma}_T(T)} \frac{(\det(\mathbf{\Sigma}))^T}{\det(\mathbf{V}(-\mathbf{\Sigma}))} \det(\mathbf{\Delta}_1(x)), \quad (110)$$

where $\mathbf{\Delta}_1(x)$ is an $R \times R$ matrix function of x whose entries are

$$\{\mathbf{\Delta}_1(x)\}_{i,j} = \begin{cases} \sigma_i^{-j}\gamma(j, \sigma_i x), & j = 1, \cdots, T \\ (-\sigma_i)^{T+1-j}, & j = T+1, \cdots, R. \end{cases} \quad (111)$$

In (111), $\gamma(\cdot, \cdot)$ is the incomplete Gamma function [60, eq. 8.350.1].

The joint eigenvalue distribution of $\mathbf{R}$ is largely governed by the distribution of $\tilde{\mathbf{R}} = \mathbf{H_I P_I H_I^H}$, and the joint eigenvalue distribution of $\tilde{\mathbf{R}}$ is one of the quadratic forms of $\mathbf{Y} \sim \tilde{N}_{R,L}(\mathbf{0}, \mathbf{I}_R, \mathbf{P_I})$ for ρ distinct power interferers $p_{<1>} > p_{<2>} > \cdots > p_{<\rho>}$with L in total.

The exact cdf of the largest eigenvalue of $\mathbf{Z}$ can be derived by averaging the conditional cdf in (110) over the joint eigenvalue distribution of $\mathbf{R}$. The exact cdf of the maximum output SINR of MIMO-OC system is obtained using the generalized Binet-Cauchy formula in Chapter II. Let $\Gamma_D = P_D/\sigma^2, \Gamma_i = P_i/\sigma^2$, $\gamma_{<k>} = p_{<k>}/\sigma^2$ and $\mathbf{\Gamma}_I = \mathrm{diag}(\Gamma_1, \Gamma_2, \cdots, \Gamma_L)$. Then, a closed-form expression of outage probability of maximum output SINR of MIMO-OC system is

$$P_{\text{out}}(\gamma_0) = \Pr\{\gamma \leq \gamma_0\} = F_{\lambda_{\max}}(\gamma_0/P_D) = \tilde{K}_1(T, R, \mathbf{\Gamma}_I) \det\left(\tilde{\mathbf{\Delta}}_1(\gamma_0)\right) \quad (112)$$

where $\tilde{\mathbf{\Delta}}_1(x)$ is an $L \times L$ matrix function

$$\tilde{\mathbf{\Delta}}_1(x) = \begin{bmatrix} \tilde{\boldsymbol{Y}}_1(x) & \tilde{\boldsymbol{Y}}_2(x) & \cdots & \tilde{\boldsymbol{Y}}_\rho(x) \\ \tilde{\boldsymbol{Z}}_{(L-R),1} & \tilde{\boldsymbol{Z}}_{(L-R),2} & \cdots & \tilde{\boldsymbol{Z}}_{(L-R),\rho} \end{bmatrix}, \quad (113)$$

and

$$\tilde{K}_1\left(R, L, \mathbf{\Gamma}_I\right) = \frac{(-1)^{T(R-T)+R(R-1)/2}\, \pi^{T(T-1)} \prod_{i=R-T+1}^{R} \Gamma(i)}{\tilde{\Gamma}_T(R)\tilde{\Gamma}_T(T)\ \det\left(\left[\begin{array}{cccc} \tilde{\boldsymbol{Z}}_{(L),1} & \tilde{\boldsymbol{Z}}_{(L),2} & \cdots & \tilde{\boldsymbol{Z}}_{(L)\rho} \end{array}\right]\right)} K_1\left(R, L, \mathbf{\Gamma}_I\right), \tag{114}$$

$$\left\{\tilde{\boldsymbol{Y}}_k(x)\right\}_{i,j} = \begin{cases} \Gamma(i)\mathcal{I}\left(T-i, j-1, 1, \gamma_{<k>}\right) - \Gamma(i)\exp(-\frac{x}{\Gamma_D}) & \\ \cdot \sum_{k=0}^{i-1} \frac{x^k}{k!}\mathcal{I}\left(T-i+k, j-1, 1, \frac{\Gamma_D \gamma_{<k>}}{\Gamma_D+\gamma_{<k>}x}\right) & i = 1, \cdots, T, \\ (-1)^{R-j}\mathcal{I}\left(T+R-i, j-1, 1, \gamma_{<k>}\right), \qquad i = T+1, \cdots, R, & \end{cases} \tag{115}$$

$$\left\{\tilde{\boldsymbol{Z}}_{(l),k}\right\}_{i,j} = (-1)^{(j-1)}(i-j+1)_{(j-1)}(-\gamma_{<k>})^{(j-i)}. \tag{116}$$

In (115), [60, eq. 8.352.1] is used for the alternate expression for the incomplete gamma function, and $\mathcal{I}(a,b,c,d) = \int_0^\infty (y+c)^a\ y^b\ \exp(-y/d)dy$. Using the binomial expansion and [60, eq. 3.381.4], we get the closed-form solution for $\mathcal{I}(a,b,c,d)$,

$$\mathcal{I}\left(a,b,c,d\right) = \sum_{k=0}^{a} \left(\begin{array}{c} a \\ k \end{array}\right) c^{a-k}\, d^{b+k+1}\, \Gamma(b+k+1). \tag{117}$$

5.4.1.2 MIMO-OC system with $R \leq T$ and $R \geq L$

When the number of transmit antennas is greater than the number of receive antennas, $\mathbf{Z}$ has R non-zero eigenvalues equal to the eigenvaules of $\mathbf{Y_2}\mathbf{Y_2}^H$, where $\mathbf{Y_2} \sim \tilde{N}_{R,T}(\mathbf{0}, \mathbf{\Sigma}^{-1}, \mathbf{I}_T)$. With the same procedure above, we get the outage probability of MIMO-OC with $R \leq T$ is

$$P_{\text{out}}\left(\gamma_0\right) = \Pr\left\{\gamma \leq \gamma_0\right\} = F_{\lambda_{\max}}\left(\gamma_0/P_D\right) = \tilde{K}_2\left(T, R, \mathbf{\Gamma}_I\right) \det\left(\tilde{\mathbf{\Delta}}_2\left(\gamma_0\right)\right) \tag{118}$$

where $\tilde{\mathbf{\Delta}}_2\left(x\right)$ is an $L \times L$ matrix function

$$\tilde{\mathbf{\Delta}}_2\left(x\right) = \left[\begin{array}{cccc} \tilde{\boldsymbol{Y}}_1(x) & \tilde{\boldsymbol{Y}}_2(x) & \cdots & \tilde{\boldsymbol{Y}}_\rho(x) \\ \tilde{\boldsymbol{Z}}_{(L-R),1} & \tilde{\boldsymbol{Z}}_{(L-R),2} & \cdots & \tilde{\boldsymbol{Z}}_{(L-R),\rho} \end{array}\right], \tag{119}$$

and

$$\tilde{K}_2(R, L, \mathbf{\Gamma}_I) = \frac{(-1)^{R(R-1)/2}\pi^{R(R-1)}\prod_{i=1}^{R}\Gamma(i)}{\tilde{\Gamma}_R(T)\tilde{\Gamma}_R(R)\ \det\left(\left[\begin{array}{cccc} \tilde{\boldsymbol{Z}}_{(L),1} & \tilde{\boldsymbol{Z}}_{(L),2} & \cdots & \tilde{\boldsymbol{Z}}_{(L)\rho}\end{array}\right]\right)} K_1(R, L, \mathbf{\Gamma}_I), \tag{120}$$

$$\begin{aligned}\left\{\tilde{\boldsymbol{Y}}_k(x)\right\}_{i,j} = \quad & \Gamma(T-R+i)\mathcal{I}(R-i, j-1, 1, \gamma_{<k>}) \\ & -\Gamma(T-R+i)\exp(-\frac{x}{\Gamma_D})\sum_{k=0}^{T-R+i-1}\frac{x^k}{k!}\mathcal{I}\left(R-i+k, j-1, 1, \frac{\Gamma_D\gamma_{<k>}}{\Gamma_D+\gamma_{<k>}x}\right) \qquad (121)\\ \left\{\boldsymbol{Z}_{(l),k}\right\}_{i,j} = \quad & (-1)^{(j-1)}(i-j+1)_{(j-1)}(-\gamma_{<k>})^{(j-i)}. \qquad (122)\end{aligned}$$

5.4.2 Pdf of SINR

The pdf of the SINR for MIMO-OC can be found by taking the derivative of the cdf of SINR of MIMO-OC. By using the formula for the derivative of determinant [74]

$$\frac{d}{dx}\det(\mathbf{\Delta}(x)) = \det(\mathbf{\Delta}(x))\operatorname{tr}\left(\mathbf{\Delta}^{-1}(x)\frac{d}{dx}\mathbf{\Delta}(x)\right). \tag{123}$$

Using (123), the pdf of maximum output SINR of the MIMO-OC system is

$$f_\gamma(x) = \left\{\begin{array}{ll} \frac{1}{\Gamma_D}\tilde{K}_1(T, R, \mathbf{\Gamma}_I)\det\left(\tilde{\mathbf{\Delta}}_1(x)\right)\operatorname{tr}\left(\tilde{\mathbf{\Delta}}_1^{-1}(x)\,\breve{\mathbf{\Delta}}_1(x)\right), & R \geq T, \\ \frac{1}{\Gamma_D}\tilde{K}_2(R, T, \mathbf{\Gamma}_I)\det\left(\tilde{\mathbf{\Delta}}_2(x)\right)\operatorname{tr}\left(\tilde{\mathbf{\Delta}}_2^{-1}(x)\,\breve{\mathbf{\Delta}}_2(x)\right), & T \geq R, \end{array}\right., \tag{124}$$

where $\breve{\mathbf{\Delta}}_1(x)$ and $\breve{\mathbf{\Delta}}_2(x)$ are $L \times L$ matrices

$$\breve{\Delta}_1(x) = \left[\begin{array}{cccc} \widetilde{\boldsymbol{Y}}_1^1(x) & \widetilde{\boldsymbol{Y}}_2^1(x) & \cdots & \widetilde{\boldsymbol{Y}}_\rho^1(x) \\ \multicolumn{4}{c}{\mathbf{0}_{(L-T),L}} \end{array}\right], \tag{125}$$

$$\breve{\Delta}_2(x) = \left[\begin{array}{cccc} \widetilde{\boldsymbol{Y}}_1^2(x) & \widetilde{\boldsymbol{Y}}_2^2(x) & \cdots & \widetilde{\boldsymbol{Y}}_\rho^2(x) \\ \multicolumn{4}{c}{\mathbf{0}_{(L-R),L}} \end{array}\right], \tag{126}$$

where $\mathbf{0}_{A,B}$ is $A \times B$ null matrix, and $\widetilde{\boldsymbol{Y}}_k^1$ and $\widetilde{\boldsymbol{Y}}_k^2$ are $T \times l_k$ and $R \times l_k$ matrices respectively whose entries are defined by

$$\{\widetilde{\boldsymbol{Y}}_k^1(x)\}_{i,j} = x^{i-1}\exp(-\frac{x}{\Gamma_D})\ \mathcal{I}\left(T-1, j-1, 1, \frac{\Gamma_D\gamma_{<k>}}{\Gamma_D+\gamma_{<k>}x}\right), \tag{127}$$

$$\{\widetilde{\boldsymbol{Y}}_k^2(x)\}_{i,j} = x^{T-R+i-1}\ \exp(-\frac{x}{\Gamma_D})\,\mathcal{I}\left(T-1, j-1, 1, \frac{\Gamma_D\gamma_{<k>}}{\Gamma_D+\gamma_{<k>}x}\right). \tag{128}$$

5.4.3 SER of MPSK

Based on the outage probability in (112) and (118), we can derive a single integral formula for the SER of coherent MPSK in a MIMO-OC system. The SER of MPSK system is

$$\bar{P}_s = \frac{1}{\pi}\int_0^{\pi-\pi/M}\int_0^{\infty} \exp\left(-\frac{g_{\text{PSK}}}{\sin^2\theta}\gamma\right) f_\gamma(\gamma) d\gamma\, d\theta, \tag{129}$$

where $g_{\text{PSK}} = \sin^2(\pi/M)$ and M is the number of modulation symbols of MPSK systems. Using the integration by parts, the SER of above equation can be expressed as

$$\begin{aligned}\bar{P}_s &= \frac{1}{\pi}\int_0^{\pi-\pi/M}\int_0^{\infty} \exp\left(-\frac{g_{\text{PSK}}}{\sin^2\theta}\gamma\right) \frac{d}{d\gamma} P_{\text{out}}(\gamma) d\gamma\, d\theta \\ &= \frac{1}{\pi}\int_0^{\infty} P_{\text{out}}(\gamma)\int_0^{\pi-\pi/M} \frac{g_{\text{PSK}}}{\sin^2\theta}\exp\left(-\frac{g_{\text{PSK}}}{\sin^2\theta}\gamma\right) d\theta d\gamma\,.\end{aligned} \tag{130}$$

By changing the variable $\theta = \cot^{-1} y$, the average SER of MPSK can be expressed as a single integral formula, which is easier to handle for evaluating the performance of MIMO-MRC system,

$$\bar{P}_s = \sqrt{\frac{g_{\text{psk}}}{\pi}}\int_0^{\infty} \frac{e^{-g_{\text{PSK}}\gamma}}{2\sqrt{\gamma}}\left(1+\operatorname{erf}\left(\sqrt{(1\text{-g}_{\text{PSK}})\gamma}\right)\right) P_{\text{out}}(\gamma)\, d\gamma, \tag{131}$$

where $\operatorname{erf}(x) = 2/\sqrt{\pi}\int_0^x \exp(-t^2)dt$. Finally, the error probability of MPSK in MIMO-OC system is given by

$$\bar{P}_s = \begin{cases} \tilde{K}_1(T,R,\Gamma_I)\,\frac{\sqrt{g_{\text{psk}}}}{2\sqrt{\pi}}\int_0^{\infty}\frac{e^{-g_{\text{PSK}}\gamma}}{\sqrt{\gamma}}\left(1+\operatorname{erf}\left(\sqrt{(1\text{-g}_{\text{PSK}})\gamma}\right)\right)\det\left(\tilde{\boldsymbol{\Delta}}_1(\gamma)\right) d\gamma, & R \geq T, \\ \tilde{K}_2(R,T,\Gamma_I)\,\frac{\sqrt{g_{\text{psk}}}}{2\sqrt{\pi}}\int_0^{\infty}\frac{e^{-g_{\text{PSK}}\gamma}}{\sqrt{\gamma}}\left(1+\operatorname{erf}\left(\sqrt{(1\text{-g}_{\text{PSK}})\gamma}\right)\right)\det\left(\tilde{\boldsymbol{\Delta}}_2(\gamma)\right) d\gamma, & T \geq R. \end{cases} \tag{132}$$

5.5 *MGF-Based Performance Analysis of Optimum Combining of SIMO Systems With Interference and Thermal Noise*

A closed-form expression for the exact MGF of output SINR of SIMO-OC is derived in the presence of thermal noise and arbitrary-power interferers. Using the MGF of output SINR of SIMO-OC, we derive moments of output SINR of OC, particulary the average output SINR of OC. The symbol error probabilities of various M-ary modulation schemes are also studied. We only consider the overload case for the brevity ($L \geq R$). However, the same framework can be applied to the underload case.

5.5.1 MGF

Since $\mathbf{R}$ is decomposed as $\mathbf{U}^H\mathbf{\Sigma}\mathbf{U}$, the output SINR γ can be expressed as $\gamma = P_D \sum_{i=1}^{R} v_i/\sigma_i$, where $\mathbf{v} = \mathbf{U}\mathbf{h}_D = [v_{D,1}, v_{D,2}, \cdots, v_{D,R}]^T$, and $v_i = |h_{D,i}|^2$. Since $\mathbf{v}$ has the same statistical properties as $\mathbf{h}_D$ due to the unitary transformation of $\mathbf{U}$, v_i is a chi-square random variable with two degrees of freedom. Then the moment-generating function (MGF) of γ conditioned on the eigenvalues σ_i of $\mathbf{R}$, $i = 1, 2, \cdots, R$, is given by [63]

$$\Phi_{\gamma}^{\mathrm{OC}}(s\,; \sigma_1, \sigma_2, \cdots, \sigma_R) = \prod_{i=1}^{R} \left(\frac{\sigma_i}{\sigma_i - P_D s} \right) \tag{133}$$

Integrating (133) over the distribution of eigenvalues of $\mathbf{R}$ and using the generalized Binet Cauchy formula in Chapter II, the exact MGF of OC is,

$$\Phi_{\gamma}^{\mathrm{OC}}(s) = \frac{K_1(R,L,\mathbf{\Gamma_I})}{\det\begin{bmatrix} \boldsymbol{Z}_{(L),1} & \boldsymbol{Z}_{(L),2} & \cdots & \boldsymbol{Z}_{(L),\rho} \end{bmatrix}} \det(\Delta_1(s)) \;, \tag{134}$$

where $\Delta_1(s)$ is an $L \times L$ matrix functions of s given by

$$\Delta_1(s) \;=\; \begin{bmatrix} \boldsymbol{Y}_1^1 & \boldsymbol{Y}_2^1 & \cdots & \boldsymbol{Y}_\rho^1 \\ \boldsymbol{Z}_{(L-R),1} & \boldsymbol{Z}_{(L-R),2} & \cdots & \boldsymbol{Z}_{(L-R),\rho} \end{bmatrix} \tag{135}$$

where $\boldsymbol{Y}_k^1$, and $\boldsymbol{Z}_{(l),k}$ are $R \times l_k$, and $l \times l_k$ matrices respectively whose entries are defined by

$$\begin{aligned} \{\boldsymbol{Y}_k^1\}_{i,j} &= (-1)^{j-1}\mathcal{I}_1(i, j-1, 1, \gamma_{<k>}, s), & (136) \\ \left\{\boldsymbol{Z}_{(l),k}\right\}_{i,j} &= (-1)^{(j-1)}(i-j+1)_{(j-1)}(-\gamma_{<k>})^{(j-i)}, & (137) \end{aligned}$$

$$\mathcal{I}_1(a,b,c,d,s) = \int_0^\infty \frac{(y+1)^a \ y^b}{(y+1-\Gamma_D s)^c} \ \exp(-y/d)dy$$
$$= \sum_{k=0}^{a} \begin{pmatrix} a \\ k \end{pmatrix} \mathcal{I}_2(b+k,c,d,s), \tag{138}$$

for non-negative integer a with

$$\mathcal{I}_2(a,b,c,s) = \int_0^\infty \frac{y^a}{(y+1-P_D s)^b} \exp(-y/c)dy \tag{139}$$
$$= \Gamma(a+1) \ (1-\Gamma_D s)^{a-b+1} \ \Phi(a+1,a-b+2;(1-\Gamma_D s)/c) \tag{140}$$

where $\Phi(\cdot)$ is a confluent hypergeometric function defined as [60, eq. 9.210.2], and [60, eq. 9.211.4] is applied for (140).

5.5.2 Average output SINR

The moments of output SINR of OC are easily derived from MGF. The formula on the derivative of determinant is used [75]

$$\frac{d^k}{ds^k} \det\left[\Delta\left(s\right)\right] = \sum_{\boldsymbol{\mu}\in\mathcal{A}} \frac{(k)!}{\mu_1!\mu_2!\cdots\mu_m!} \det\left[\Psi_{\boldsymbol{\mu}}\left(s\right)\right] \tag{141}$$

where $\mathcal{A} = \{(\mu_1,\mu_2,\cdots,\mu_m)|\ \mu_i\text{'s are integers satisfying } \sum_{i=1}^m \mu_i = k\}$ and $\Psi_{\boldsymbol{\mu}}(s)$ is an $m\times m$ matrix function whose entries are given by $\{\Psi_{\boldsymbol{\mu}}(s)\}_{i,j} = \{\Delta(s)\}_{i,j}^{(\mu_i)}$. For the derivative of matrix, the identity, $I^{(k)}(a,b,c,d,s) = (c)_k(\Gamma_D)^k I\left(a,b+k,c,s\right)$, is used.

The kth moment of output SINR of OC is for the overload case is

$$M_{OC}^k = \left.\frac{d^k}{ds^k}\Phi_\gamma^{\text{OC}}\left(s\right)\right|_{s=0}, \tag{142}$$
$$= \frac{K_1\left(R,L,\boldsymbol{\Gamma}_{\mathbf{I}}\right)}{\det\left[\begin{array}{cccc} \boldsymbol{Z}_{(L),1} & \boldsymbol{Z}_{(L),2} & \cdots & \boldsymbol{Z}_{(L),\rho}\end{array}\right]} \sum_{\boldsymbol{\mu}\in\mathcal{A}} \frac{(k)!}{\mu_1!\mu_2!\cdots\mu_m!} \det\left[\Psi_{\boldsymbol{\mu}_1}\left(0\right)\right] \tag{143}$$

and the kth moment of output SINR of OC for the underload case is

$$
\begin{aligned}
M_{OC}^{k} \;=\; & \frac{K_2\left(L, R, \mathbf{\Gamma_I}\right)}{\det\begin{bmatrix} \boldsymbol{Z}_{(L),1} & \boldsymbol{Z}_{(L),2} & \cdots & \boldsymbol{Z}_{(L),\rho} \end{bmatrix}} \\
& \cdot \left\{ \sum_{p=0}^{k} \binom{k}{p} \left(\Gamma_d\right)^p (R-L)_p \sum_{\boldsymbol{\mu}\in\mathcal{A}} \frac{(k-p)!}{\mu_1!\mu_2!\cdots\mu_m!} \det\left[\Psi_{\boldsymbol{\mu}_2}(0)\right] \right\} \quad , (144)
\end{aligned}
$$

where $\{\Psi_{\boldsymbol{\mu}_1}(s)\}_{i,j} = \{\Delta_1(s)\}_{i,j}^{(\mu_i)}$, and $\{\Psi_{\boldsymbol{\mu}_2}(s)\}_{i,j} = \{\Delta_2(s)\}_{i,j}^{(\mu_i)}$.

Especially, the first moment of output SINR of OC is easily derived using (123). The average output SINR of OC, the first moment of output SINR of OC, for overload case is

$$
M_{OC}^{1} = \frac{K_1\left(R, L, \mathbf{P_I}\right)}{\det\begin{bmatrix} \boldsymbol{Z}_{(L),1} & \boldsymbol{Z}_{(L),2} & \cdots & \boldsymbol{Z}_{(L),\rho} \end{bmatrix}} \det\left(\Delta_1(s)\right) \operatorname{tr}\left(\Delta_1^{-1}(s)\tilde{\Delta}_1(s)\right)\Bigg|_{s=0} \quad (145)
$$

where $\tilde{\Delta}_1(s)$ is an $L \times L$ matrix function of s given by

$$
\tilde{\Delta}_1(s) = \begin{bmatrix} \widetilde{\boldsymbol{Y}}_1^1 & \widetilde{\boldsymbol{Y}}_2^1 & \cdots & \widetilde{\boldsymbol{Y}}_\rho^1 \\ & \mathbf{0}_{(L-R),L} & & \end{bmatrix}, \tag{146}
$$

where $\mathbf{0}_{(L-R),L}$ is $(L-R) \times L$ null matrix, and $\widetilde{\boldsymbol{Y}}_k^1$ is $R \times l_k$ matrix whose entries are defined by

$$
\{\widetilde{\boldsymbol{Y}}_k^1\}_{i,j} = (-1)^{j-1}\,\Gamma_D\,\mathcal{I}_1(i, j-1, 2, \gamma_{<k>}, s). \tag{147}
$$

5.5.3 Pdf and Outage Probability Approximation

Although the exact distribution is derived, it is worth considering the approximation of pdf and cdf using MGF. To investigate the statistical properties of the maximum SINR for the OC, such as pdf $f_\gamma(\gamma)$ and outage probability $P_{\text{out}}(\gamma_0)$, we need to evaluate the inverse Laplace transform of the MGF, i.e.,

$$
f_\gamma(\gamma) = \frac{1}{2\pi i}\int_{c-i\infty}^{c+i\infty} \Phi_\gamma(s)e^{-\gamma s}ds, \tag{148}
$$

and

$$P_{\text{out}}(\gamma_0) = \Pr\left[\gamma_s < \gamma_0\right] = \frac{1}{2\pi i} \int_{c-i\infty}^{c+i\infty} \Phi_\gamma(s) e^{-\gamma_0 s} \frac{ds}{s}. \tag{149}$$

Usually, the inverse Laplace transforms is hard to derive as a closed-form expression. Instead of deriving a closed-form solution, we may use numerical integrations. However, it sometimes requires even more computational time than Monte Carlo simulations for a large m. To solve this problem, there have been proposed approximations and numerical algorithms for the inverse Laplace transform [83]. We only considers the Gaver-Wynn-Rho (GWR) algorithm as the simple and efficient techniques for evaluating the inverse Laplace transform.

As a numerical algorithm for inverse Laplace transform, Euler summation technique with Bromwich inversion integral has been used for evaluating the outage probabilities of MRC and equal-gain combiner without co-channel interference in the generalized fading channels [84]. Although this algorithm is a simple and accurate technique for the inverse Laplace transform of the MGF, several free parameters must be adjusted for determining the accuracy of the numerical evaluation. As an efficient solution for the inherent problem of a number of free parameters, Valkó and Abate have recently proposed the GWR algorithm, which contains only one free parameter ν [85, 86]. In GWR algorithm, the Gaver functional can be defined as [87]

$$g_k(\gamma) = \frac{k \ln 2}{\gamma} \binom{2k}{k} \sum_{j=0}^{k} (-1)^k \binom{k}{j} \Phi\left(-\frac{(k+j)\ln 2}{\gamma}\right) \tag{150}$$

where $\Phi(s) = \Phi_{\gamma_s}(s)$ for pdf and $\Phi(s)\Phi_{\gamma_s}(s)/s$ for outage probability. The Gaver functional itself provides a simple approximation for inverse Laplace transform as $k \to \infty$. However, the convergence is too slow to obtain the accurate evaluation, e.g, $g_k(\gamma)$ with $k = 1000$ provides only 2 or 3 digits of accuracy [85]. To overcome the convergence problem of the Gaver functional, Valkó and Abate have investigated the convergence acceleration algorithms and found the Wynn-Rho algorithm as the best acceleration scheme for the Gaver functionals, which is given by the recursive formula [86]

$$\rho_{n,-1}(\gamma) = 0, \quad \rho_{n,0}(\gamma) = g_n(\gamma), \tag{151}$$

and

$$\rho_{n,k}(\gamma) = \rho_{n+1,k-2}(\gamma) + \frac{k}{\rho_{n+1,k-1}(\gamma) - \rho_{n,k-1}(\gamma)}, \tag{152}$$

for $n \geq 0$ and $k \geq 1$. Using the ν consecutive Gaver functionals $g_1(\gamma), g_2(\gamma), \cdots, g_\nu(\gamma)$, where ν is even integer, we finally obtain $\rho_{0,\nu}(\gamma)$ as the approximate pdf or outage probability for the OC. Since the relative error estimate for the GWR algorithm is approximately $10^{-0.8\nu}$ [85], the number of significant digits in $\rho_{0,\nu}(\gamma)$ is about equal to ν. Therefore, we can easily handle the accuracy of the numerical inverse Laplace transform of the MGF by only adjusting one free parameter ν.

5.5.4 SERs of various M-ary Modulation Schemes

With the MGF derived in the last section, we can evaluate various modulation schemes. From the MGF-based approach for evaluating the error probability in [63], the average SER's for various M-ary modulation schemes with OC are

$$P_S^{MPSK} = \Upsilon\left(\pi - \frac{\pi}{M}; -\frac{g_{MPSK}}{\sin^2\theta}\right), \tag{153}$$

$$P_S^{MQAM} = 4q_{MQAM}\Upsilon\left(\pi - \frac{\pi}{2}; -\frac{g_{MQAM}}{\sin^2\theta}\right) - 4q_{MQAM}^2\Upsilon\left(\pi - \frac{\pi}{4}; -\frac{g_{MQAM}}{\sin^2\theta}\right),$$

$$P_S^{BFSK} = \Upsilon\left(\pi - \frac{\pi}{2}; -\frac{g_{BFSK}}{\sin^2\theta}\right), \tag{154}$$

and

$$P_S^{MDPSK} = \Upsilon\left(\pi - \frac{\pi}{M}; -\frac{g_{MDPSK}}{1+\cos(\pi/M)\sin\theta}\right), \tag{155}$$

where $P_S^{MPSK}, P_S^{MQAM}, P_S^{BFSK}, P_S^{MDPSK}$ are the average SER of MPSK, MQAM, BFSK, and MDPSK respectively, $\Upsilon(\alpha; h(\theta)) = 1/\pi \int_0^\alpha \Phi_\gamma(h(\theta))d\theta$, $g_{MPSK} = g_{MDPSK} = \sin^2(\pi/M)$, $g_{MQAM} = 3/(2(M-1))$, $q_{MQAM} = 1 - 1/\sqrt{M}$, $g_{BFSK} = 1/2$ for coherent orthogonal BFSK, and g_{BFSK} for coherent BFSK with minimum correlation.

5.6 Numerical Examples

This section presents some numerical results to illustrate the performance of OC in the presence of equal and unequal-power interferers and thermal noise. The performance of OC is compared with MRC or MRT as a reference. The input SINR is defined as $\Gamma_D/(1+\sum_{i=1}^{L}\Gamma_i)$.

Figure 13 and Fig. 14 show the performance of (3,2,4) and (2,3,4) MIMO-OC systems with $\Gamma_D = 1, \Gamma_1 = 0.9, \Gamma_2 = 0.9, \Gamma_3 = 0.7$, and $\Gamma_4 = 0.5$, respectively. The accuracy of the analytical results derived in section IV are verified by comparing with Monte Carlo simulation results.

We consider effects of the number of antennas at both transmitter and receiver on the outage probability of MIMO-OC systems. Figure 15 and Fig. 16 show the outage probability versus output SINR for (T,2,5) and (2,R,5) MIMO-OC systems with $\Gamma_D = 1, \Gamma_1 = 0.9, \Gamma_2 = 0.7, \Gamma_3 = 0.5, \Gamma_4 = 0.3$, and $\Gamma_5 = 0.1$, respectively. As expected, we observe that outage probability improves as the number of transmit or receive antennas increases. In particular, it is shown that increasing the number of receive antennas gives lower outage probability for MIMO-OC system than increasing the number of transmit antennas.

To investigate the effect of various combinations of antenna pairs on the performance of MIMO-OC systems in detail, Fig. 17 shows the outage probability versus output SINR for MIMO-OC systems with $L = 5$, $\Gamma_D = 1, \Gamma_1 = 0.9, \Gamma_2 = 0.7, \Gamma_3 =$

$0.5, \Gamma_4 = 0.3$, and $\Gamma_5 = 0.1$ when the total number of transmit and receive antennas is fixed. It is interesting to note that (2,4,5) MIMO-OC systems outperform (3,3,5) MIMO-OC systems slightly in the sense of outage probability, whereas (2,2,5) MIMO-OC systems outperform (1,3,5) MIMO-OC systems. This trends are different from the previous results for MIMO-OC systems, i.e., the evenly distributed antenna configuration provides minimum outage probability for fixed number of total transmit and receive antennas in the interference-limited environment [71]. It is because the receive antennas play more important roles than the transmit antennas to null the interference efficiently, even if the number of receive antennas is equal to the number of transmit antennas.

The effects of interfering power distribution on MIMO-OC performance are shown in Fig. 18. Figure 18 shows the outage probability versus output SINR for (4,4,5) MIMO-OC system with $\Gamma_D = 1$. We observe that the MIMO-OC system with unequal-power interferers has better performance than that with equal-power interferers. This is consistent with the results on the the performance of OC with a single transmit antenna.

Figure 19 shows the average SER of MPSK for (2,R,4) MIMO-OC system versus input SINR in the presence of unequal-power interferers with $M = 4$, $\Gamma_1 = 0.9, \Gamma_2 = 0.7, \Gamma_3 = 0.3$, and $\Gamma_4 = 0.1$. We can see that there is a good agreement between the theoretical analysis in (132) with simulation results. As expected, the performance of MIMO-OC improves as the number of antennas increases. The slope of the SER, which is understood as the diversity order, becomes steeper as the number of antennas increases: the diversity order increases. It is also shown that the use of OC in MIMO adaptive antenna system considerably improves the system performance. For example, the MIMO-OC provides output SINR gain over 1.5 dB at 0.1% SER for QPSK systems between OC and MRT when $T = 2$ and $R = 4$.

Though the number of interferers is assumed to be equal or greater than the

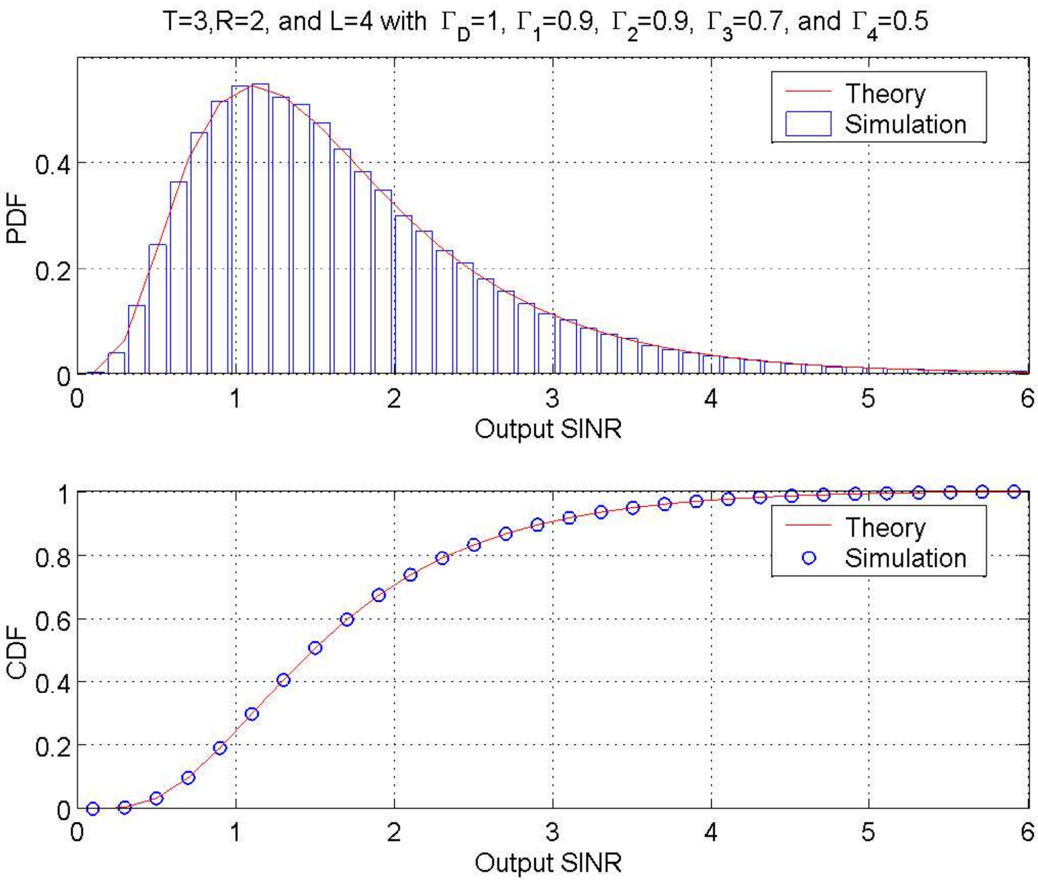

Figure 13: Comparison between the analytical results of pdf and cdf of SINR of MIMO-OC and Monte Carlo simulations when $T = 3$ and $R = 2$ L=4 with $\Gamma_D = 1, \Gamma_1 = 0.9, \Gamma_2 = 0.9, \Gamma_3 = 0.7$, and $\Gamma_4 = 0.5$

number of receive antennas in the previous sections, all the analytical results can be extended to the case in which the number of receive antennas is equal or greater than the number of interferers by assigning very small power to virtual interferers. For example, for (2,5,4) MIMO systems, we assign a virtual interferer with insignificant power such as $\Gamma_5 = -20$ dB and apply the analysis for (2,5,5) MIMO systems. The analytical results and simulation results for (2,5,4) MIMO systems is also included in Fig. 19. We can see that there is a good agreement between the theoretical analysis with simulation results.

Figure 20 and Fig. 21 show characteristics of average output SINR of SIMO-OC. The average output SINR is an important factor to determine the system performance,

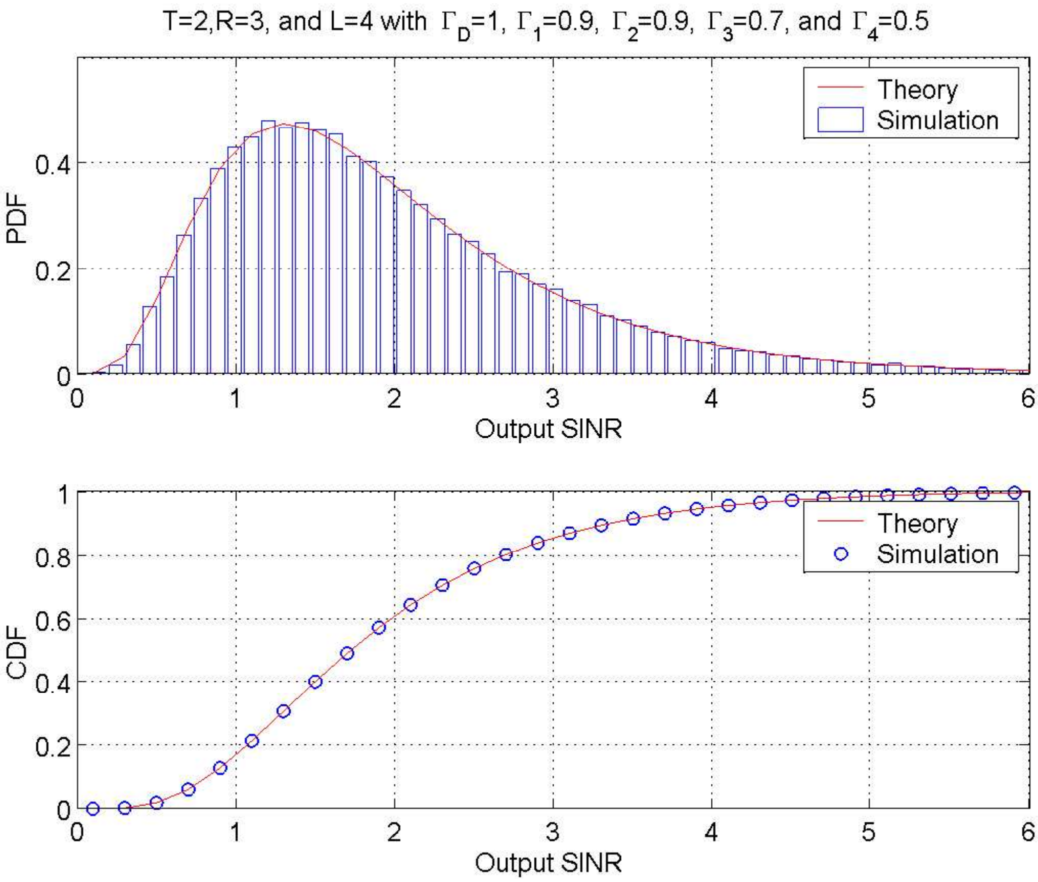

Figure 14: Comparison between the analytical results of pdf and cdf of SINR of MIMO-OC and Monte Carlo simulations when $T = 2$ and $R = 3$ L=4 with $\Gamma_D = 1, \Gamma_1 = 0.9, \Gamma_2 = 0.9, \Gamma_3 = 0.7$, and $\Gamma_4 = 0.5$

which indicates the average performance improvement in general. Although it is well known that the diversity order of OC and MRC is the same, there is a significant difference in the performance of average SINR. Figure 20 shows the performance of average SINR of OC and MRC when $R = 4$ and $L = 5$ with different power profiles of interference. It shows that average SINR of OC is the function of the power profile of interference, while MRC is not. It is observed that the equal power profile of interference is the worst case. OC significantly outperforms MRC for all the cases. Simulation results for equal and unequal power interferers are in good agreement with the theoretical analysis. Figure 21 shows the performance trend of the average SINR against the number of receive antennas with 5 interferes of

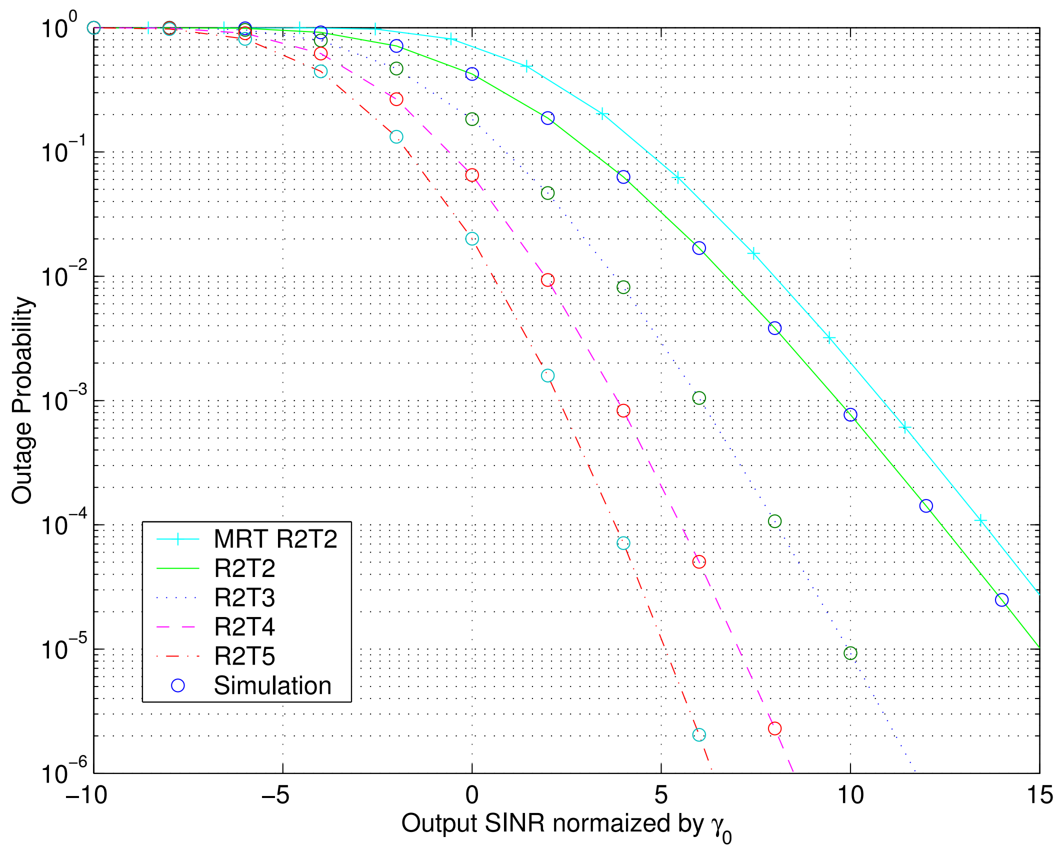

Figure 15: Outage probability varing number of transmit antennas when $R = 2$ and L=5 with $\Gamma_D = 1, \Gamma_1 = 0.9, \Gamma_2 = 0.7, \Gamma_3 = 0.5, \Gamma_4 = 0.3$, and $\Gamma_5 = 0.1$

$\Gamma_1 = 0.9, \Gamma_2 = 0.7, \Gamma_3 = 0.5, \Gamma_4 = 0.3$, and $\Gamma_5 = 0.1$. We see that the performance difference between OC and MRC is significant, and it increases as the number of receive antennas increases.

Finally, we can see that all simulation results are in good agreement with the theoretical analysis given in the previous section.

5.7 Conclusion

This chapter presented an analytical framework for OC in the presence of co-channel interference and thermal noise on a flat Rayleigh fading channel. We develop some new results in the joint eigenvalue distributions in quadratic forms of Gaussian matrices, which can be used for the analysis on OC with arbitrary power interferers

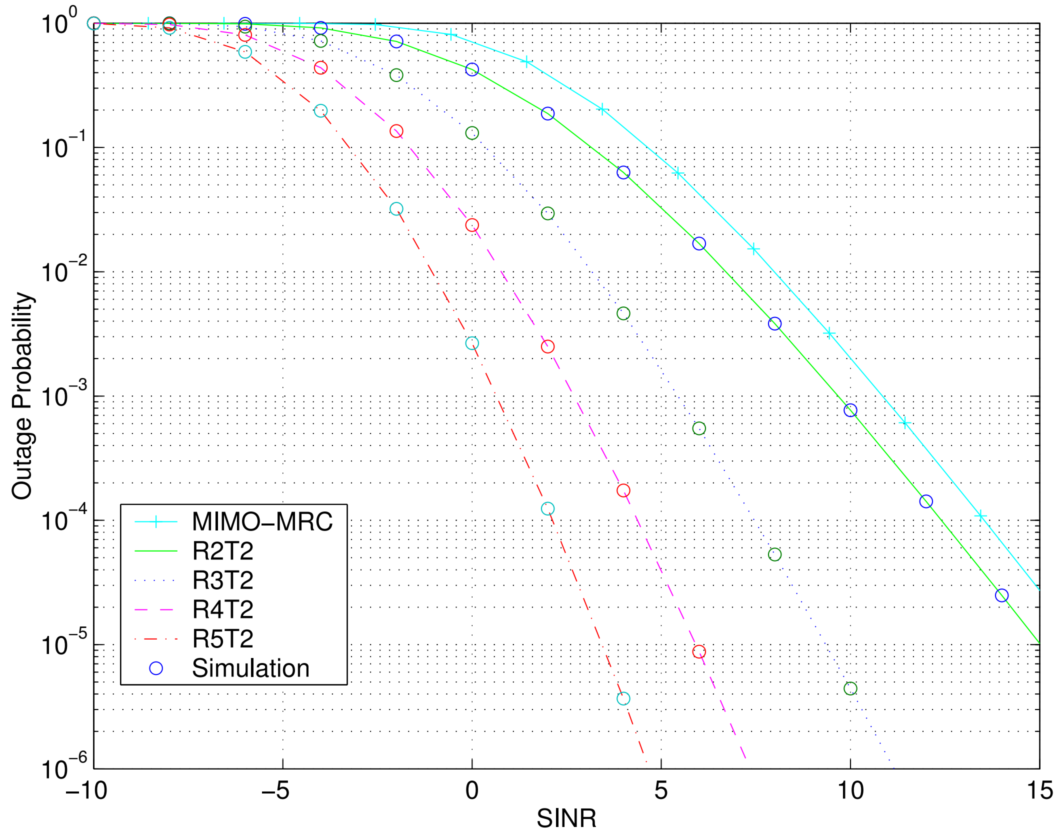

Figure 16: Outage probability varing number of receve antennas when $T = 2$ and L=5 with $\Gamma_D = 1, \Gamma_1 = 0.9, \Gamma_2 = 0.7, \Gamma_3 = 0.5, \Gamma_4 = 0.3$, and $\Gamma_5 = 0.1$

and thermal noise. Based on the joint eigenvalue distributions, we derived a closed-form expression for the distributions of output SINR of MIMO-OC, and we also derived a closed-form formula for the MGF of the output SINR of SIMO-OC. We also investigated the average output SINR, outage probability, and the SER of M-ary modulation schemes. From the numerical examples, we verified the accuracy of our analytical results. This theoretical approach gives a simple and accurate way to assess the performance of MIMO adaptive antenna systems.

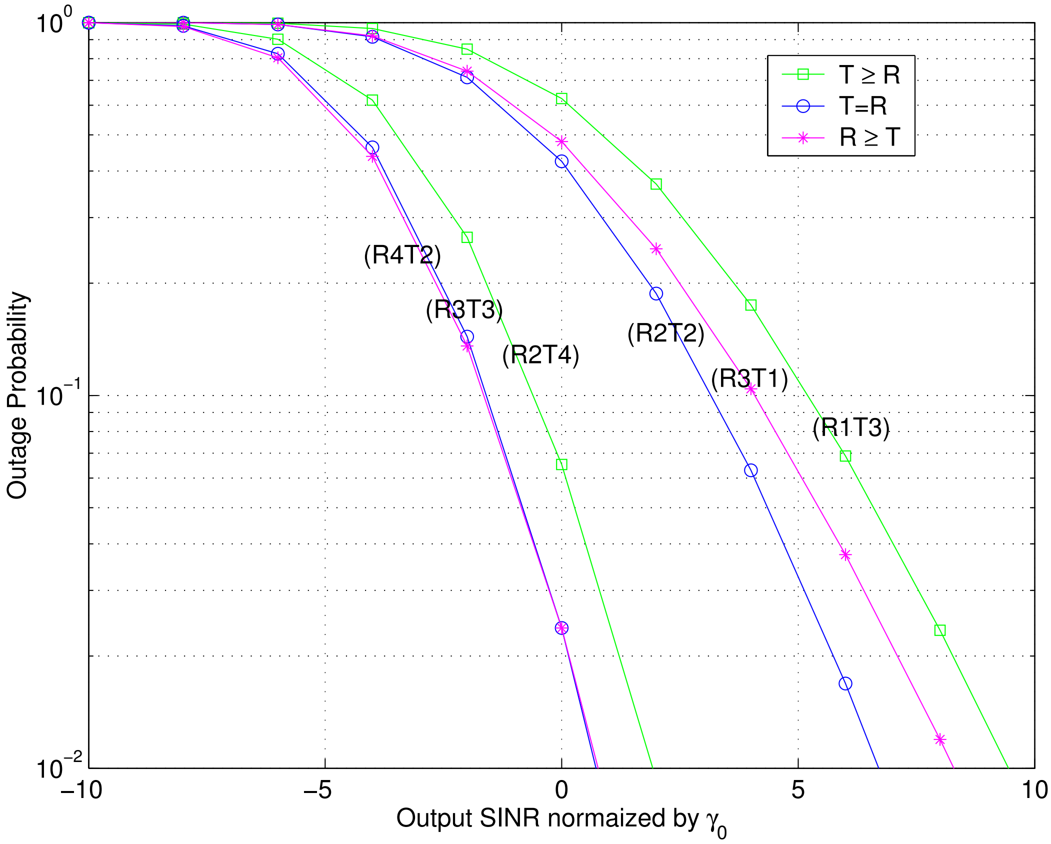

Figure 17: Comparison of outage probability with different pairs of transmit and receive antennas with fixed number of total antennas when L=5 with $\Gamma_D = 1, \Gamma_1 = 0.9, \Gamma_2 = 0.7, \Gamma_3 = 0.5, \Gamma_4 = 0.3$, and $\Gamma_5 = 0.1$

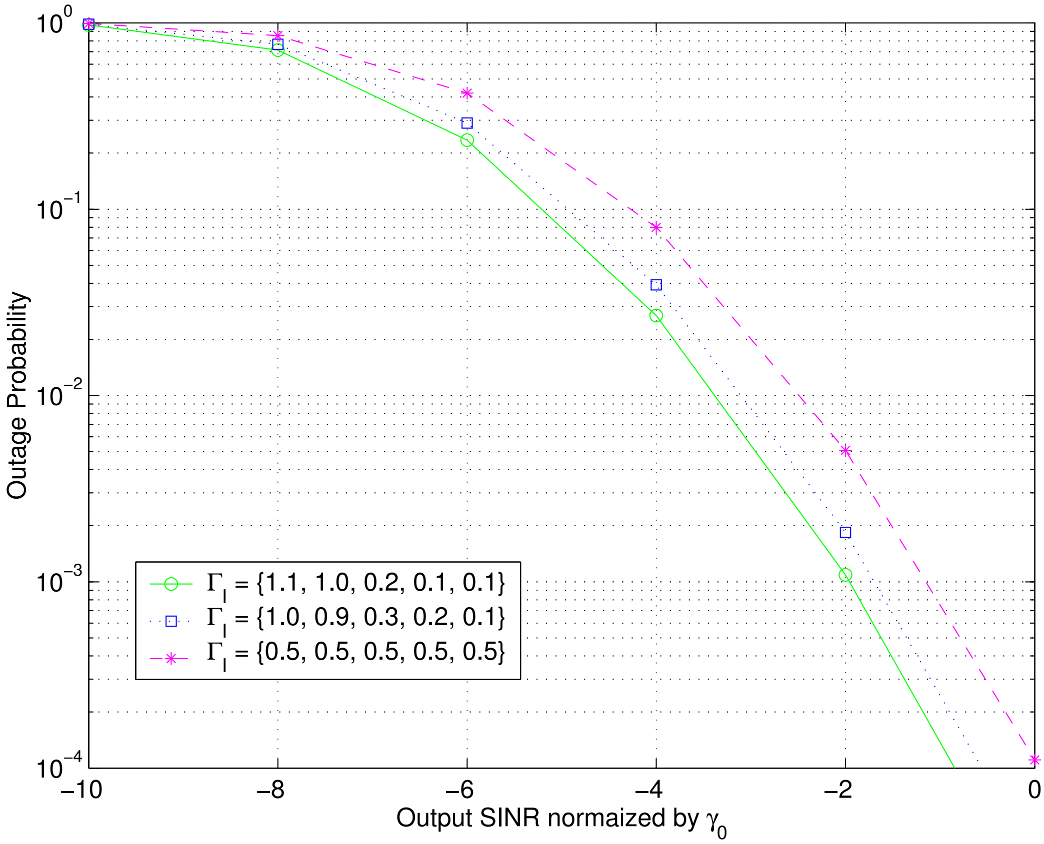

Figure 18: The trend of outage probability with different profiles of interference when $R = 4, T = 4$, and L=5 with $\Gamma_D = 1$

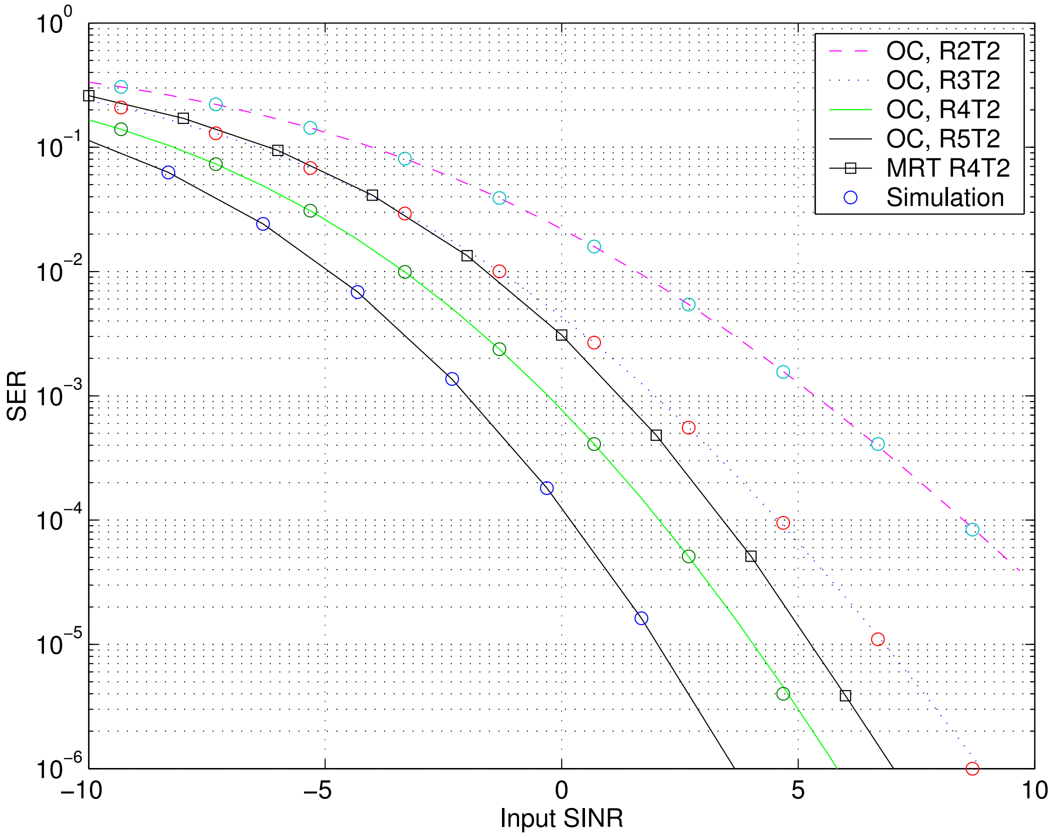

Figure 19: Comparison between the analitical results of SER for QPSK systems and Monte Carlo simulations with varying number of transmit antennas when L=4 with $\Gamma_1 = 0.9\Gamma_2 = 0.7, \Gamma_3 = 0.5$, and $\Gamma_4 = 0.3$

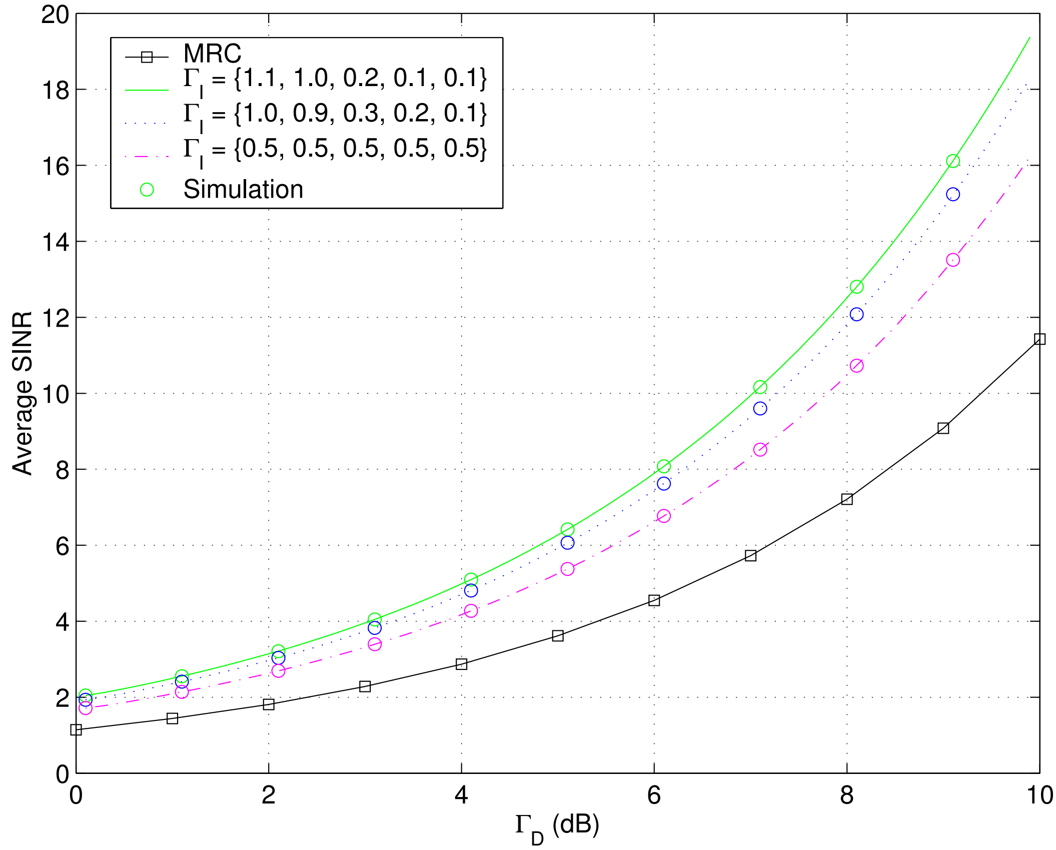

Figure 20: Average SINR of OC with different profiles of interference when $R = 4$ and L=5

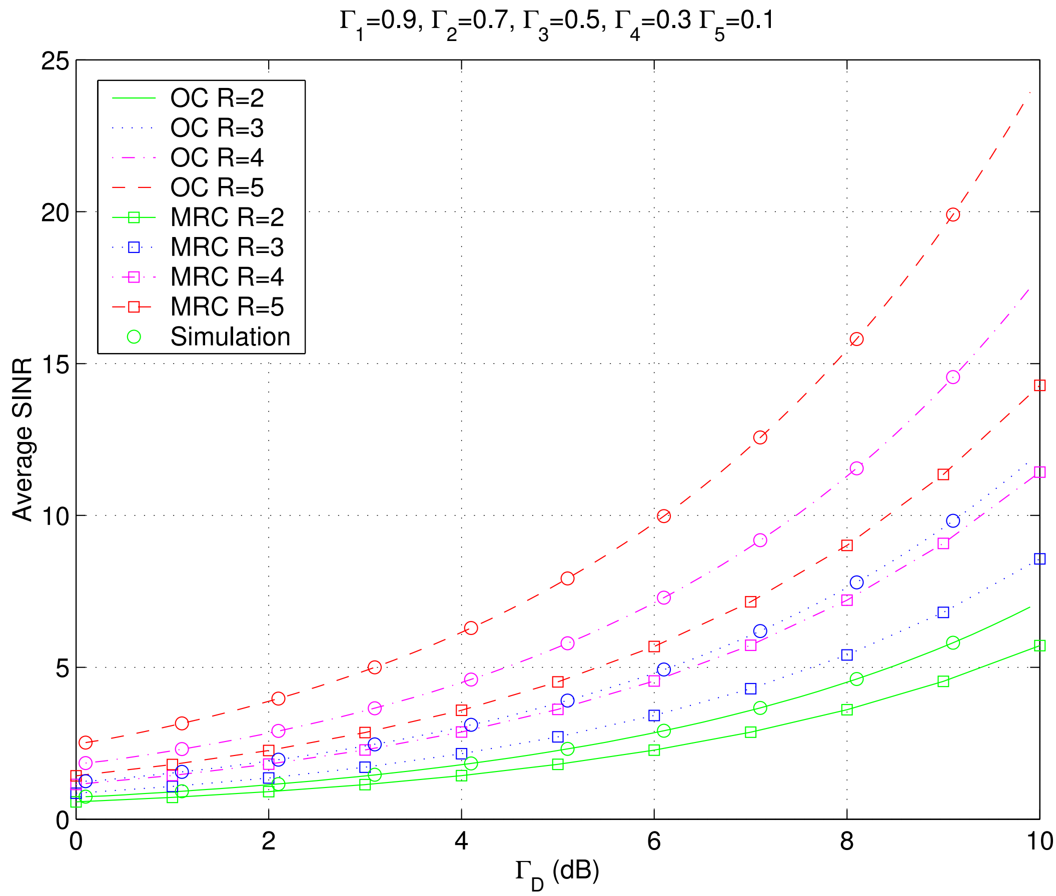

Figure 21: Average SINR of OC and MRC with various number of receive antennas when L=5 with $\Gamma_1 = 0.9, \Gamma_2 = 0.7, \Gamma_3 = 0.5, \Gamma_4 = 0.3$, and $\Gamma_5 = 0.1$

CHAPTER VI

EFFECTS OF SPATIAL CORRELATION ON MIMO SYSTEMS

6.1 Overview

In this chapter, we investigate the effects of the spatial fading correlation on the performance of MIMO adaptive antenna systems with OC in the presence of multiple co-channel interferers over a Rayleigh fading channel. Based on the Khatri's distribution functions of quadratic forms in complex Gaussian random matrices, we develop the determinant representations of those joint eigenvalue distributions. Then, closed-form formulas for the probability density function and outage probability of the maximum output signal-to-interference ratio are derived for the MIMO-OC system with the spatial correlation among the antenna elements at the transmitter or receiver. From numerical examples, we show that a new theoretical approach gives a simple and accurate way to assess the performance of the MIMO-OC system over arbitrarily correlated fading channels.

The rest of this chapter is organized as follows. Section 6.2 shows some lemmas on the random matrices and matrix functions. We briefly consider the system model in Section 6.3. Section 6.4 presents the closed-form expressions of the exact outage probability and pdf of maximum SIR when the spatial correlation exists at the transmitter or receiver. In Section 6.5, we show some numerical examples to confirm our analysis by comparing with simulation results and to investigate the effects of the antenna correlation on the performance of MIMO-OC systems. Finally, the main results of the chapter are summarized in Section 6.6.

6.2 Lemmas on Random Matrices and Matrix Functions

We briefly review some density functions of a quadratic forms in complex Gaussian random matrices to analyze the statistical properties of MIMO-OC systems with spatial fading correlation.

LEMMA 1 (Khatri's Density Functions) *Let* $\mathbf{X} \sim \tilde{N}_{p,m}(\mathbf{0}, \mathbf{\Sigma}, \mathbf{\Psi})$ *and* $\mathbf{Y} \sim \tilde{N}_{p,n}(\mathbf{0}, \mathbf{\Sigma}_1, \mathbf{I}_n)$ *be independent, where* $\mathbf{\Sigma}$, $\mathbf{\Sigma}_1$, *and* $\mathbf{\Psi}$ *are Hermitian positive definite matrices. Then, the density function of* $\mathbf{Z}_0 = \mathbf{X}^H(\mathbf{Y}\mathbf{Y}^H)^{-1}\mathbf{X}$ *for* $m \le p \le n$ *is given by*

$$f_{\mathbf{Z}_0}(\mathbf{Z}_0) = \frac{\tilde{\Gamma}_p(m+n)}{\tilde{\Gamma}_p(n)\tilde{\Gamma}_m(p)} (\det \mathbf{\Psi})^{-p} (\det \mathbf{\Omega})^{-m} (\det \mathbf{Z}_0)^{p-m} \left(\det\left(\mathbf{I}_m + (q\mathbf{\Psi})^{-1}\mathbf{Z}_0\right)\right)^{-m-n} \times {}_1\tilde{F}_0^{(p)}\left(m+n; \mathbf{I}_p - q\mathbf{\Omega}^{-1}, \mathbf{Z}_0\left(q\mathbf{\Psi} + \mathbf{Z}_0\right)^{-1}\right) \tag{156}$$

and the density function of $\mathbf{Z}_1 = (\mathbf{Y}\mathbf{Y}^H)^{-1/2}(\mathbf{X}\mathbf{X}^H)(\mathbf{Y}\mathbf{Y}^H)^{-1/2}$ *for* $m \ge p$ *and* $n \ge p$ *is given by*

$$f_{\mathbf{Z}_1}(\mathbf{Z}_1) = \frac{\tilde{\Gamma}_p(m+n)}{\tilde{\Gamma}_p(m)\tilde{\Gamma}_p(n)} (\det \mathbf{\Omega})^{-m} (\det \mathbf{\Psi})^{-p} (\det \mathbf{Z}_1)^{m-p} \left(\det\left(\mathbf{I}_p + (q\mathbf{\Omega})^{-1}\mathbf{Z}_1\right)\right)^{-m-n} \times {}_1\tilde{F}_0^{(m)}\left(m+n; \mathbf{I}_m - q\mathbf{\Psi}^{-1}, \mathbf{Z}_1\left(q\mathbf{\Omega} + \mathbf{Z}_1\right)^{-1}\right) \tag{157}$$

where $q > 0$ *is an arbitrary constant,* $\mathbf{\Omega} = \mathbf{\Sigma}^{1/2}\mathbf{\Sigma}_1^{-1}\mathbf{\Sigma}^{1/2}$, $\tilde{\Gamma}_m(n) = \pi^{m(m-1)/2}\prod_{k=1}^{m}\Gamma(n-k+1)$ *is the complex multivariate gamma function, and* ${}_1\tilde{F}_0^{(p)}(\cdot)$ *denotes the complex hypergeometric function with matrix arguments* [58, eq. (2b)].

Proof. See [58, sec. 5]. $\square$

LEMMA 2 *The alternative distribution functions of (156) and (157) are given by*

$$f_{\mathbf{Z}_0}(\mathbf{Z}_0) = \frac{\tilde{\Gamma}_p(m+n)}{\tilde{\Gamma}_p(n)\tilde{\Gamma}_m(p)} (\det \mathbf{\Psi})^{-p} (\det \mathbf{\Omega})^{-m} (\det \mathbf{Z}_0)^{p-m} {}_1\tilde{F}_0^{(p)} \left(m+n; -\mathbf{\Omega}^{-1}, \mathbf{Z}_0 \mathbf{\Psi}^{-1}\right) \tag{158}$$

and

$$\begin{aligned} f_{\mathbf{Z}_1}(\mathbf{Z}_1) &= \frac{\tilde{\Gamma}_m(m+n)}{\tilde{\Gamma}_p(m)\tilde{\Gamma}_m(m+n-p)} (\det \mathbf{\Psi})^{-p} (\det \mathbf{\Omega})^{-m} (\det \mathbf{Z}_1)^{m-p} \\ &\quad \cdot {}_1\tilde{F}_0^{(m)} \left(m+n; -\mathbf{\Psi}^{-1}, \mathbf{Z}_1 \mathbf{\Omega}^{-1}\right). \end{aligned} \tag{159}$$

Proof. . Taking the limit $q \to \infty$ in (156), we simplify the density function of $\mathbf{Z}_0$

$$\begin{aligned} f_{\mathbf{Z}_0}(\mathbf{Z}_0) =& \frac{\tilde{\Gamma}_p(m+n)}{\tilde{\Gamma}_p(n)\tilde{\Gamma}_m(p)} (\det \mathbf{\Psi})^{-p} (\det \mathbf{\Omega})^{-m} (\det \mathbf{Z}_0)^{p-m} \\ & \times \lim_{q\to\infty} \left(\det\left(\mathbf{I}_m + \frac{1}{q}\mathbf{\Psi}^{-1}\mathbf{Z}_0\right)\right)^{-m-n} {}_1\tilde{F}_0^{(p)} \left(m+n; \frac{1}{q}\mathbf{I}_p - \mathbf{\Omega}^{-1}, \mathbf{Z}_0\left(\mathbf{\Psi} + \frac{1}{q}\mathbf{Z}_0\right)^{-1}\right) \\ =& \frac{\tilde{\Gamma}_p(m+n)}{\tilde{\Gamma}_p(n)\tilde{\Gamma}_m(p)} (\det \mathbf{\Psi})^{-p} (\det \mathbf{\Omega})^{-m} (\det \mathbf{Z}_0)^{p-m} {}_1\tilde{F}_0^{(p)} \left(m+n; -\mathbf{\Omega}^{-1}, \mathbf{Z}_0 \mathbf{\Psi}^{-1}\right). \end{aligned} \tag{160}$$

In (157), taking the limit $q \to \infty$ and using the identity

$$\begin{aligned} \frac{\tilde{\Gamma}_p(m+n)}{\tilde{\Gamma}_p(n)} &= \frac{\pi^{m(m-1)/2} \prod_{k=1}^{m} \Gamma(m+n-k+1)}{\pi^{m(m-1)/2} \prod_{k=1}^{p} \Gamma(n-k+1) \prod_{k=p+1}^{m} \Gamma(m+n-k+1)} \\ &= \frac{\tilde{\Gamma}_m(m+n)}{\tilde{\Gamma}_m(m+n-p)} \end{aligned} \tag{161}$$

yield the density function of $\mathbf{Z}_1$. $\square$ $\square$

6.3 MIMO-OC System Model

As seen in the previous chapter,the received signal vector into matrix form is

$$\mathbf{r} = \sqrt{P_D}\mathbf{H}_D\mathbf{w}_T s_D + \mathbf{H}_I\mathbf{P}_I^{1/2}\mathbf{s}_I + \mathbf{n} \tag{162}$$

where $\mathbf{P}_I = \mathrm{diag}\{P_1, P_2, \cdots, P_L\}$ and $\mathbf{s}_I = (s_1, s_2, \cdots, s_L)^T$.

To maximize the output SINR at the receiver, the optimum weighting vector for a given $\mathbf{w}_T$ at the receiver is given by

$$\mathbf{w}_R = \alpha\mathbf{R}^{-1}\mathbf{H}_D\mathbf{w}_T \tag{163}$$

where $\mathbf{R} = \mathbf{H}_I\mathbf{P}_I\mathbf{H}_I^H + \sigma^2\mathbf{I}_R$ and the arbitrary non-zero constant α does not affect the output SINR. Then, the maximum output SINR per symbol is given by

$$\gamma_s = P_D\mathbf{w}_T^H\mathbf{H}_D^H\mathbf{R}^{-1}\mathbf{H}_D\mathbf{w}_T. \tag{164}$$

For analytical tractability, the interference-limited environment has been assumed, i.e., the effect of thermal noise $\mathbf{n}$ is neglected. This assumption is reasonable when the signal-to-noise ratio (SNR) and interference-to-noise ratio (INR) are high or when the system operates in an interference-rich environment, in which the number of antenna elements at the receiver is less than or equal to the number of interferers [43, 50, 90]. In addition, to obtain useful insights for the performance bound in a worst case when the aggregate interfering power is fixed, we assume that the multiple co-channel interferers have the same average power P_I [71]. Then, the maximum output SIR for the MIMO-OC system in the interference-limited environment is rewritten as [71]

$$\gamma_s = \Gamma_0\lambda_{\max} \tag{165}$$

where $\Gamma_0 = P_D/P_I$ and $\lambda_{\max}$ is the largest eigenvaules of $\mathbf{Z} = \mathbf{H}_D^H(\mathbf{H}_I\mathbf{H}_I^H)^{-1}\mathbf{H}_D$.

6.4 Performance of MIMO-OC System with Spatial Fading Correlation

In this section, we develop a theoretical approach to analyze the performance of MIMO-OC systems with spatial correlation at the transmitter or receiver in the presence of L effective co-channel interferers. For the correlated MIMO fading channel, we assume that $\mathbf{H}_I$ is a zero-mean complex Gaussian random matrix with covariance matrix $\mathbf{\Sigma}_{R,I}$ at the receiver and $\mathbf{H}_D$ is a zero-mean complex Gaussian random matrix with covariance matrices $\mathbf{\Sigma}_T$ at the transmitter and $\mathbf{\Sigma}_{R,D}$ at the receiver.

6.4.1 Spatially correlated MIMO-OC system with $T \leq R \leq L$

First, we investigate the statistical properties of maximum output SIR for the MIMO-OC system with $T \leq R \leq L$ in the presence of a spatial fading correlation at the transmitter or receiver.

6.4.1.1 Receiver-sided correlated MIMO channels

To evaluate the SIR distribution and outage probability of the MIMO-OC system with spatial fading correlation matrices, $\mathbf{\Sigma}_{R,D}$ and $\mathbf{\Sigma}_{R,I}$, at the receiver only ($\mathbf{\Sigma}_T = \mathbf{I}_T$), it is required to determine the pdf and cdf of the largest eigenvalue of $\mathbf{Z} = \mathbf{H}_D^H(\mathbf{H}_I\mathbf{H}_I^H)^{-1}\mathbf{H}_D$. First, we derive the joint eigenvalue distribution of $\mathbf{Z}$ by using the alternative representation of the Khatri's density function of $\mathbf{Z}$ in (158).

Theorem 4. *Let $\mathbf{H}_D \sim \tilde{N}_{R,T}(\mathbf{0}, \mathbf{\Sigma}_{R,D}, \mathbf{I}_T)$ and $\mathbf{H}_I \sim \tilde{N}_{R,L}(\mathbf{0}, \mathbf{\Sigma}_{R,I}, \mathbf{I}_L)$ be independent, where $\mathbf{\Sigma}_{R,D}$ and $\mathbf{\Sigma}_{R,I}$ are $R \times R$ Hermitian positive definite matrices. If $\mathbf{\Omega}_R = \mathbf{\Sigma}_{R,D}^{1/2}\mathbf{\Sigma}_{R,I}^{-1}\mathbf{\Sigma}_{R,D}^{1/2}$ is $R \times R$ Hermitian positive definite matrix with distinct eigenvalues $\omega_1 > \omega_2 > \cdots > \omega_R$, then, the joint density function of $\mathbf{\Lambda} = diag\{\lambda_1, \lambda_2, \cdots, \lambda_T\}$ with the ordered eigenvalues $\lambda_1, \lambda_2, \cdots, \lambda_T$ of $\mathbf{Z} = \mathbf{H}_D^H(\mathbf{H}_I\mathbf{H}_I^H)^{-1}\mathbf{H}_D$ for $T \leq R \leq L$ is given by*

$$f_{\mathbf{\Lambda}}\left(\lambda_1, \lambda_2, \cdots, \lambda_T\right) = K_0\left(T, R, L, \mathbf{\Omega}_R\right) \det\left(\mathbf{V}\left(\mathbf{\Lambda}\right)\right) \det\left(\mathbf{Q}_R\left(\mathbf{\Omega}_R, \mathbf{\Lambda}\right)\right) \tag{166}$$

where $\mathbf{V}(\mathbf{X})$ *denotes the Vandermonde matrix of the ordered eigenvalues of* $\mathbf{X}$,

$$K_0\left(T, R, L, \mathbf{\Omega}_R\right) = (-1)^{\lfloor \frac{T}{2} \rfloor + \lfloor \frac{R}{2} \rfloor} \frac{\pi^{T(T-1)} \tilde{\Gamma}_R(T+L) \left(\det \mathbf{\Omega}_R\right)^{-T}}{\tilde{\Gamma}_T(T) \tilde{\Gamma}_R(L) \tilde{\Gamma}_T(R) \det\left(\mathbf{V}\left(-\mathbf{\Omega}_R^{-1}\right)\right)} \prod_{k=R-T}^{R-1} \frac{k!}{(T-R+L+1)_k}, \tag{167}$$

and

$$\left\{\mathbf{Q}_R\left(\mathbf{\Omega}_R, \mathbf{\Lambda}\right)\right\}_{i,j} = \begin{cases} \left(1 + \lambda_j/\omega_i\right)^{R-T-L-1}, & j = 1, \cdots, T, \\ \left(-\omega_i\right)^{j-R}, & j = T+1, \cdots, R. \end{cases} \tag{168}$$

Proof. By substituting $\mathbf{\Psi} = \mathbf{I}_T$ into (158) and applying the identity in [94, eq.(3.9)], the density function of ordered eigenvalues of $\mathbf{Z}$ is given by

$$\begin{aligned} f_{\mathbf{\Lambda}}\left(\lambda_1, \lambda_2, \cdots, \lambda_T\right) &= \frac{\pi^{T(T-1)}}{\tilde{\Gamma}_T\left(T\right)} \left(\det\left(\mathbf{V}\left(\Lambda\right)\right)\right)^2 \int_{U(T)} f_{\mathbf{Z}}\left(\mathbf{E}\mathbf{\Lambda}\mathbf{E}^H\right) (d\mathbf{E}) \\ &= \frac{\pi^{T(T-1)} \tilde{\Gamma}_R(T+L)}{\tilde{\Gamma}_T(R) \tilde{\Gamma}_T(T) \tilde{\Gamma}_R(L) \left(\det \mathbf{\Omega}_R\right)^T} \frac{\left(\det\left(\mathbf{V}\left(\mathbf{\Lambda}\right)\right)\right)^2}{\left(\det \mathbf{\Lambda}\right)^{T-R}} {}_1\tilde{F}_0^{(R)}\left(T+L; -\mathbf{\Omega}_R^{-1}, \mathbf{\Lambda}\right). \end{aligned} \tag{169}$$

where $\mathbf{Z} = \mathbf{E}\mathbf{\Lambda}\mathbf{E}^H$ is an eigen-decomposition and $U(T)$ is the group of all $T \times T$ complex unitary matrices $\mathbf{E}$, i.e., the unitary group [94]. Adding the $R-T$ eigenvalues $\varepsilon_1 > \varepsilon_2 > \cdots > \varepsilon_{R-T-1} > \varepsilon_{R-T} = 0$ in $\mathbf{\Lambda}$ and taking the limit $\{\varepsilon_i\} \to 0$ for $i = 1, 2, \cdots, R-T-1$, ${}_1\tilde{F}_0^{(R)}\left(T+L; -\mathbf{\Omega}_R^{-1}, \mathbf{\Lambda}\right)$ can be expressed as

$${}_1\tilde{F}_0^{(R)}\left(T+L; -{\mathbf{\Omega}_R}^{-1}, \mathbf{\Lambda}\right) = \lim_{\{\varepsilon_i\} \to 0} {}_1\tilde{F}_0^{(R)}\left(T+L; -{\mathbf{\Omega}_R}^{-1}, \hat{\mathbf{\Lambda}}\right) \tag{170}$$

where $\hat{\mathbf{\Lambda}}$ is an $R \times R$ diagonal matrix $\hat{\mathbf{\Lambda}} = diag\{\hat{\lambda}_1, \cdots, \hat{\lambda}_R\} = diag\{\lambda_1, \cdots, \lambda_T, \varepsilon_1, \cdots, \varepsilon_{R-T-1}, 0\}$. The determinant representation of the complex hypergeometric function with classical hypergeometric function ${}_1F_0(a; bx)$ is given by

$$
{}_1\tilde{F}_0^{(R)}\left(T+L;-\mathbf{\Omega}_R{}^{-1},\hat{\mathbf{\Lambda}}\right)=\prod_{k=1}^{R}\frac{\Gamma(k)}{(\alpha)_{R-k}}\frac{\det\left(\mathbf{Q}_0\left(\mathbf{\Omega}_R,\hat{\mathbf{\Lambda}}\right)\right)}{\det\left(\mathbf{V}\left(-\mathbf{\Omega}_R^{-1}\right)\right)\det\left(\mathbf{V}\left(\hat{\mathbf{\Lambda}}\right)\right)}
$$

$$
=\hat{K}_0\left(T,R,L,\mathbf{\Omega}_R\right)\frac{\det\left(\left[\mathbf{h}\left(\lambda_1\right)\ \cdots\mathbf{h}\left(\lambda_T\right)\mathbf{h}\left(\varepsilon_1\right)\ \cdots\mathbf{h}\left(\varepsilon_{R-T-1}\right)\mathbf{h}\left(0\right)\right]\right)}{\det\left(\left[\mathbf{g}\left(\lambda_1\right)\ \cdots\mathbf{g}\left(\lambda_T\right)\mathbf{g}\left(\varepsilon_1\right)\ \cdots\mathbf{g}\left(\varepsilon_{R-T-1}\right)\mathbf{g}\left(0\right)\right]\right)}
\tag{171}
$$

where $\mathbf{Q}_0(\mathbf{\Omega}_R,\hat{\mathbf{\Lambda}})$ is a $R\times R$ matrix whose entries are $\{\mathbf{Q}_0(\mathbf{\Omega}_R,\hat{\mathbf{\Lambda}})\}_{i,j}={}_1F_0(\alpha;-\hat{\lambda}_i\omega_j^{-1})$, $\alpha=T-R+L+1$, $(a)_q=a(a+1)\cdots(a+q-1)$ is the Pochhammer symbol, $\hat{K}_0(T,R,L,\mathbf{\Omega}_R)=\prod_{k=1}^{R}\Gamma(k)/\{(\alpha)_{R-k}\det\left(\mathbf{V}\left(-\mathbf{\Omega}_R^{-1}\right)\right)\}$, $\mathbf{h}(x)=[\ {}_1F_0(\alpha;-x\omega_1^{-1})\ {}_1F_0(\alpha;-x\omega_2^{-1}$ and $\mathbf{g}(x)=[1\ x\ x^2\cdots x^{R-1}]^T$. Applying the Cauchy's mean value theorem in [81] and using the k-th derivatives of ${}_1F_0(a;bx)$,

$$
\frac{d^k}{dx^k}\ {}_1F_0(a;bx)=(a)_k b^k{}_1F_0(a+k;bx),
\tag{172}
$$

${}_1\tilde{F}_0^{(R)}\left(T+L;-\mathbf{\Omega}_R{}^{-1},\mathbf{\Lambda}\right)$ becomes

$$
{}_1\tilde{F}_0^{(R)}\left(T+L;-\mathbf{\Omega}_R{}^{-1},\mathbf{\Lambda}\right)=\hat{K}_0\left(T,R,L,\mathbf{\Omega}_R\right)\frac{\det\left(\left[\mathbf{h}\left(\lambda_1\right)\ \cdots\mathbf{h}\left(\lambda_T\right)\mathbf{h}^{(R-T-1)}\left(0\right)\ \cdots\mathbf{h}^{(0)}\left(0\right)\right]\right)}{\det\left(\left[\mathbf{g}\left(\lambda_1\right)\ \cdots\mathbf{g}\left(\lambda_T\right)\mathbf{g}^{(R-T-1)}\left(0\right)\ \cdots\mathbf{g}^{(0)}\left(0\right)\right]\right)}
\tag{173}
$$

where $\mathbf{h}^{(k)}(x)$ and $\mathbf{g}^{(k)}(x)$ denote the kth derivatives of $\mathbf{h}(x)$ and $\mathbf{g}(x)$, respectively. Since the effect of interchanging operation between two rows upon the determinant is to multiply it by -1 [5], ${}_1\tilde{F}_0^{(R)}\left(T+L;-\mathbf{\Omega}_R{}^{-1},\mathbf{\Lambda}\right)$ is rewritten as

$$
{}_1\tilde{F}_0^{(R)}\left(T+L;-\mathbf{\Omega}_R^{-1},\mathbf{\Lambda}\right)=(-1)^{\lfloor\frac{T}{2}\rfloor+\lfloor\frac{R}{2}\rfloor}\prod_{k=R-T}^{R-1}\frac{k!}{(\alpha)_k}\frac{\left(\det\mathbf{\Lambda}\right)^{T-R}\det\left(\mathbf{Q}_R\left(\mathbf{\Omega}_R,\mathbf{\Lambda}\right)\right)}{\det\left(\mathbf{V}\left(-\mathbf{\Omega}_R^{-1}\right)\right)\det\left(\mathbf{V}\left(\mathbf{\Lambda}\right)\right)}.
\tag{174}
$$

Finally, substituting (174) into (169) yields the distribution (166) of the ordered eigenvalues of $\mathbf{Z}$. □

We get the cdf of largest eigenvalue $\lambda_{\max}=\lambda_1$ given by

$$F_{\lambda_{\max}}(x) = \int_D K_0(T, R, L, \mathbf{\Omega}_R) \det(\mathbf{V}(\mathbf{\Lambda})) \det(\mathbf{Q}_R(\mathbf{\Omega}_R, \mathbf{\Lambda}))(d\mathbf{\Lambda}) \tag{175}$$

where $D = \{0 \le \lambda_T \le \lambda_{T-1} \le \cdots \le \lambda_1 \le x\}$. With the help of the generalized integral version for Binet-Cauchy formula in Section II, the cdf of $\lambda_{\max}$ of $\mathbf{Z}$ is given by

$$F_{\lambda_{\max}}(x) = K_0(T, R, L, \mathbf{\Omega}_R) \det(\Delta_R(\mathbf{\Omega}_R, x)) \tag{176}$$

where $\Delta_R(\mathbf{\Omega}_R, x)$ is an $R \times R$ matrix function of x whose entries are given by

$$\{\Delta_R(\mathbf{\Omega}_R, x)\}_{i,j} = \begin{cases} \int_0^x y^{j-1}(1 + y/\omega_i)^{R-T-L-1} dy, & j = 1, \cdots, T, \\ (-\omega_i)^{j-R}, & j = T+1, \cdots, R. \end{cases} \tag{177}$$

Using the identity [60, eq. (3.194.1)], we have a single determinant expression for the outage probability of the MIMO-OC system in the interference-limited environment, which can be written as

$$P_{\text{out}}(\gamma_0) = F_{\lambda_{\max}}(\gamma_0/\Gamma_0) = K_0(T, R, L, \mathbf{\Omega}_R) \det(\Delta_R(\mathbf{\Omega}_R, \gamma_0/\Gamma_0)) \tag{178}$$

where $\Delta_R(\mathbf{\Omega}_R, x)$ is an $R \times R$ matrix function of x whose entries are given by

$$\{\Delta_R(\mathbf{\Omega}_R, x)\}_{i,j} = \begin{cases} \dfrac{x^j}{j\Gamma_0^j}\,{}_2F_1\left(T - R + L + 1, j; j+1; -\dfrac{x}{\omega_i \Gamma_0}\right), & j = 1, \cdots, T, \\ (-\omega_i)^{j-R}, & j = T+1, \cdots, R. \end{cases} \tag{179}$$

The Gauss hypergeometric function ${}_2F_1(\,\cdot\,)$ is easily evaluated by using the alternative expression in terms of the elementary functions as shown in [51].

The pdf of the maximum SIR is then obtained by taking the derivative at the outage probability with respect to γ_0. Using the formula on the derivative of determinant in [71], we derive a closed-form expression for the pdf of the maximum SIR in the MIMO-OC system in the interference-limited environment,

$$f_{\gamma_s}(\gamma) = \Gamma_0 K_0(T, R, L, \mathbf{\Omega}_R) \det\left(\Delta_R(\mathbf{\Omega}_R, \gamma/\Gamma_0)\right) \operatorname{tr}\left(\Delta_R^{-1}(\mathbf{\Omega}_R, \gamma/\Gamma_0)\, \tilde{\Delta}_R(\mathbf{\Omega}_R, \gamma/\Gamma_0)\right) \tag{180}$$

where $\tilde{\Delta}_R(\mathbf{\Omega}_R, x)$ is an $R \times R$ matrix function of x whose entries are given by

$$\left\{\tilde{\Delta}_R(\mathbf{\Omega}_R, x)\right\}_{i,j} = \begin{cases} x^{j-1}\left(1 + x/\omega_i\right)^{R-T-L-1}, & j = 1, \cdots, T, \\ 0, & j = T+1, \cdots, R. \end{cases} \tag{181}$$

6.4.1.2 Transmitter-sided correlated MIMO channels

Let us consider the MIMO-OC system with the spatial fading correlation with covariance matrix $\mathbf{\Sigma}_T$ at the transmitter for the desired user and uncorrelated fading at the receiver, i.e., $\mathbf{\Sigma}_{R,D}$=$\mathbf{\Sigma}_{R,D}$=$\mathbf{I}_R$. As shown in the previous section, we first determine the joint eigenvalue distribution of $\mathbf{Z}$ based on the density function of $\mathbf{Z}$ with $T \leq R \leq$ Ł.

Theorem 5. *Let* $\mathbf{H}_D \sim \tilde{N}_{R,T}(\mathbf{0}, \mathbf{I}_R, \mathbf{\Sigma}_T)$ *and* $\mathbf{H}_I \sim \tilde{N}_{R,L}(\mathbf{0}, \mathbf{I}_R, \mathbf{I}_L)$ *be independent, where* $\mathbf{\Sigma}_T$ *is* $T \times T$ *Hermitian positive definite matrix with distinct eigenvalues* $\sigma_1 > \sigma_2 > \cdots > \sigma_T$*, then, the joint density function of the ordered eigenvalues* $\lambda_1, \lambda_2, \cdots, \lambda_T$ *of* $\mathbf{Z} = \mathbf{H}_D^H(\mathbf{H}_I\mathbf{H}_I^H)^{-1}\mathbf{H}_D$ *with* $T \leq R \leq L$ *is given by*

$$f_{\mathbf{\Lambda}}(\lambda_1, \lambda_2, \cdots, \lambda_T) = K_1(T, R, L, \mathbf{\Sigma}_T)\left(\det \mathbf{\Lambda}\right)^{R-T} \det\left(\mathbf{V}(\mathbf{\Lambda})\right) \det\left(\mathbf{Q}_T(\mathbf{\Sigma}_T, \mathbf{\Lambda})\right) \tag{182}$$

where

$$K_1(T, R, L, \mathbf{\Sigma}_T) = \frac{\pi^{T(T-1)}\tilde{\Gamma}_R(T+L)\left(\det \mathbf{\Sigma}_T\right)^{-R}}{\tilde{\Gamma}_T(T)\tilde{\Gamma}_R(L)\tilde{\Gamma}_T(R)\det\left(\mathbf{V}\left(-\mathbf{\Sigma}_T^{-1}\right)\right)} \prod_{i=1}^{T} \frac{(i-1)!}{(L+1)_{T-i}}, \tag{183}$$

and

$$\{\mathbf{Q}_T(\mathbf{\Sigma}_T, \mathbf{\Lambda})\}_{i,j} = {}_1F_0(L+1; -\lambda_j/\sigma_i) = (1+\lambda_j/\sigma_i)^{-L-1}. \tag{184}$$

Proof. Setting $\mathbf{\Sigma} = \mathbf{\Sigma}_1 = \mathbf{I}_R$ and $\mathbf{\Psi} = \mathbf{\Sigma}_T$ in (158), we have the density function of $\mathbf{Z}$

$$\begin{aligned} f_{\mathbf{Z}}(\mathbf{Z}) &= \frac{\tilde{\Gamma}_R(T+L)}{\tilde{\Gamma}_R(L)\tilde{\Gamma}_T(R)} (\det \mathbf{\Sigma}_T)^{-R} (\det \mathbf{Z})^{R-T} \, {}_1\tilde{F}_0\left(T+L; -\mathbf{Z}\mathbf{\Sigma}_T^{-1}\right) \\ &= \frac{\tilde{\Gamma}_R(T+L)}{\tilde{\Gamma}_R(L)\tilde{\Gamma}_T(R)} (\det \mathbf{\Sigma}_T)^{-R} (\det \mathbf{Z})^{R-T} \left(\det\left(\mathbf{I}_T + \mathbf{Z}\mathbf{\Sigma}_T^{-1}\right)\right)^{-T-L} \end{aligned} \tag{185}$$

where ${}_1\tilde{F}_0(a; \mathbf{A}) = (\det(\mathbf{I}+\mathbf{A}))^{-a}$. Since $\det(\mathbf{I}_T + \mathbf{Z}\mathbf{\Sigma}_T^{-1}) = \det(\mathbf{I}_T + \mathbf{\Sigma}_T^{-1}\mathbf{Z})$, we can derive the density function of the ordered eigenvalues of $\mathbf{Z}$ as

$$\begin{aligned} f_{\mathbf{\Lambda}}(\lambda_1, \lambda_2, \cdots, \lambda_T) &= \frac{\pi^{T(T-1)}\tilde{\Gamma}_R(T+L)}{\tilde{\Gamma}_T(R)\tilde{\Gamma}_T(T)\tilde{\Gamma}_R(L)} (\det \mathbf{\Sigma}_T)^{-R} (\det \mathbf{\Lambda})^{R-T} (\det(\mathbf{V}(\mathbf{\Lambda})))^2 \\ &\quad \times \int_{U(T)} {}_1\tilde{F}_0\left(T+L; -\mathbf{\Sigma}_T^{-1}\mathbf{E}\mathbf{\Lambda}\mathbf{E}^H\right)(d\mathbf{E}) \\ &= \frac{\pi^{T(T-1)}\tilde{\Gamma}_R(T+L)}{\tilde{\Gamma}_T(R)\tilde{\Gamma}_T(T)\tilde{\Gamma}_R(L)} \frac{(\det \mathbf{\Lambda})^{R-T}}{(\det \mathbf{\Sigma}_T)^R} (\det(\mathbf{V}(\mathbf{\Lambda})))^2 \, {}_1\tilde{F}_0^{(T)}\left(T+L; -\mathbf{\Sigma}_T^{-1}, \mathbf{\Lambda}\right). \end{aligned} \tag{186}$$

Using the alternative formulation for the complex hypergeometric function with two matrix arguments with classical hypergeometric functions in Section II, i.e.,

$${}_1\tilde{F}_0^{(T)}\left(T+L; -\mathbf{\Sigma}_T^{-1}, \mathbf{\Lambda}\right) = \prod_{k=1}^{T} \frac{\Gamma(k)}{(L+1)_{T-k}} \frac{\det\left(\left\{{}_1F_0\left(L+1; -\lambda_j\sigma_i^{-1}\right)\right\}\right)}{\det\left(\mathbf{V}\left(-\mathbf{\Sigma}_T^{-1}\right)\right)\det(\mathbf{V}(\mathbf{\Lambda}))} \tag{187}$$

yields the closed-form expression for the joint eigenvalue distribution of $\mathbf{Z}$ in (182).

□

Using the similar approach in case of receiver-sided correlation, we readily derive the outage probability and pdf of the maximum output SIR for the interference-limited MIMO-OC system by applying the generalized Binet-Cauchy formula in Section II,

$$P_{\text{out}}(\gamma_0) = K_1(T, R, L, \mathbf{\Sigma}_T) \det\left(\Delta_T\left(\mathbf{\Sigma}_T, \gamma_0/\Gamma_0\right)\right) \tag{188}$$

and

$$f_{\gamma_s}(\gamma) = \Gamma_0 K_1(T, R, L, \mathbf{\Sigma}_T) \det\left(\Delta_T\left(\mathbf{\Sigma}_T, \gamma/\Gamma_0\right)\right) \operatorname{tr}\left(\Delta_T^{-1}\left(\mathbf{\Sigma}_T, \gamma/\Gamma_0\right) \tilde{\Delta}_T\left(\mathbf{\Sigma}_T, \gamma/\Gamma_0\right)\right), \tag{189}$$

respectively, where $\Delta_T(\mathbf{\Sigma}_T, x)$ is an $T \times T$ matrix function of x whose entries are given by

$$\left\{\Delta_T\left(\mathbf{\Sigma}_T, x\right)\right\}_{i,j} = \frac{x^{R-T+j}}{\Gamma_0^{R-T+j}(R-T+j)}\, {}_2F_1\left(L+1, R-T+j; R-T+j+1; -\frac{x}{\sigma_i \Gamma_0}\right) \tag{190}$$

and $\tilde{\Delta}_T(\mathbf{\Sigma}_T, x)$ is an $T \times T$ matrix function of x whose entries are given by

$$\left\{\tilde{\Delta}_T\left(\mathbf{\Sigma}_T, x\right)\right\}_{i,j} = \frac{x^{R-T+j-1}}{\left(1 + x/\sigma_i\right)^{L+1}}. \tag{191}$$

6.4.2 Spatially correlated MIMO-OC system with $T \geq R$ and $L \geq R$

Next, we consider the MIMO-OC system with $T \geq R$ and $L \geq R$. To investigate the statistical properties of the MIMO-OC system, the following theorem enables us to find the equivalent MIMO-OC system with $T \leq R \leq L$.

Theorem 6. *Let the MIMO adaptive antenna system with OC be $(T, R, L, \mathbf{\Sigma}_T, \mathbf{\Omega}_R)$ MIMO-OC system with $L \geq R$, where $\mathbf{\Omega}_R = \mathbf{\Sigma}_{R,D}^{1/2} \mathbf{\Sigma}_{R,I}^{-1} \mathbf{\Sigma}_{R,D}^{1/2}$ denotes the effective correlation at the receiver. Then, an one-sided correlated MIMO-OC system with $T \geq R$ is exactly equivalent to a system with $T \leq R$, i.e., for $T \geq R$ and $L \geq R$,*

$$(T, R, L, \mathbf{\Sigma}_T, \mathbf{I}_R) \text{ MIMO-OC system} \longleftrightarrow (R, T, L+T-R, \mathbf{I}_R, \mathbf{\Sigma}_T) \text{ MIMO-OC system}$$

and

$(T, R, L, \mathbf{I}_T, \mathbf{\Omega}_R)$ *MIMO-OC system* $\longleftrightarrow$ $(R, T, L+T-R, \mathbf{\Omega}_R, \mathbf{I}_T)$ *MIMO-OC system*

where $A \longleftrightarrow B$ *denotes the equivalence between* A *and* B.

Proof. Since the non-zero distinct eigenvalues of $\mathbf{Z}_1 = (\mathbf{H}_I {\mathbf{H}_I}^H)^{-1/2}(\mathbf{H}_D {\mathbf{H}_D}^H)(\mathbf{H}_I {\mathbf{H}_I}^H)^{-1/2}$ are equal to those of $\mathbf{Z} = {\mathbf{H}_D}^H(\mathbf{H}_I {\mathbf{H}_I}^H)^{-1}\mathbf{H}_D$ [5, p.53], the joint eigenvalue distributions of $\mathbf{Z}$ for $(T, R, L, \mathbf{\Sigma}_T, \mathbf{I}_R)$ and $(T, R, L, \mathbf{I}_T, \mathbf{\Omega}_R)$ MIMO-OC systems in the case of $T \geq R$ and $L \geq R$ are readily derived as

$$f_{\mathbf{\Lambda}}(\lambda_1, \lambda_2, \cdots, \lambda_R) = \frac{\pi^{R(R-1)}\tilde{\Gamma}_T(L+T)\left(\det \mathbf{\Lambda}\right)^{T-R}}{\tilde{\Gamma}_R(T)\tilde{\Gamma}_R(R)\tilde{\Gamma}_T(L+T-R)} \frac{\left(\det\left(\mathbf{V}\left(\mathbf{\Lambda}\right)\right)\right)^2}{\left(\det \mathbf{\Sigma}_T\right)^R} {}_1\tilde{F}_0^{(T)}\left(L+T; -\mathbf{\Sigma}_T^{-1}, \mathbf{\Lambda}\right) \tag{192}$$

and

$$f_{\mathbf{\Lambda}}(\lambda_1, \lambda_2, \cdots, \lambda_R) = \frac{\pi^{R(R-1)}\tilde{\Gamma}_T(L+T)\left(\det \mathbf{\Omega}_R\right)^{-T}}{\tilde{\Gamma}_R(T)\tilde{\Gamma}_R(R)\tilde{\Gamma}_T(L+T-R)} \frac{\left(\det\left(\mathbf{V}\left(\mathbf{\Lambda}\right)\right)\right)^2}{\left(\det \mathbf{\Lambda}\right)^{T-R}} {}_1\tilde{F}_0^{(R)}\left(L+T; -\mathbf{\Omega}_R^{-1}, \mathbf{\Lambda}\right), \tag{193}$$

respectively. Comparing (192) and (193) with (169) and (186), we can find that the joint eigenvalue distribution of $\mathbf{Z}$ is obtained by applying the substitution in Theorem 6. Consequently, the PDF and cdf of largest eigenvalue of $\mathbf{Z}$ can be also derived by making the same substitution, which completes the proof of Theorem 6. □

Theorem 6 reveals that the pdf of maximum output SIR and outage probability for the MIMO-OC system with $T \geq R$ and $L \geq R$ over a correlated Rayleigh fading channel can be obtained by putting $\mathbf{\Omega}_R \rightarrow \mathbf{\Sigma}_T$ in (178) and (180) for the transmitter-sided correlation and $\mathbf{\Sigma}_T \rightarrow \mathbf{\Omega}_R$ in (200) and (189) for the receiver-sided correlation with making the substitution $T \rightarrow R$, $R \rightarrow T$, and $L \rightarrow L+T-R$. In the special case of $N_A \triangleq T = R$, if we let $\mathbf{\Xi}$ be the $N_A \times N_A$ Hermitian positive definite correlation matrix, then, we get the unified expressions for the outage probability and pdf of maximum output SIR of the MIMO-OC system in the one-sided correlated fading channel,

$$P_{\text{out}}(\gamma_0) = K(N_A, L, \Xi) \det(\Delta(\Xi, \gamma_0/\Gamma_0)) \tag{194}$$

and

$$f_{\gamma_s}(\gamma) = \Gamma_0 K(N_A, L, \Xi) \det(\Delta(\Xi, \gamma/\Gamma_0)) \operatorname{tr}\Big(\Delta^{-1}(\Xi, \gamma/\Gamma_0)\, \tilde{\Delta}(\Xi, \gamma/\Gamma_0)\Big), \tag{195}$$

where $K(N_A, L, \Xi) \triangleq K_0(N_A, N_A, L, \Xi) = K_1(N_A, N_A, L, \Xi)$, $\Delta(\Xi, x) \triangleq \Delta_R(\Xi, x) = \Delta_T(\Xi, x)$, and $\tilde{\Delta}(\Xi, x) \triangleq \tilde{\Delta}_R(\Xi, x) = \tilde{\Delta}_T(\Xi, x)$. This means that, when the numbers of antennas are same at both transmitter and receiver ($T = R$), the MIMO-OC system with spatial correlation at the transmitter is equivalent to the system with the same spatial correlation at the receiver in the interference-limited environment and vice versa.

6.4.3 Capapcity MGF

After whitening the received vector by $\mathbf{R}^{-\frac{1}{2}}$, the capacity for the uniformed transmitter with $T \leq R \leq L$ can be expressed as [95]

$$\begin{aligned} C &= E\,[\, \log_2(\det(\mathbf{I}_T + \frac{\rho}{T}\mathbf{H}_D^H(\mathbf{H}_I\mathbf{H}_I^H)^{-1}\mathbf{H}_D))\,] && (196)\\ &= E\,[\sum_{i=1}^{T} \log_2(1 + \frac{\rho}{T}\lambda_i)\,], && (197)\end{aligned}$$

where λ_i's are eigenvalues of $\mathbf{H}_D^H(\mathbf{H}_I\mathbf{H}_I^H)^{-1}\mathbf{H}_D$. Using the joint eigenvalue distribution derived in the previous section, we can derive the capacity MGF of correlated MIMO systems. The capacity MGF of receiver-sided correlated MIMO channels with $T \leq R \leq L$ is

$$\Phi(s) = K_0(T, R, L, \mathbf{\Omega}_R) \det(\Delta'_R(\mathbf{\Omega}_R, s)) \tag{198}$$

where $\Delta'_R(\mathbf{\Omega}_R, s)$ is an $R \times R$ matrix function of s whose entries are given by

$$\{\Delta'_R(\mathbf{\Omega}_R, s)\}_{i,j} = \begin{cases} \int_0^\infty y^{j-1}(1+y/\omega_i)^{R-T-L-1}(1+\rho y/T)^{s/\ln 2}\,dy, & j = 1, \cdots, T, \\ (-\omega_i)^{j-R}, & j = T+1, \cdots, R. \end{cases} \tag{199}$$

The capacity MGF of transmitter-sided correlated MIMO channels with $T \leq R \leq L$ is

$$\Phi(s) = K_1(T, R, L, \mathbf{\Sigma}_T)\det(\Delta'_T(\mathbf{\Sigma}_T, s)), \tag{200}$$

where $\Delta'_T(\mathbf{\Sigma}_T, s)$ is an $T \times T$ matrix function of s whose entries are given by

$$\{\Delta'_T(\mathbf{\Sigma}_T, s)\}_{i,j} = \int_0^\infty y^{R-T+j-1}(1+y/\omega_i)^{-L-1}(1+\rho y/T)^{s/\ln 2}\,dy \tag{201}$$

We only include final results for the brevity. The capacity MGF of correlated MIMO channels with $T \geq R$ and $L \geq R$ can be obtained from the equivalent model with $T \leq R \leq L$ by the theorem in the previous section, since the joint eigenvalue distributions of equivalent models are identical.

6.5 Numerical Examples

In this section, some numerical results are presented to illustrate the performance of an MIMO adaptive antenna system with optimum combining in a correlated Rayleigh fading channel. We evaluate the pdf of output SIR and outage probability of the MIMO-OC system in the presence of equal-power interferers. We first let the normalized output SIR be $\hat{\gamma}_0 \triangleq \gamma_s/\Gamma_0$ to illustrate the performance of an MIMO-OC system in the interference-limited environment. For one-sided correlated MIMO fading channels, we consider the exponential model with correlation matrix $\mathbf{C}(\rho)$ whose entries are given by [50, 93]

$$\{\mathbf{C}(\rho)\}_{p,q} = \rho^{|p-q|}\exp\left(j(p-q) \times \frac{\pi}{12}\right) \tag{202}$$

where ρ denotes the absolute value of correlation coefficient between two adjacent antennas with $0 < \rho < 1$. Then, we assume $\mathbf{\Sigma}_T = \mathbf{C}(\rho_T)$, $\mathbf{\Sigma}_{R,D} = \mathbf{C}(\rho_{R,D})$, and $\mathbf{\Sigma}_{R,I} = \mathbf{C}(\rho_{R,I})$.

Figure 22 and 23 show the pdf of the maximum output SIR and outage probability of MIMO-OC systems versus normalized output SIR comparing the theoretical results with Monte-Carlo simulation results in a correlated Rayleigh fading channel. The performance of MIMO-OC systems in Fig. 22 and 23 is evaluated for $T = 3$ with $\rho_T = 0.5$ and $R = 4$ with $\rho_{R,D} = 0.6$ and $\rho_{R,I} = 0.3$, respectively. It is shown that the pdf of output SIR and outage probability from the theoretical analysis agree with those from Monte-Carlo simulation. As expected, we find that increasing the number of transmit(or receive) antennas or decreasing the number of co-channel interferers improves the chance for the system to take on larger SIR values, which implies a better outage performance in MIMO-OC systems.

Figure 24 shows the required normalized output SIR to achieve 10^{-6} outage probability versus correlation coefficient ρ_T for the a MIMO-OC system with $R = 6$, $L = 8$, and spatial correlation $\mathbf{\Sigma}_T$ at the transmitter only. We observe that the performance degradation of MIMO-OC systems in highly correlated fading channel at the transmitter increases as the number of transmit antennas increases. For example, the required normalized output SIR for $T = 6$ with $\rho_T = 0.8$ is smaller than that for $T = 5$ with $\rho_T < 0.5$.

Figure 25 shows the required normalized output SIR to achieve 10^{-6} outage probability versus correlation coefficient $\rho_{R,I}$ with various spatial correlation coefficient for the desired user $\mathbf{\Sigma}_{R,D}$ when $T = 2$ and $L = 6$. It is observed that increasing signal correlation of the interferers at the receiver improves the outage performance of MIMO-OC systems. Furthermore, for given $\rho_{R,D}$ and $\rho_{R,I}$, the spatial correlation affects MIMO-OC systems a little bit more as the number of receive antennas increases. We can also find that the required output SIR's for MIMO-OC systems are equal when both desired and interfering signals suffer from the same spatial correlation, since $\mathbf{\Omega}_R = \mathbf{\Sigma}_{R,D}^{1/2}\mathbf{\Sigma}_{R,I}^{-1}\mathbf{\Sigma}_{R,D}^{1/2} = \mathbf{I}_R$. It is noted that, from Fig. 24 and 25, the effect of the spatial correlation is negligible when the maximum correlation between pairs of antenna branches ρ is less than 0.4 as a consistent result of the MIMO system capacity over the exponentially correlated fading channel in [91].

Finally, we compare the outage performance of MIMO-OC systems with one-sided spatial correlation at the transmitter or receiver. Fig. 26 shows the outage performance of the MIMO-OC systems with $T = 3$ and $L = 6$. We observe again that increasing the spatial correlation of the interferers improves the outage performance of MIMO-OC systems. As mentioned in the previous section , the performance of MIMO-OC systems with correlated transmit antennas is exactly equal to the performance of the system with same correlation at the receive antennas when the number of antennas is evenly distributed at both transmitter and receiver. In the case where the number of receive antennas is larger than that of transmit antennas, however, there is a slight improvement in outage performance of MIMO-OC systems, when the spatial correlation exists at the transmit antennas.

6.6 Conclusions

In this chapter, we investigated the effects of the spatial fading correlation at the transmitter or receiver on the performance of MIMO-OC systems with multiple co-channel interferers. We first developed the determinant representations of the exact joint eigenvalue distributions of quadratic forms in complex Gaussian random matrices with different covariance matrices. We also derived closed-form formulas of the maximum output SIR for MIMO-OC systems. We presented some numerical examples, which verify the accuracy of our analytical results and showed the effects of arbitrarily correlated signals on the outage performance of MIMO-OC systems.

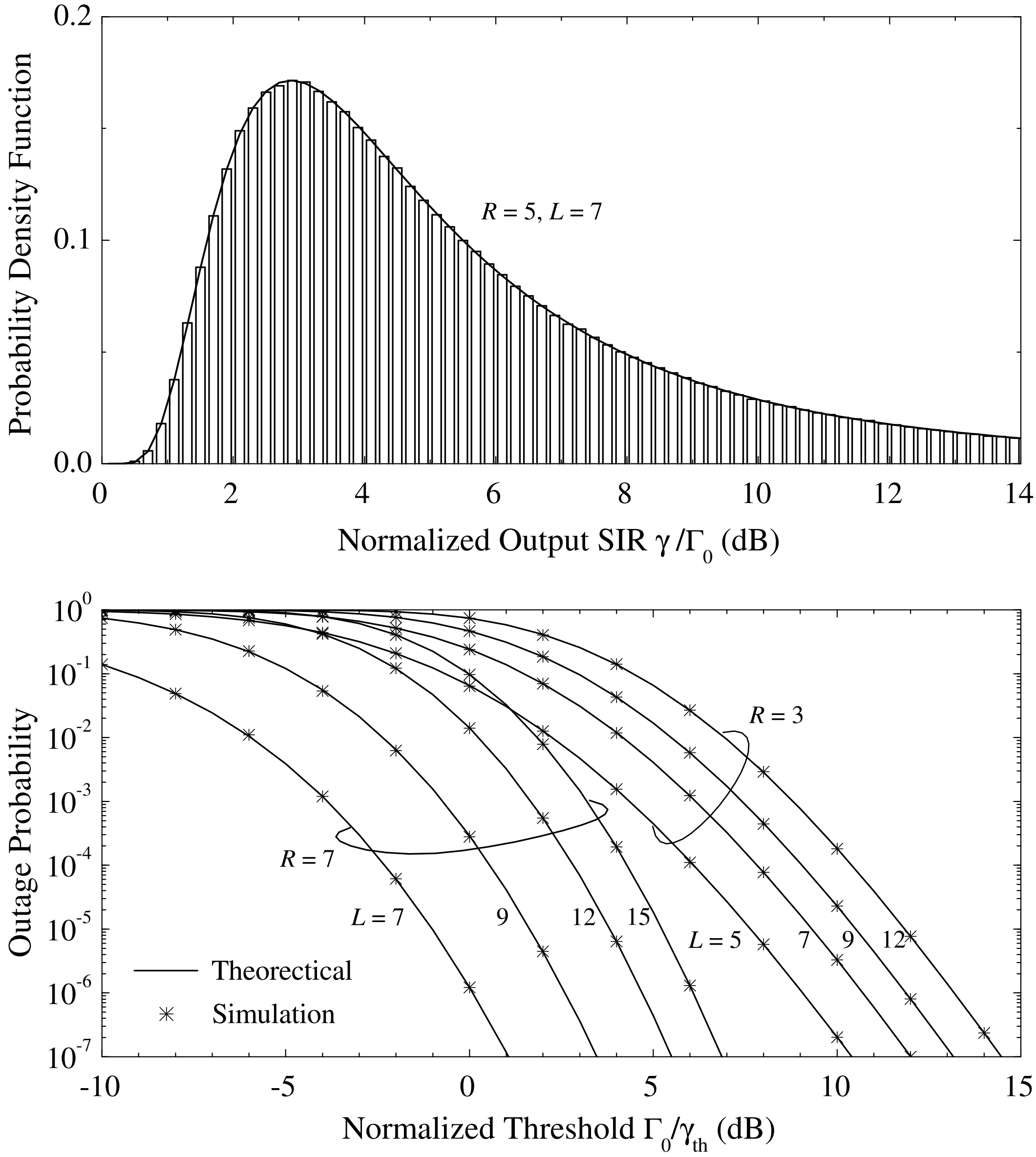

Figure 22: pdf and outage probability comparison between theoretical analysis and Monte-Carlo simulation for a MIMO-OC system with spatial correlation at the transmitter, when $T = 3$ and $\rho_T = 0.5$.

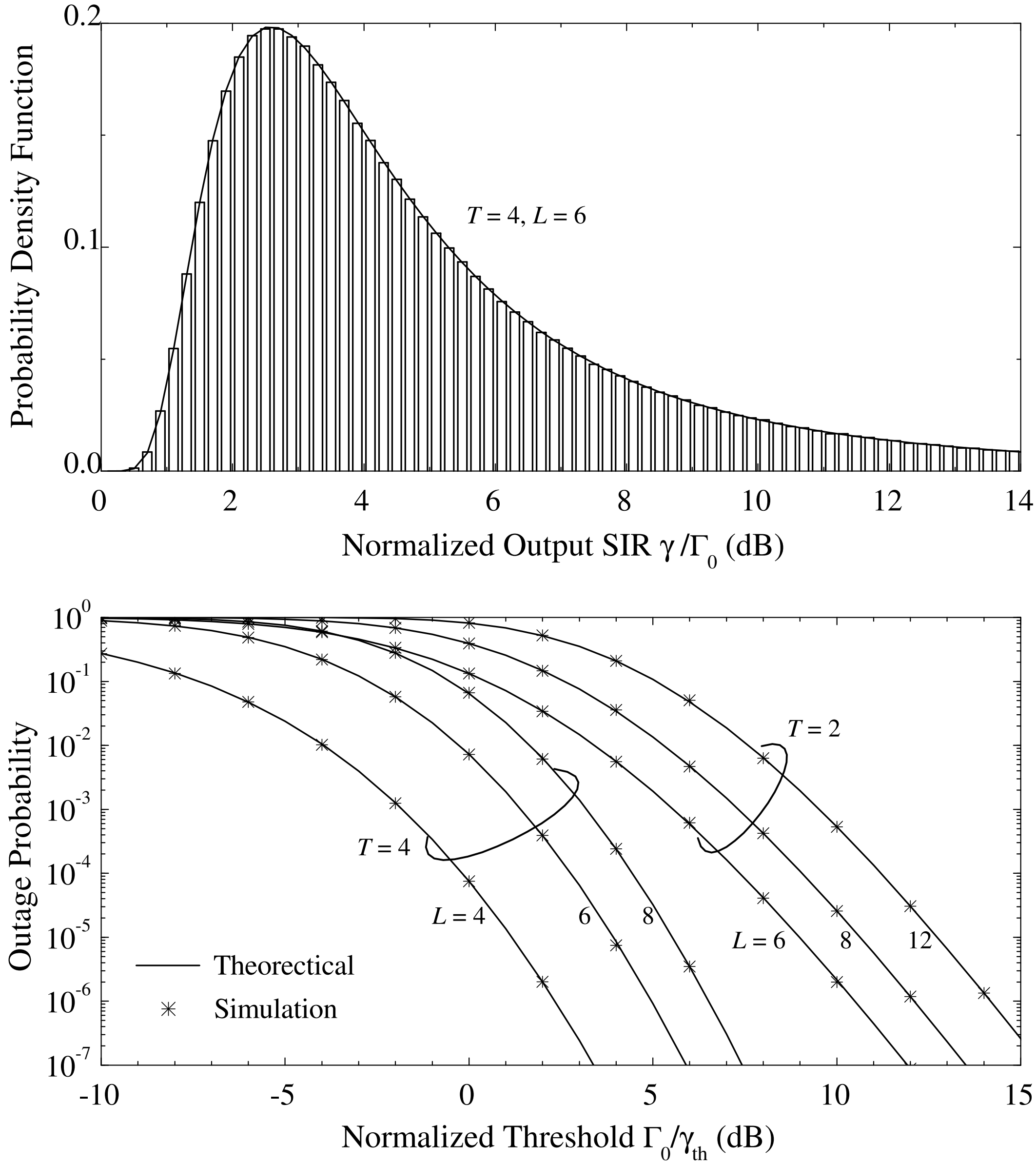

Figure 23: pdf and outage probability comparison between theoretical analysis and Monte-Carlo simulation for a MIMO-OC system with spatial correlation at the receiver, when $R = 4$, $\rho_{R,D} = 0.6$, and $\rho_{R,I} = 0.3$

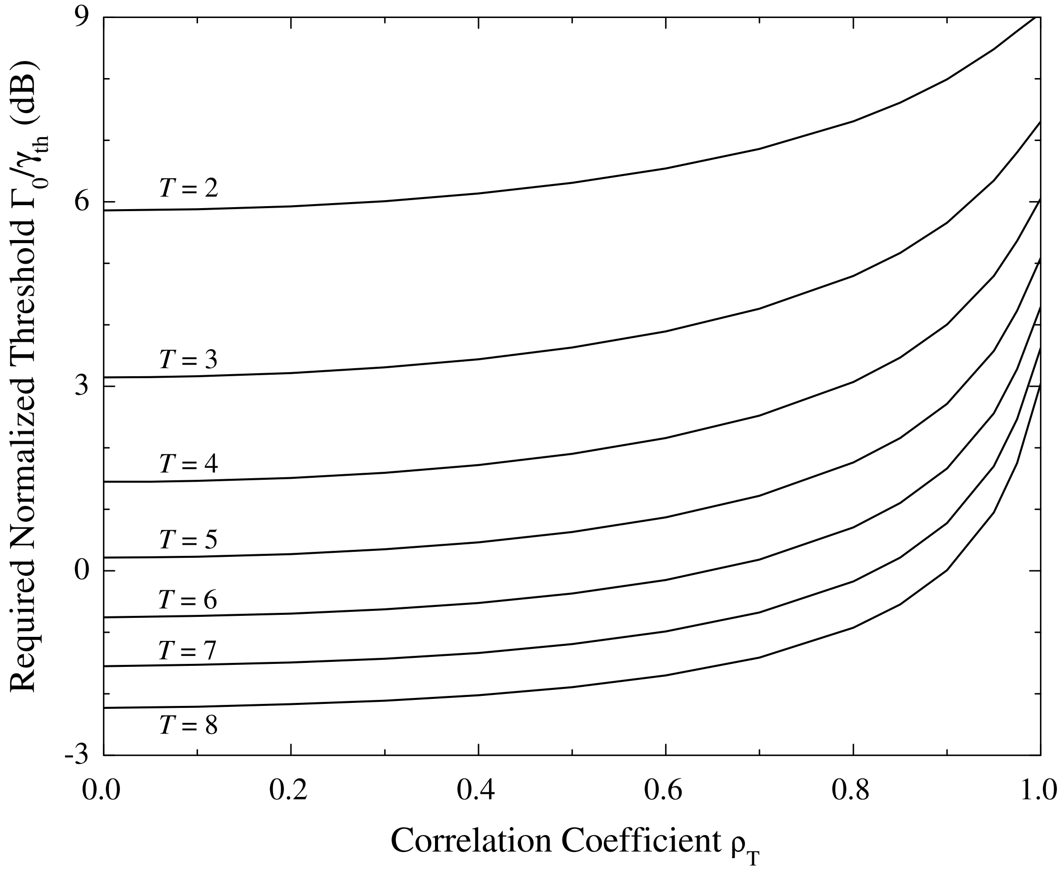

Figure 24: Required normalized output SIR to achieve 10^{-6} outage probability versus correlation coefficient ρ_T for a MIMO-OC system with $R = 6$, $L = 8$, and spatial correlation $\mathbf{\Sigma}_T$ at the transmitter only.

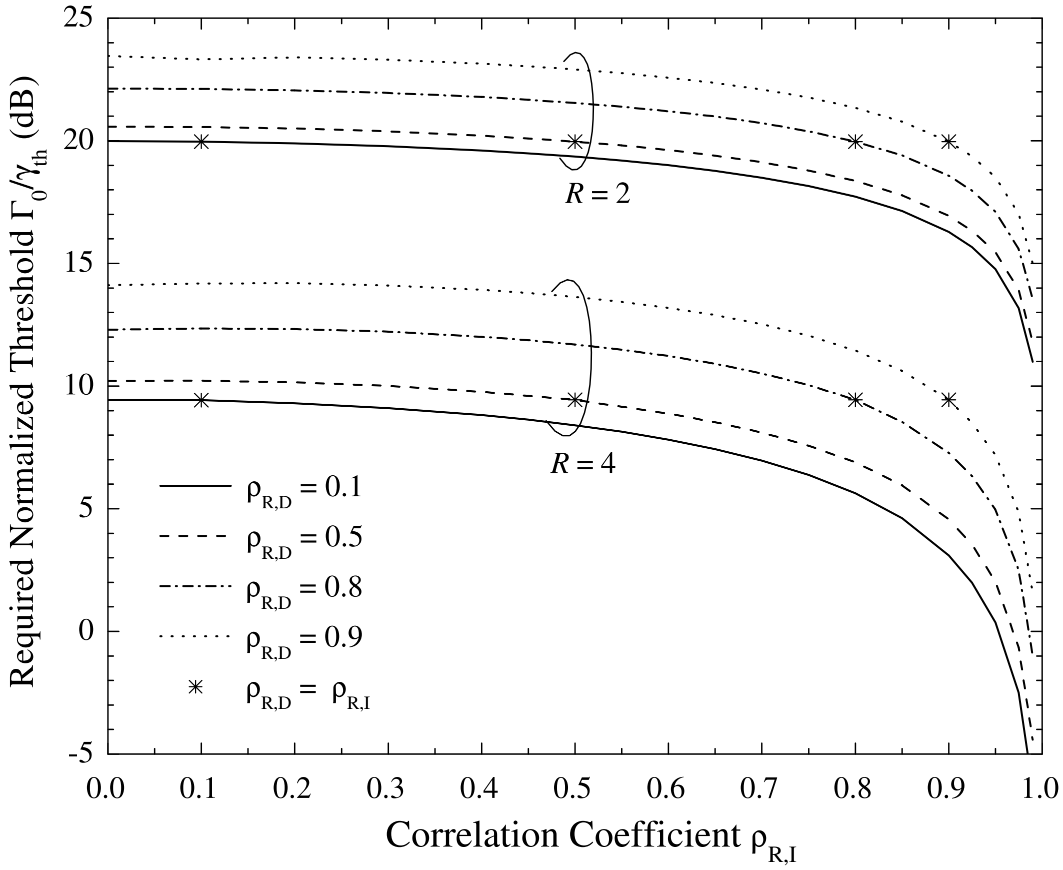

Figure 25: Required normalized output SIR to achieve 10^{-6} outage probability versus correlation coefficient $\rho_{R,I}$ with various spatial correlation coefficient for the desired user $\mathbf{\Sigma}_{R,D}$, when $T = 2$ and $L = 6$

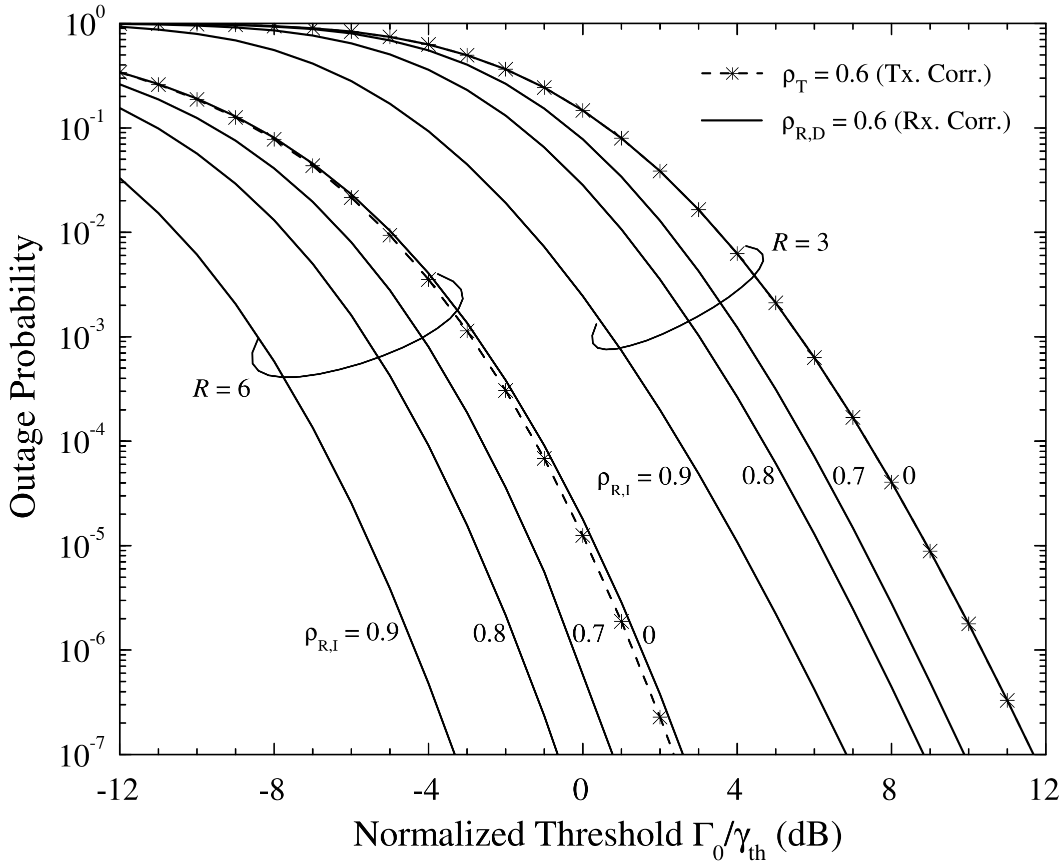

Figure 26: Outage probability of the MIMO-OC system versus normalized output SIR with $T = 3$ and $L = 6$.

CHAPTER VII

MULTI-USER MIMO SYSTEMS

7.1 Overview

Uncorrelated antennas provide antenna diversity (AD), and multi-user diversity (MUD) is inherent in wireless communications. Though both diversity techniques can increase the system capacity, the combined advantages or trade-offs are not clear. In the chapter, we study the relation between MUD and AD by investigating capacity of the single-mode-beamforming (SB) broadcast channel. We show that there is a conflict between AD and MUD, and systems with non-diversity antennas provide larger capacity than those with diversity antennas. Huge capacity is achieved at high signal-to-nose ratio (SNR) by exploiting multiple-mode-beamforming(MB) without requiring multiple antennas at each receiver. The problem of MB is the complexity for selecting users to achieve the best sum capacity. We propose an efficient suboptimal algorithm for selecting users to exploit MUD in MB. The algorithm is nearly optimal with significantly reduced complexity.

The remainder of this chapter is organized as follows. In Section 7.2, we define the multi-user MIMO system. The review of the capacity of multi-user systems with single antenna is presented in Section 7.3. Section 7.4 presents main results of this chapter which has three subsections considering the capacity of multi-user MIMO systems. We show that non-diversity antennas performs better in multi-user SB in the first subsection. In the second subsection, we show that multi-user diversity is more efficient in a system with multiple antennas than one with a single antenna, but it has a complexity problem. In the last subsection, we propose a suboptimal but efficient algorithm that performs close to optimal with significantly reduced complexity. We briefly discuss the capacity of multi-user MIMO systems with multiple antennas at the receivers in Section 7.5. Finally, conclusions are presented in Section 7.6.

7.2 System Model

One end of communication link of the kth user is a transmitter with M antennas, and the other end is a receiver with N antennas. We designate this configuration as an (M,N) MIMO system. The bandwidth of signal is narrow enough for the channel to be frequency flat. We also assume that the channel is "quasi-static". The channel may change from burst-to-burst, but remains constant during a burst.

The transmitted signal $\mathbf{s}$ is an $M \times 1$ vector, and the received signal $\mathbf{r}$ is an $N \times 1$ vector. Then, channel is represented by an $N \times M$ channel matrix $\mathbf{H}$. H_{ij}, the element of ith row and jth column of the channel matrix $\mathbf{H}$, represents the complex channel gain between the jth transmitting antenna and the ith receiving antenna. The noise $\mathbf{n}$ is an $N \times 1$ zero mean complex Gaussian vector whose real and imaginary parts are i.i.d. $N(0, \sigma^2/2)$, and its covariance matrix is equal to an $N \times N$ identity matrix multiplied by σ^2.

Then, as noted in [104], simple, but powerful expression for the received signal of kth user associated with an (M,N) MIMO multi-user system is

$$\mathbf{r}_k = \mathbf{H}_k \mathbf{s}_k + \mathbf{n}_k, \qquad k = 1, 2, \ldots, K \tag{203}$$

The time index is omitted for conciseness. For a multi-user MIMO system, we designate the MIMO system with n_T users each having with M antennas and n_R users each having with N antennas as (M,N, n_T, n_R).

7.3 Multi-user diversity of single-antenna systems

Multi-user diversity of single-antenna systems has been studied by many researchers. We briefly review the multi-user diversity gain of single antenna systems to gain insight about multi-user diversity.

It is well known that the capacity of an additive white Gaussian noise (AWGN) channel with SNR γ is

$$C_\gamma = \log(1 + \gamma) \tag{204}$$

If γ is a random variable, the capacity is a random variable too, and it must be integrated over the distribution of the random variable.

$$C = E[C_\gamma] = \int \log(1 + \gamma) p(\gamma) d\gamma, \tag{205}$$

where $p(\gamma)$ is the pdf of the random variable γ. Since the logarithm is a concave function, the capacity of a Rayleigh fading channel is less than the capacity of an AWGN channel with the same SNR using Jensen's inequality [108].

$$C_{Rayleigh} = E_\gamma[\log(1 + \gamma)] \leq \log(1 + E[\gamma]) = C_{AWGN} \tag{206}$$

However, this capacity degradation in a fading channel is dramatically restored and reversed when there are multiple users to schedule. While there is no multi-user diversity gain in an AWGN channel, the multi-user diversity gain grows as the number of users increases in a fading channel. By selecting the user above the average rate, it is always possible to obtain a higher rate than the average rate. With enough number of users, the probability that at least one user has the rate above the average is 1. The optimal strategy for single-antenna system is to schedule only one user with the best channel among users.

More precisely, when users receive an average power of unity, the average power achievable by a scheme that schedules the best user is increased. The gain of SNR converges to l_K in distribution [97, 107] with

$$F(l_K) = 1 - 1/K, \tag{207}$$

where $F()$ is the cdf of the random variable and K is the number of users. By increasing the number of users, l_K corresponds to a farther point to the right from the center in the distribution, which means more power and more gain. By a simple calculation for i.i.d. Rayleigh variables with unit variance, $l_K = \log K$, so the average power of multi-user diversity is increased to $\log K$ from unity. Therefore,

$$C_{AWGN,Multi-user} \propto \log(1+\gamma) \tag{208}$$

$$C_{Rayleigh,Mulit-user} \propto \log(1+\gamma \log K) \tag{209}$$

Figure 27 shows total throughputs of single-user Rayleigh, and Multi-user Rayleigh channels when signal to noise ratio (SNR) is 20 dB. It shows that

$$C_{Rayleigh} < C_{AWGN} = C_{AWGN,Multi-user} < C_{Rayleigh,Mulit-user} \tag{210}$$

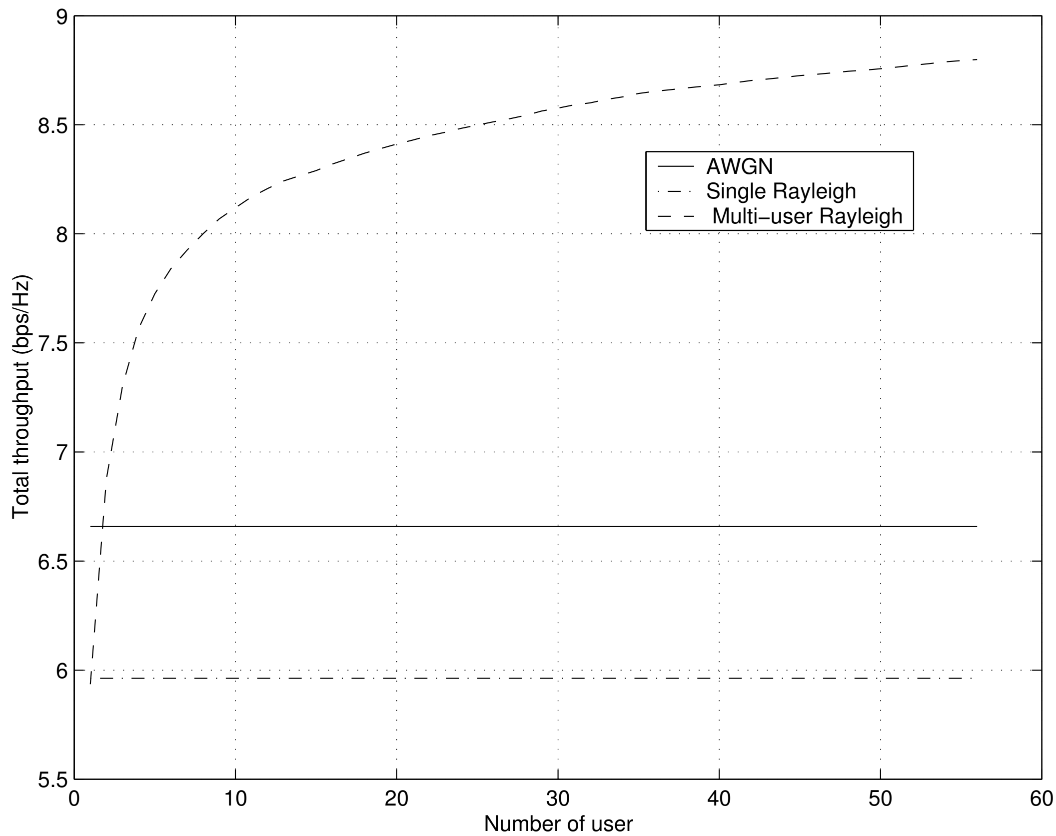

Figure 27: Total throughputs for AWGN, single Rayleigh and multi-user Rayleigh with SNR 20 dB

7.4 *Multi-user diversity of* $(M, 1, 1, n_R)$ *MIMO systems*

When there are multiple antennas in the transmitter and no feedback of CSI from the receiver, we use transmission diversity to increase the link reliability. The effective received signal of user k is given by

$$r_k = \frac{1}{M}\mathbf{h}_k^{\dagger} \cdot \mathbf{h}_k \cdot s_k + n_k, \tag{211}$$

where $\mathbf{h}_k$ is an M dimensional column vector which represents channel gain from all transmit antennas to the antenna of user k, M is the number of transmit antenna, and $(\cdot)^{\dagger}$ is the conjugate transpose of the matrix. To deliver this type of effective channel, the transmitter employs techniques like delay diversity and space-time coding [109].

Transmit diversity averages the fluctuations of each signal by providing multiple independent sources to be combined. It gives a lower BER in a fading channel than a non-diversity scheme in the point to point communication. Therefore, the capacity increases as we increase the number of antennas.

By allowing the feedback of only SNR of each user, we can exploit the multi-user diversity.

Theorem 7. *The MUD gain of Transmit diversity system vanishes as the number of antennas increases.*

$$\lim_{M\to\infty} C_{Rayleigh,Transmit-Diversity,Multi-user} = C_{AWGN,Single-Antenna,Multi-user} \tag{212}$$

Proof. The pdf of the random variable (R.V.) Y, the signal portion the effective channel r_k, is the normalized chi-square distribution with $2M$ degrees of freedom, mean $= 1$ and variance $= 1/M$ when each element of h_k is the independent identically distributed (i.i.d) circular complex Gaussian random variable with mean zero and unit variance.

$$f_Y(y) = \frac{1}{\sigma^{2M}2^M\Gamma(M)} y^{M-1}\exp^{-y/2\sigma^2}, \tag{213}$$

where $\Gamma(x)$ is the gamma function, defined as

$$\Gamma(x) = \int_0^\infty y^{x-1} \exp^{-x} dy, \quad x > 0 \tag{214}$$

By the central limit theorem (CLT), the pdf of R.V. Y approaches a normal distribution with the same mean and variance. The variance converges to 0 as $M \to \infty$, which means no variation on the signal with the same mean. $\square$

A similar conclusion is drawn from MIMO systems with a large number of transmit antennas and fixed number of receive antennas, known as channel hardening [98]. The theorem hints us that the MUD gain decreases while the gain by transmit diversity increases as the number of antennas increases. It indicates that multi-user diversity has a conflict with multi-antenna diversity. From (210) and(212), single antenna multi-user system may outperform the transmit-diversity multi-user system as the number of user increases. They are confirmed by simulation as shown in fig. 28.

One of the benefit in transmit-diversity multi-user system is that all users are equally good. Therefore, any user can be served in any time. The sum capacity loss is the penalty.

When there are multiple users in the system, transmit diversity technique is not the capacity achieving technique in a delay-tolerated system. It tells us that multi-user environment is very different from the single-user environment. In a single-user environment, fading is the impairment to be mitigated for a reliable communication, but fading should not be removed in multi-user environment, but should be exploited. The transmit diversity with multiple antennas is worse than a single antenna in a multi-user delay tolerated environment.

When there are multiple antennas at the transmitter, it forms a vector Gaussian broadcast channel. Unlike the scalar Gaussian broadcast channel, the channel is non-degraded, and the capacity region is not fully known in general. We address this problem by dividing our analysis in following three sections. The first section is for a simple single beamforming (SB) approach, which is mostly adopted in the current commercial system, the second is for optimal multiple beamforming (MB) for multi-user MIMO systems, and a sub-optimal but efficient solution for MB is considered in the last section.

7.4.1 Single-mode-beamforming (SB)

In this section we study whether a antenna diversity is desirable in multi-user communications when we deploy SB, which is adopted by most of the current commercial systems. With a feedback of CSI from each user, we can select the user to achieve the best SNR after beamforming. The effective received signal of user k with beamforming is given by

$$r_k = \mathbf{h}_k^\dagger \cdot \mathbf{h}_k \cdot s_k + n_k, \tag{215}$$

The significant difference compared with (211) is SNR improvement due to antenna gain by beamforming. By beamforming in the transmitter, we can achieve SNR boost as well as diversity gain, so its capacity increases as the number of antennas increases. As shown in [110], the single-mode-diversity beamforming (SDB, with diversity antennas) outperforms single-mode-non-diversity beamforming (SNDB, with correlated antennas) for the single-user case.

However, this is not the case for the multi-user environment. The pdf of the random variable (R.V.) Z, the signal portion the effective channel r_k of (215), is the normalized chi-square distribution with a mean ($= M$) and variance ($=M$). The pdf of the signal portion of SNDB is the single exponential distribution with mean ($= M$) and variance ($=M^2$). Although there is no closed-form solution to identify the gain of MUD for both cases, it can be shown that SNDB has better performance as the number of users increase by investigating the statistical properties of two R.V..

We find an interesting observation: If we have more correlated antennas, we have a larger sum capacity. The capacity of SDB is larger than SNDB for a single user.

However, the capacity gap between them is reduced and inverted as the number of user increases.

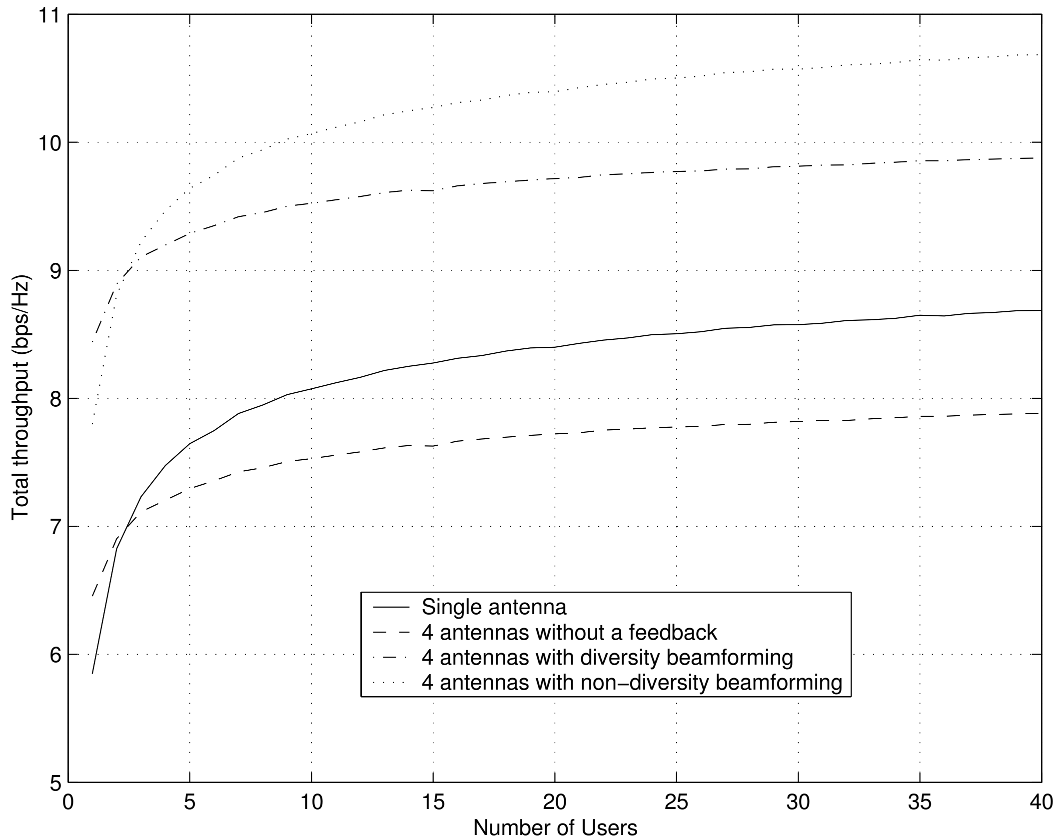

Figure 28: Capacity of SDB and SNDB vs. number of users at SNR=20dB

Figure 28 shows simulation results for SDB and SNDB when SNR = 20dB. For the comparison, multi-user capacities of single antenna and multiple diversity antennas without a CSI feedback but only with SNR feedback are included. As seen in the figure, both SDB and SNDB provide larger capacities than a non-beamforming scheme (a scheme without CSI feedback). They outperform the single-antenna systems mainly as a result of the SNR boost. We also can see that SNDB outperforms SDB as the number of users increases.

Allowing correlation has a practical advantage in the deployment of multiple antennas in the system. It overcomes the difficulty in deploying antennas in a limited space of communication node. We can easily add more antennas in the limited space, particulary for the mobile station.

7.4.2 Optimal Multiple-mode-beamforming (MB)

Although SB with multi-user diversity is a simple technique to improve the capacity of the system, it is not an optimal strategy. By exploiting all possible spatial dimensions, we can select the best multiple modes of transmission at the same time.

The simplest scheme is the zero-forcing (ZF) beamforming solution. When there are M users in the system ($n_R = M$), transmitter can transmit multiple beams

$$\begin{aligned} \mathbf{s} &= \sum_{i=1}^{M} \mathbf{H}_i^{\perp} s_i &(216)\\ \mathbf{H}^{\perp} &= \mathbf{H}^{\dagger}(\mathbf{H}\mathbf{H}^{\dagger})^{-1}, &(217)\end{aligned}$$

where $\mathbf{H} = [\mathbf{h}_1, \mathbf{h}_2, \cdots, \mathbf{h}_M]$, $\mathbf{H}^{\perp}$ is pseudo-inverse of $\mathbf{H}$, $\mathbf{H}_i^{\perp}$ is ith column vector of $\mathbf{H}_i^{\perp}$, and s_i is the data of user i. Substituting (216) to the system equation, we have non-interfering M parallel scalar channels. The received signal of each user is

$$r_i = s_i + n_i, \;\; i = 1, \cdots, M \tag{218}$$

The covariance of $\mathbf{s}$ and the effective SNR of each user, ρ_i, is

$$\begin{aligned} E\{\mathbf{s}\mathbf{s}^{\dagger}\} &= \frac{1}{(\mathbf{H}\mathbf{H}^{\dagger})^{-1}} &(219)\\ \rho_i &= \frac{1}{[(\mathbf{H}\mathbf{H}^{\dagger})^{-1}]_{i,i}}, \quad i = 1, \cdots, M, &(220)\end{aligned}$$

where $\mathrm{A}_{i,i}$ is the element of the ith row and the ith column of matrix A. The capacity with the ZF solution is

$$C_{ZF} = \sum_{i=1}^{M} [\log(\xi \rho_i)]_+, \tag{221}$$

where $[a]_+ = \min(0, a)$, and ξ is the "water-filling" solution of the following equation [108]

$$\sum_{i=1}^{M} [\xi - 1/\rho_i]_+ = P_{tot}, \tag{222}$$

where P_{tot} is the total power allowed for the transmitter. One important observation is that the capacity of MB linearly increases with the number of modes, which is the minimum between M and n_R.

Higher capacity is achieved by Costa's dirty-paper coding [111]. Using QR decomposition [5],

$$\mathbf{H}^{\dagger} = \mathbf{QR} \tag{223}$$

$$\mathbf{H} = \mathbf{LQ}^{\dagger} \tag{224}$$

$$\mathbf{L} = \mathbf{R}^{\dagger}, \tag{225}$$

where $\mathbf{R}$ and $\mathbf{L}$ are upper and lower triangular matrices respectively. By transmitting $\mathrm{Q} \cdot \mathrm{s}$, the effective channel of each user is [104]

$$r_i = l_{i,i}s_i + \sum_{j<i} l_{i,j}s_j + n_i, \;\; i = 1, \cdots, M \tag{226}$$

The non-causally known interference, $\sum_{j<k} l_{k,j}s_j$, can not be seen to user k by dirty-paper coding, referred as the zero-forcing dirty-paper coding (ZF-DP) in [104]. The resulting effective SNR of user k with a unit noise variance is $l_{k,k}^2$. The capacity of ZF-DP is

$$C_{ZF-DP} = \sum_{i=1}^{M} [\log(\xi\gamma_i)]_+, \tag{227}$$

where $\gamma_i = l_{i,i}^2$, and ξ is the solution of $\sum_{i=1}^{M} [\xi - 1/\gamma_i]_+ = P_{tot}$. It is shown in [112] that the ZF-DP is the optimal scheme for achieving the sum capacity.

When there are more users than the number of transmit antennas ($n_R > M$), a larger capacity is achieved by selecting the best users to maximize the sum capacity. The maximum number of supportable users is limited by the number of transmit antennas. The total number of groups to consider is $n_R!/(n_R - M)!/M!$. Unfortunately, there is no easy way to select the best group. It should noted that ZF-DP is order sensitive (it has different $\mathbf{L}$ depending on the order of users in the group). Therefore, $n_R!/(n_R - M)!/M!$ pseudo-inverses for ZF and $n_R!/(n_R - M)!$ QR decompositions are required in general, which is computationally prohibitive. Therefore an efficient algorithm to achieve the most of capacity is proposed in the next section.

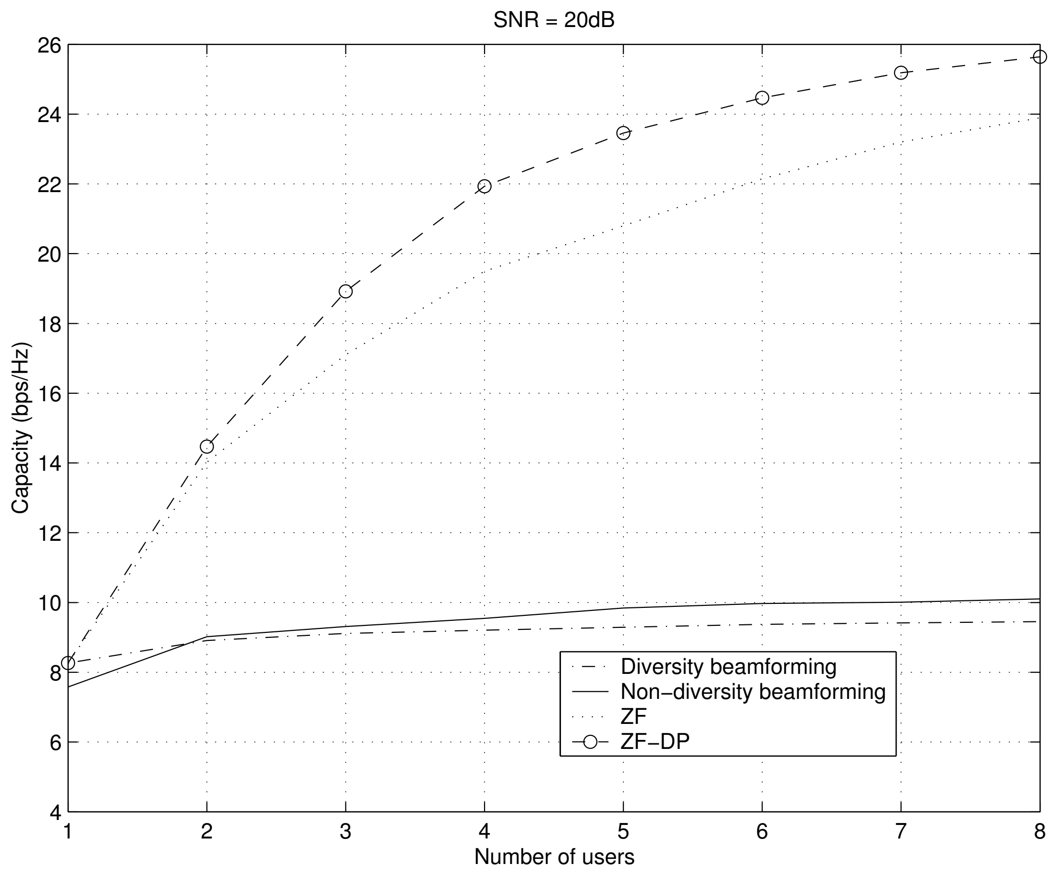

Figure 29: Capacities of multiple beamforming and single beamforming at SNR=20dB with $M = 4$ and various n_R's

Figure 29 shows the simulation results of MB and SB in the multi-user environment when SNR = 20 dB. It is shown that the capacity of MB far exceeds the capacity of SB schemes. One interesting observation is that multi-user diversity of MB is much more efficient than SB. The slope of the capacity increase is much steeper than SB even after the number of users reaches the number of transmit antennas, M. The multi-user diversity is understood as the power gain, so the capacity is increased logarithmically. However, the capacity of MB is amplified by multiplying the average capacity increase of each spatial mode by the total number of spatial modes. The

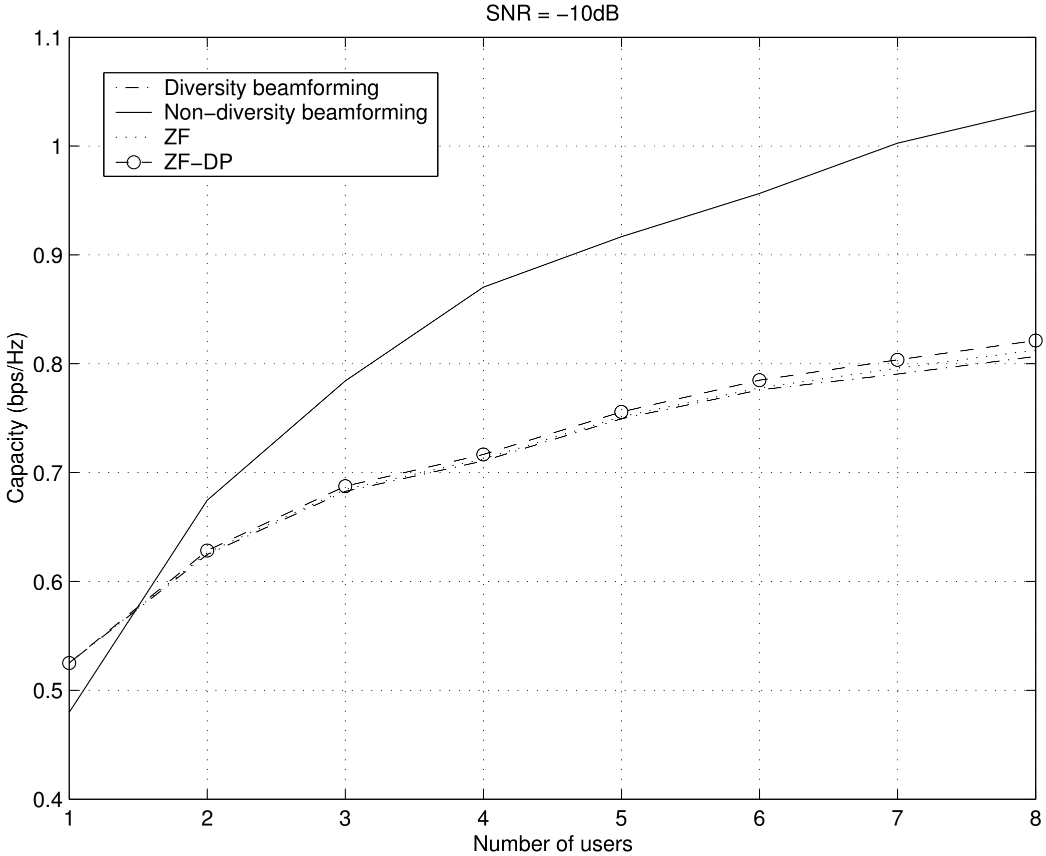

Figure 30: Capacities of multiple beamforming and single beamforming at SNR=-10dB with $M = 4$ and various n_R's

multi-user diversity gain in MB is huge as a consequence, and should not be ignored.

We found another interesting observation that the SNDB outperforms all the diversity beamforming schemes at low SNR as shown in fig. 30. ZF and ZF-DP become equal to SB at low SNR due to insufficient power which can not be distributed to other modes as seen in (222), so the capacity of MB at low SNR equals that of the SDB. Therefore, SNDB outperforms all diversity beamforming schemes at low SNR since SNDB outperforms SDB when there are large number of users.

7.4.3 Suboptimal Multiple-mode-beamforming

As seen in the previous section, the multi-user diversity gain in MB is huge and must be exploited. The main problem in exploiting the multi-user diversity is in its complexity. In this section, we propose a suboptimal but efficient algorithm for ZF-DP to reduce the complexity significantly.

`Algorithm 1: Ordered QR (OQ)`

`initialize` : $\mathbf{B} = \{\mathbf{h}_1, \mathbf{h}_2, \cdots, \mathbf{h}_{n_R}\}, \ \mathbf{S} = \phi$

$\| \mathbf{B}_j \|_2 = \max_B(\| \mathbf{B}_i \|_2)$

`Update` $\mathbf{S}$ `and` $\mathbf{B}$: `remove` $\mathbf{B}_j$ `from` $\mathbf{B}$ `and include to` $\mathbf{S}$: $\mathbf{S}_1 = \mathbf{B}_j$

$\mathbf{R}_{1,1} = \| \mathbf{B}_j \|_2$

$\mathbf{Q}_1 = \mathbf{B}_j / \mathbf{R}_{1,1}$

`for` $k = 2 : M$

  $\mathbf{E} = \mathbf{Q}^\dagger \mathbf{B}$

  $\mathbf{T} = \mathbf{B} - \mathbf{Q}\,\mathbf{E}$

  $\| \mathbf{T}_j \|_2 = \max_T(\| \mathbf{T}_i \|_2)$

  `Update` $\mathbf{S}$ `and` $\mathbf{B}$: `remove` j`th column of` $\mathbf{B}$ `and` $\mathbf{S}_k = \mathbf{B}_j$

  $\mathbf{R}_{k,k} = \| \mathbf{T}_j \|_2$

  $\mathbf{R}_{1:k-1,k} = \mathbf{E}_{1:k-1,k}$

  $\mathbf{Q}_k = \mathbf{T}_j / \mathbf{R}_{k,k}$

`end`

The OQ algorithm for ZF-DP (ZF-DP-OQ) is the general modification of classical Gram-Schmidt (CGS) algorithm [113]. The main idea is to find the best user in each mode without looking back. The algorithm completes the selection for each mode sequentially instead finding all modes at the same time. Therefore, the algorithm is robust and close to optimal when only a part of modes are needed.

The flops required for ZF-DP-OQ is $(Mn_R - M + 1)$ times $2M^3$ while the flops for ZF-DP is $n_R!/(n_R - M)!$ times $2M^3$. With $M = 4$ and $n_R = 10$, 4736 and 645120 flops are required for ZF-DP-OQ and ZF-DP respectively. The complexity reduction is by a factor of 136. As the number of users increases, the complexity of ZF-DP-OQ increases linearly with the number of users, but the complexity of ZF-DP increase almost Mth power of the number of users. As a consequence, ZF-DP is not feasible while ZF-DP-OQ is feasible as the number of users increases.

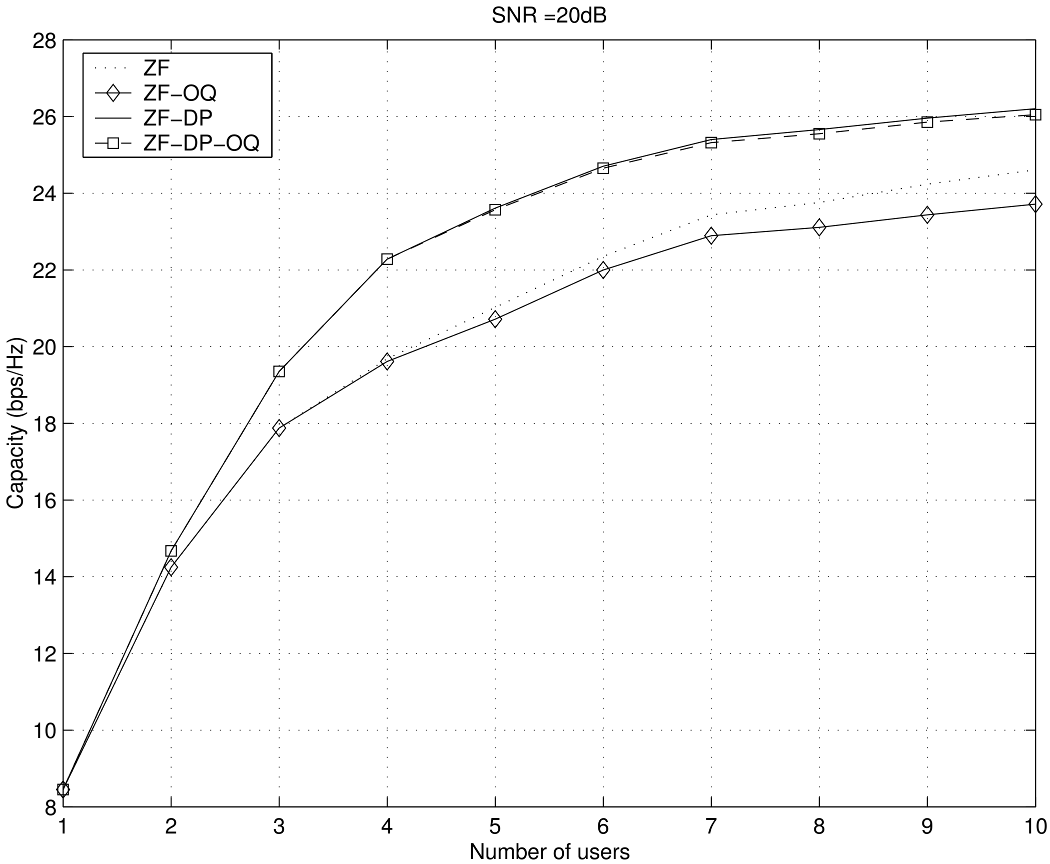

Figure 31: The capacity of ZF-DP-OQ and ZF-OQ at SNR = 20 dB

Figure 31 shows the simulation results for ZF-DP-OQ at SNR = 20 dB. It shows that the performance of ZF-DP-OQ is as good as the optimal ZF-DP. ZF-DP-OQ captures most of the MUD gain with significantly reduced complexity. We can also apply the OQ algorithm to ZF (ZF-OQ). Fig. 31 shows that ZF-OQ performs well with significantly reduced complexity. However, it is not as good as ZF-DP-OQ since OQ is optimized based on QR decomposition for ZF-DP.

7.5 *Multi-user diversity of* $(M, N, 1, n_R)$ *MIMO systems*

In this section, we briefly discuss about multi-user (M,N) MIMO system based on the studies in the previous sections.

A multi-user (M,N) MIMO system is the generalization of a multi-user (M,1) MIMO system. If every user has the same number of antennas, N, a $(M, N, 1, n_R)$ MIMO system, is lower bounded by a $(M, 1, 1, N \cdot n_R)$ MIMO system, which was discussed in the previous section. The significant difference between $(M, N, 1, n_R)$ and $(M, 1, 1, N \cdot n_R)$ MIMO systemss is that the cooperation within the data streams of the same user is possible in $(M, N, 1, n_R)$ MIMO systems. In $(M, N, 1, n_R)$ MIMO systems, there are N independent data streams in maximum within each user, and the decoder of each user can cooperated operation for streams. Therefore, the capacity of $(M, N, 1, n_R)$ MIMO systems are larger than the capacity of $(M, 1, 1, N \cdot n_R)$ MIMO systems.

The basic approach for $(M, N, 1, n_R)$ MIMO systems is to make multiple beams to be orthogonal between users and maximize the capacity within a user [114, 115]. When $N \cdot n_R$ exceeds M, we need to consider all possible combinations to collect the M best modes among $N \cdot n_R$ possible candidates. In [103], the author simplifies it to choose best user which gives the best capacity of (M,N) system, but the multi-user gain of the system from the scheme is not large as seen in the last section.

In high SNR regions, a multi-user (M, N) MIMO system gives higher capacity than any of multi-user $(M, 1)$ MIMO systems due to the increased number of effective streams from n_R to $N \cdot n_R$, and the cooperation within modes of the same user. In low SNR regions, (M, N) MIMO system can only transmit single mode, so SNDB outperforms (M,N) MIMO MB schemes. We do not include the result here for sure.

7.6 Conclusion

We study the capacity of the vector broadcast channel. Huge capacity is achieved by exploiting multiple spatial modes when there is an independent fading between antennas and between users to provide unique signatures of spatial modes. A problem arise to exploit MUD with MB because of the infeasible complexity for selecting users. We propose an efficient suboptimal algorithm to select the users to exploit MUD in MB. The algorithm is almost as good as optimal with significantly reduced complexity. With this simple algorithm, multi-user diversity can be readily exploited without significant complexity increase, and we can enjoy huge capacity gain. We showed that there is an interesting conflict between AD and MUD in SB. Antenna diversity reduces the dynamic range of channel variation, so multi-user diversity is reduced resulting from the limited scope of scheduling. As a consequence, SNDB outperforms the SDB. Allowing correlation in the antennas has a practical advantage in the deployment of multiple antennas in the system.

CHAPTER VIII

CONCLUDING REMARKS

8.1 Summary of Contributions

This dissertation primarily focuses on designing new architectures for multiple antenna wireless communication systems operating in a mobile-to-mobile environment and developing theoretical frameworks for analyzing multiple antenna systems.

In Chapter III, we proposed new architectures for MIMO systems in a mobile-to-mobile environment. Previous research has not focused on using directional antennas in MIMO systems because it is believed that directional antennas might suffer degradation of the capacity as a result of a reduction of the richness in the scattering environment. However, we find that directional antennas are very attractive in MIMO systems in a mobile-to-mobile environment. We investigate the effects of spatial correlation and multipath richness on the capacity of MIMO systems. The study shows that higher capacities are achieved for MIMO systems with directional antennas relative to MIMO systems with omni-directional antennas when antennas are closely located or when the number of scatterers is small.

In Chapter IV, we proposed new architectures for SIMO systems in a mobile-to-mobile environment. These architecture have considerable gain on output SINR over conventional systems. As a consequence of the architecture, we proposed a new combining scheme to select outputs of optimal combing (SOOC). We analyzed SOOC by deriving closed-form expressions for the pdf, the outage probability of output SIR, and average output SIR in the presence of multiple interferers of equal power in an interference-limited environment. In addition, we derived the expression for the SER of MPSK systems as the sum of single integral formulas, and a closed-form expression for the SER of BPSK as a special case.

In Chapter V, we developed a new analytical framework that provides a simple and accurate way to assess the effects of arbitrary-power interferers and thermal noise. Using some new results of joint eigenvalue distributions of complex random matrices, we derived closed-form formulas for the pdf and the cdf of the maximum output SINR of MIMO-OC and the SER of coherent MPSK as a single integral formula that can be easily evaluated by using commercial software packages. With the framework, we also derived a closed-form expression for the MGF of the output SINR of SIMO-OC in the presence of arbitrary-power interferers and thermal noise. Using the MGF, we derived an expression for average output SINR and the error performance expressions for MPSK, MQAM, and MDPSK, using the MGF-based approach. To the best of our knowledge, there has been no theoretical analysis of MIMO-OC systems with arbitrary-power interferers and thermal noise, and this work is the first to derive a closed-form expression for the exact MGF, the average output SINR, and the performance analysis of M-ary modulation schemes with SIMO-OC in the presence of arbitrary interferers and thermal noise. It is applicable even when the number of interferers is larger than the number of antennas while [55] is not.

In Chapter VI, we extended results of the performance analysis of the SIMO adaptive antenna system with OC in [50] and derived a closed-form solution of the outage probability for MIMO-OC in correlated Rayleigh fading channels. Based on the distribution functions of quadratic forms in complex Gaussian random matrices with different covariance matrices in [58, eqs. (59), (61)], we first derived the exact joint eigenvalue distributions of the quadratic-form random matrices and then investigated the statistical characteristics of maximum output SIR for the MIMO-OC system in an interference-limited environment.

In Chapter VII, we investigated the capacity of broadcast channels for a single transmitter with multiple antennas and multiple receivers with a single antenna, which is a typical downlink scenario for commercial cellular systems. We show that MUD gain decreases as AD mitigates fading, so we can conclude that there is a contention between MUD and AD. We also show that introducing intentional correlations between antennas may be beneficial in a multi-user environment. We propose an efficient algorithm for selecting users for MB, which is as good as optimal with reduced complexity.

8.2 Suggestions for Future Research

Future research can proceed in the following areas

MIMO systems in a mobile-to-mobile environment

- The characteristics of mobile-to-mobile channels differ from those of cellular channels. We show that directional antennas are attractive in MIMO systems in mobile-to-mobile channels while they are not in cellular channels. Thus, the deign of MIMO systems with different types of antennas is an open field. Possible candidates are the polarization antennas and reflection antennas currently being investigated in the software radio lab at Georgia Tech Research Institute.

- Performance analysis in mobile-to-mobile channels has been limited by lack of practical measurements of mobile-to-mobile channels. Channel measurements of mobile-to-mobile channels in the context of MIMO is an ongoing research topic.

Analysis of optimal combining

- We derived a closed-form formula for the MGF of SIMO-OC in the presence of arbitrary-power interferers and thermal noise, but a closed-form solution for the MGF of MIMO-OC is an open problem.

- The performance analysis for OC in this thesis assumed that CSI is perfectly known, but the channel gain and interference-plus-noise covariance matrix will be estimated in real implementation, which will result in estimation errors. Thus, the performance analysis of OC with estimation errors is an open problem.

Muliti-user MIMO systems

• The broadcast channel capacity is known only when both transmitters and receivers have perfect CSI of the channel. However, perfect CSI would not be realizable in practice. Hence, the capacity of broadcast channels with estimation errors is an open problem.

• Although dirty-paper coding [111] is a powerful capacity-achieving technique, it is very complex and appears to be difficult to implement in practical systems. Developing a suboptimal scheme that approaches the capacity of broadcast channels is an ongoing research topic.

REFERENCES

[1] D. Gesbert, M. Shafi, D. Shiu, and P. Smith, "From theory to practice: An overview of space-time coded MIMO wireless systems," *IEEE J. SELECT. AREAS COMMUN.*, vol. 21, pp. 281-301, Apr. 2003.

[2] G. L. Stüber, *Principles of Mobile communication*, Kluwer Academic Publishesrs, 1996.

[3] G. J. Foschini and M. J. Gans, " On Limits of wireless communications in a fading Environment when using multiple antennas," *Wireless Personal Communications*, No. 6, pp. 311-335, 1998.

[4] I. E. Teletar, "Capacity of multi-antenna Gaussian channels," AT&T *Bell Lab. Tech. Memo.*, June 1995.

[5] R. A. Horn and C. R. Johnson, *Matrix Analysis*, Cambridge University Press, 1985.

[6] A. S. Akki and F. Haber, "A Statistical model of mobile to mobile land communication channel," *IEEE Trans. Veh. Technol.*, vol. VT-35, No. 1, pp. 2 - 7,

[7] R. Wang, and D. C. Cox, " When double mobility improves link performance in ad hoc wireless networks," *Proceedings of the 12th Virginia Tech/MPRG Symposium on Wireless Personal Communications.*

Feb. 1986.

[8] A. S. Akki, "Statistical properties of mobile-to-mobile land communication channels," *IEEE Trans. Veh. Technol.*, vol. 43, No. 4, pp. 826-831, Feb. 1994.

[9] W. C. Jakes, *Microwave Mobile Communications*, New York: IEEE, 1993.

[10] K. sheikh, D. Gesbert, D. Gore, and A. Paulraj, "Smart antennas for broadband wireless access," *IEEE Commun. Mag.*, Nov. 1999.

[11] L. C. Godara, "Applications of antenna arrays to mobile communications, part I: performance improvement, feasibility, and system considerations," *Proc. IEEE*, vol. 85, no. 7, pp. 1031-1060, July 1997.

[12] J. D. Gibson, *The Mobile Communications Handbook.* 2nd ed, IEEE Press, 1999.

[13] R. T. Compton, Jr., *Adaptive Antennas: Concepts and Performance,* Prentice-Hall, 1988.

[14] L. E. Brennan, J. D. Mallett, and I. S. Reed, "Adaptive arrays in airbone MTI radar," *IEEE Trans Aerosp. Propagation,* vol. 24, no. 5, Sept. 1976.

[15] I. S. Reed, J. D. Mallett, and L. E. Brennan, "Rapid convergence cate in adaptive arrays," *IEEE Trans Aerosp. Electronic Sys.,* vol. 10, no. 6, Nov. 1974.

[16] L. L. Horowitz, H. Blatt, W. G. Brodsky, and K. D. Senne, "Controlling adaptive antenna arrays with sample matrix inversion algorithm," *IEEE Trans Aerosp. Electronic Sys.,* vol. 15, no. 6, Nov. 1979.

[17] A. T. James, " Distributions of matrix variates and latent roots derived from normal samples," *Ann. Math. Stat.*, vol. 35, pp. 475-501, 1964.

[18] A. T. James, "Zonal polynomials of the real positive definite symmetric matrices," *Ann. Math.*, vol. 74, pp. 456-469, 1961.

[19] K. I. Gross and D. P. Richards, "Total positivity, spherical series, and hypergeometric functions of matrix argument," *J. Approx. Theory*, vol. 59, pp. 224-246, 1989.

[20] P. R. Krishnaiah, "Some recent developments on complex multivariate distributions," *J. Multivariate Anal.,* vol. 6, pp. 1-30, 1976.

[21] 3rd Generation Partnership Project, " Opportunity driven multiple access," *3G TR25.924* .

[22] T. J. Harold and A. R. Nix, " Capacity enhancement using intelligent relaying for future personal communication systems," *Vehicular Technology Conference 2000*, Sep 2000.

[23] D. Shiu, G. J. Foschini, M. J. Gans, and J. M. Kahn, " Fading correlation and its effect on the capacity of multi-element antenna systems," *ICUPC 1998*, vol.1, pp. 429 -433, 1998.

[24] R. H. Clark, " A Statistical theory of mobile radio reception", *Bell. Syst. Tech. J.*, pp. 957 -1000, 1968.

[25] W. C. Y. Lee, " Effects on correlation between two mobile radio base station antennas," *IEEE Trans. Commun.*, vol. COM-21, pp. 1214 -1224, Nov 1973.

[26] J. Salz, and J. H. Winters, " Effect of fading correlation on adaptive arrays in digital mobile radio," *IEEE Trans. Veh. Technol.*, vol. 43, pp. 1049 -1057, 1994.

[27] A. G. Burr, " Cpacity bounds and estimation for the finite sccatterers MIMO wireless channel ," *IEEE J. SELECT. AREAS COMMUN.*, vol. 21, No. 5, pp. 812 - 818, 2003.

[28] G. G. Raleigh and V. K. Jones, " Multivariate modulation and coding for wireless communications," *IEEE J. SELECT. AREAS COMMUN.*, vol. 17, pp. 851 - 866, May 2003.

[29] R. R. Müller, “ A random matrix theory of communication via antenna arrays,” *IEEE Trans. Inform. Theory*, vol. 48, No. 9, pp. 2495 - 2506, Sep. 2002.

[30] H. Kang, G. L. Stüber, T. Pratt, and M. Ingram, “ Studies on the spatial correlation of MIMO systems in mobile-to-mobile environment,” *CTA 2003 Sympsium.*

[31] C. S. Patel, G. L. Stüber, and T. G. Pratt, “ Generation of Rayleigh faded waveforms for mobile-to-mobile communication ,” *CTA 2003 Sympsium.*

[32] C. S. Patel, G. L. Stüber, and T. G. Pratt, “Simulation of Rayleigh faded channels for mobile-to-mobile communications,” *IEEE Trans. Commun.*, vol. 53, No. 11, pp. 1876 - 1884, Nov. 2005.

[33] M. J. Gans, N. Amitay, Y. S. Yeh, H. Xu, T. C. Damen, R. A. Valenzuela, T. Sizer, R. Storz, D. Taylor, W. M. MacDonald, T. Cuong , and A. Adamiecki, “ Outdoor BLAST measurement system at 2.44 GHz: calibration and initial results ,” *IEEE J. SELECT. AREAS COMMUN.*, vol. 20, pp. 570 -583, 2002.

[34] R. S. Kennedy, *Fading dispersive communication channels*, New York: Wireley-Interscience, pp. 12, 1969.

[35] S. Loyka and A. Kouri, “New compound upper bound on MIMO channel capacity,” *IEEE Comm. Lett.*, vol. 6, No. 6.,pp. 96-99, Mar. 2002.

[36] H. Kang, G. L. Stuber, T. G. Pratt, and M. Ingram, “Studies on the capacity of MIMO Systems in Mobile-to-mobile environment,” *Proc. of IEEE Wireless Communications and Networking Conference*, vol. 1, 363-368, March 2004.

[37] G. V. Tsoulos, M. A. Beach, and S. C. Swales, “ Smart antenna arrays for CDMA systems,” *Proc. of the 45th Vehicular Technology Conference*, vol., pp. 45-49, July 1995.

[38] R. G. Vaughan, “On optimum combining at the mobile,” *IEEE Tran. Vehicul. Technol.*, vol. 37, pp. 181-188, 1988.

[39] K. K. Wong, K. B. Letaief, and R. D. Murch, “Investigating the performance of smart antenn systems at the mobile and base stations in the down and uplinks,” *IEEE Tran. Vehicul. Technol.*, vol. 2, pp. 880-884, May 1988.

[40] J. H. winters, “ Optimum combing in digital mobile radio with cochannel interference,” *IEEE J. Select. Areas Commun.*, vol. SAC-2, pp. 528-539, July 1984.

[41] J. H. winters, J. Salz, and R. D. Gitlin, “ The impact of antenna diversity on the capacity of wireless communication systems,” *IEEE Tran. Commun.*, vol. 42, pp. 1740-1751, 1994.

[42] J. H. Winters, J. Salz, and R. D. Gitlin, “Upper bounds on the bit-error rate of optimum combining in wireless systems,” *IEEE Tran. Commun.*, vol. 46, pp. 1619-1624, Dec. 1998.

[43] A. Shah and A. M. Haimovich, "Performance analysis of optimum combing in wireless communications with Rayleigh fading and co-channel interference," *IEEE Trans. Commun.*, vol. 46, pp.473-479, Apr. 1998.

[44] ——, "Performance analysis of maximal ratio combing and comparison with optimal comnbining for mobile radio communications with cochannel interference," *IEEE Trans. Veh. Technol.*, vol. 49, pp.1454-1463, July 2000.

[45] T. D. Pham and K. G. Balmain, " Multipath performance of adaptive antennas with multiple interferers and correlated fadings," *IEEE Tran. Veh. Technol.*, vol. 48, pp. 342-352, Mar. 1999.

[46] E. Villier, " Performace analysis of optimum combining with multiple interferers in flat Rayleigh fading," *IEEE Tran. Commun.*, vol. 47, pp. 1503-1510, Oct. 1999.

[47] J. S. Kwak and J. H. Lee, "Performance analysis of optimum combining for dual-antenna diversity with multiple interferers in a Rayleigh fading channel," *IEEE Commun. Lett.,* vol. 6, pp. 541-543, Dec. 2002.

[48] R. K. Mallik, M. Z. Win, M. Chiani, and A. Zanella, "Bit-error probability for optimum combining of binary signals in the presence of interference and noise," *IEEE Trans. Wireless Commun.*, vol. 3, no. 2, pp. 395-407, Mar 2004.

[49] M. Chiani, M. Z. Win, and A. Zanella, " Error Probability for optimum combining of M-ary PSK signals in the presence of interference and noise," *IEEE Tran. Commun.*, vol. 51, No. 11, pp. 1949-1957, Nov. 2003.

[50] Q. T. Zang, and X. W. Cui, " Outage probability for optimum combining of arbitary faded signals in the presence of correlated Rayleigh interferers," *IEEE Tran. Veh. Technol.*, vol. 53, No. 4, pp. 1043-1051, July 2004.

[51] J. S. Kwak and J. H. Lee, "Closed-form expressions of approximate error rates for optimum combining with multiple interferers in a Rayleigh fading channel," accepted for publication in *IEEE Trans. Veh. Technol.*, Feb. 2005.

[52] H. Gao, P. J. Smith, and M. V. Clark, " Theoretical reliability of MMSE linear diversity combining in Rayleigh-fading additive interference channels," *IEEE Tran. Commun.*, vol. 46, No. 5, 1998.

[53] Y. Tokgoz, B. D. Rao, M. Wengler, and B. Judson, "Performance analysis of optimum combining in antenna array systems with multiple interferers in flat Rayleigh fading", *IEEE Trans. Commun.*, vol. 52, pp. 1047 - 1050 , July 2004.

[54] D. Lao and A. M. Haimovich, "Exact closed-form performance analysis of optimum combining with multiple cochannel interferers and Rayleigh fading," *IEEE Trans. Commun.*, vol. 50, pp. 995-1003, June 2003.

[55] M. Chiani, M. Z. Win, and A. Zanella, "On optimum combining of M-PSK signals with unequal-power interferers and noise," *IEEE Trans. Commun.*, vol. 53, no. 1, pp. 44-47, Jan. 2005.

[56] T. G. Pratt, B. Walkenhorst, and H. Kang " Analysis of multi-antenna architectures for non-lOS mobile-to-mobile communications in co-channel interference," *accepted to IEEE Tran. Veh. Technol.*

[57] B. Walkenhorst, and T. G. Pratt, ' Antenna Down-Selection for Co-Channel Interference Mitigation in a Non-LOS Mobile-to-Mobile Channel," *IEEE WCNC 2006*, Jul., 2006.

[58] C. G. Khatri, " On certain distribution problems based on positive definite quadratic functions in normal vectors," *Ann. Math. Stat.*, vol. 37, pp. 468-479, 1966.

[59] M. Abramowitz and I. S. Stegun, *Handbook of mathematical functions with formulas, graphs and mathematical tables*, Dover Publications, 1972.

[60] I. S. Gradshteyn, and I. M. Ryzhik, *Table of Integrals, Series and Products*, New York: Macmillan, 1985.

[61] A. Erdelyi(ed.), *Tables of Integral Transforms: Vol II.*, New York: McGraw-Hill, 1954.

[62] A. Erdelyi(ed.), *Higher Transcendental Functions: Vol I.*, New York: McGraw-Hill, 1953.

[63] M. K. Simon and M. S. Alouini, *Digital Communication over Fading Channels: A Unified Approach to Performance Analysis*, New York, John Wiley, 2000.

[64] T. G. Pratt, B. Walkenhorst, and H. Kang, " Multiple-antenna architectures for non-LOS mobile-to-mobile communications," *4GMF2005*, July 2005.

[65] H. Kang and T. G. Pratt, " Performance analysis of slection combining of outputs of optimum combing with co-channel interference," *submitted to IEEE Tran. Wireless. Commun.*, 2006.

[66] T. K. Y. Lo, "Maximum ratio transmission," *IEEE Trans. Commun.,* vol. 47, no. 10, pp. 1458-1461, Oct. 1999.

[67] P. A. Dighe, R. K. Mallik, and S. S. Jamuar, "Analysis of transmit-receive diversity in Rayleigh fading," *IEEE Trans. Commun.,* vol. 51, no. 4, pp. 694-703, Apr. 2003.

[68] M. Kang and M.-S. Alouini, "Largest eigenvalue of complex Wishart matrices and performance analysis of MIMO MRC systems," *IEEE J. Select. Areas Commun.*, vol. 21, no. 3, pp. 418-426, Apr. 2003.

[69] K.-K. Wong, R. D. Murch, and K. B. Letaief, "Optimizing time and space MIMO antenna system for frequency selective fading channels," *IEEE J. Select. Areas Commun.*, vol. 19, no. 7, pp. 1395-1407, July 2001.

[70] K.-K. Wong, R. S.-K. Cheng, K. B. Letaief, and R. D. Murch, "Adaptive antennas at the mobile and base stations in an OFDM/TDMA system," *IEEE Trans. Commun.,* vol. 49, no. 1, pp. 195-206, Jan. 2001.

[71] M. Kang and M.-S. Alouini, "Quadratic forms in complex Gaussian matrices and performance analysis of MIMO systems with cochannel interference," *IEEE Trans. Wireless Commun.,* vol. 3, no. 2, pp. 418-431, Mar. 2004.

[72] M. Kang. L. Yang, and M.-S. Alouini, "Performance analysis of MIMO systems in presence of MIMO systems in presence of co-channel interference and additive Gaussian noise," in *Proc. 37th CISS'2003, Baltimore, MD* , , Mar. 2003.

[73] H. Shin and J. H. Lee, "Capacity of multiple-antenna fading channels: spatial fading correlation, double scattering and keyhole," *IEEE Trans. Inform. Theory,* vol. 49, no. 10, pp. 2636-2647, Oct. 2003.

[74] M. A. Golberg, "The derivative of determinant," *American Math. Monthly,* vol. 79, pp. 1124-1126, Dec. 1972.

[75] J. G. Christiano and J. E. Hall, "On the n-th derivative of a determinant of the j-th order," *Math. Mag.,* vol. 37, pp. 215-217, Sep.-Oct. 1964.

[76] J. Abate and P. P. Valkó, "Multi-precision Laplace transform inversion," *Comput. Math. Appl.,* vol. 60, pp. 979-993, 2004.

[77] P. P. Valkó and J. Abate, "Comparison of sequence accelerators for the Gaver method of numerical Laplace transform inversion," *Comput. Math. Appl.,* vol. 48, pp. 629-636, 2004.

[78] D. P. Gaver, "Observing stochastic processes and approximate transform inversion," *Oper. Res.,* vol. 14, pp. 444-459, 1966.

[79] R. J. Muirhead, *Aspects of Multivariate Statistical Theory,* Wiley, 1982.

[80] A. Takemura, *Zonal Polynomials,* Hayward, CA: Institute of Mathematical Statistics Lecture Note-Monograph Series, vol. 4, 1984.

[81] H. Gao and P. J. Smith, "A determinant representation for the distribution of quadratic forms in complex normal vectors," *J. Multivariate Anal.,* vol. 73, pp. 155-165, 2000.

[82] H. Shin, M. Z. Win, and J. S. Kwak, "Orhtogonal space time block codes in the presence of double scattering," submitted to *IEEE Trans. Inform. Theory,* 2005.

[83] B. Davies and B. Martin, "Numerical inversion of the Laplace transform: a survey and comparison of methods," *J. Comput. Phys.,* vol. 33, pp. 1–32, 1979.

[84] Y.-C. Ko, M.-S. Alouini, and M. K. Simon, "An MGF-based numerical technique for the outage probability evaluation of diversity systems," *IEEE Trans. Commun.*, vol. 48, pp. 1783–1787, Nov. 2000.

[85] J. Abate and P. P. Valkó, "Multi-precision Laplace transform inversion," *Comput. Math. Appl.,* vol. 60, pp. 979-993, 2004.

[86] P. P. Valkó and J. Abate, "Comparison of sequence accelerators for the Gaver method of numerical Laplace transform inversion," *Comput. Math. Appl.,* vol. 48, pp. 629-636, 2004.

[87] D. P. Gaver, "Observing stochastic processes and approximate transform inversion," *Oper. Res.,* vol. 14, pp. 444-459, 1966.

[88] H. Kang, J. Kwak, H. Shin, G. L. Stuber, and T. G. Pratt, "Optimal combining with arbitrary power interferers and thermal noise," *ICC 2006,* June 2006.

[89] H. Kang, J. Kwak, H. Shin, G. L. Stuber, and T. G. Pratt, "Analytical framework for optimal combining with arbitrary power interferers and thermal noise," *submitted to IEEE TRan. Veh. Technol.,* 2006.

[90] M. Kang, M. -S. Alouini, and L. Yang, "Outage probability and spectrum efficiency of cellular mobile radio systems with smart antennas," *IEEE Trans. Commun.*, vol. 50, no. 12, pp. 1871-1877, Dec. 2002.

[91] M. Chiani, M. Z. Win, and A. Zanella, "On the capacity of spatially correlated MIMO Rayleigh-fading channels," *IEEE Trans. Inform. Theory,* vol. 49, no. 10, pp. 2363-2371, Oct. 2003.

[92] C. N. Chuah, D. Tse, J. M. Kahn, and R. A. Valenzuela, "Capacity scaling in MIMO wireless systems under correlated fading," *IEEE Inform. Theory*, vol. 48, no. 3, pp. 637-650, Mar. 2002.

[93] S. L. Loyka, "Channel capacity of MIMO architecture using the exponential correlation matrix, ," *IEEE Commun. Lett.*, vol. 5, no. 9, pp. 369-371, Sept. 2001.

[94] A. Edelman, *Eigenvalues and condition number of random matrices*, Ph.D. dissertation, MIT, Cambridge, MA, 1989.

[95] R. S. Blum, J. H. winters, and N. R. Sollenberger, "On the capacity of cellular systems with MIMO, ," *IEEE Commun. Lett.*, vol. 6, no. 6, pp. 242-244, Jun. 2002.

[96] J. Kwak, H. Kang, Y. Li, and G. L. Stuber, "Effects of spatial correlation on MIMO adaptive antenna system with optimum combining," *accepted to IEEE Trans. On Wireless Commun..*

[97] P. Viswanath, D. N. C. Tse, and R. Laroia, " Opportunistic beamforming using dumb antennas," *IEEE Tran. Inform. Theory*, vol. 48, No. 6, pp. 1277-1294, June 2002.

[98] B. M. Hochwald, T. M. Marzeeta, and V. Tarokh, " Mulitple-antenna channel hardening and its implications for feedback and scheduling," *IEEE Tran. Inform. Theory*, vol. 50, No. 9, pp. 1893-1909, Sep. 2004.

[99] W. Rhee, W. Yu, and J. M. Cioffi, " Utilizing multiuser diversity for multiple antenna systems,"in *Proc. IEEE WCNC*, pp. 420-425, Sep. 2000.

[100] R. Knopp, and P. Humblet, " Information capacity and power control in single cell multiuser Communications," in *Proc. IEEE Int. Computer Conf. (ICC'95)*, Seatle WA, June 1995.

[101] E. Esteves, " The high data rate evolution of the cdma2000 cellular system," in Multiaccess, mobility, and teletraffic for wireless communications: vol. 5, pp61-72, Kluwer Academic Publishesrs, Dec. 1996.

[102] TIA/EIA/IS-856, " CDMA 2000:High rate packet data air interface apecification," Std., Nov. 2000.

[103] S. Borst and P. Whiting, " The use of diversity antennas in high-speed wireless systems: Capacity gains, firness issues, multi-user scheduling," *Bell Labs. Tech. Mem.*, 2001.

[104] G. Caire, and S. S. Shamai, " On the achievable throughput of a multiantenna Gaussian broadcast channel," *IEEE Tran. Inform. Theory*, vol. 49, No. 7, pp. 1691-1706, Jul. 2003.

[105] R. B. Ertel, P. Carldieri, K. W. Sowerby and T. S. Rappaport, " Overview of spatial channel models for antenna array communication systems," *IEEE Personal Commun. Sys.*, pp. 10-22, Feb. 1998.

[106] D. Gesbert, H. Bölskei, D. A. Gore, and A. J. Paulaj, " Outdoor MIMO wireless channels: models and performance prediction," *IEEE Tran. Commun.*, vol. 50, pp. 1926-1934, Dec. 2002.

[107] H. A. David, *Order Statistics*, Newyork:Wiley, 1970.

[108] T. cover and J. Thomas, *elements of Information theory*, Newyork:Wiley, 1991.

[109] V. Tarokh, N. Seshadri, A. R. Calderbank, " Spacetime codes for high data rate wireless communication: Performance criterion and code construction," *IEEE Tran. Inform. Theory*, vol. 44, pp. 744-765, Mar. 1998.

[110] R. Knopp, and G. Caire, " Power control and beamforming for systems with multiple transmit and receive antennas," *IEEE Tran. Wireless Commun.*, vol. 1, N0. 4, pp. 638-648, Oct. 2002.

[111] M. Costa, " Writing on dirty paper," *IEEE Tran. Inform. Theory.*, vol. IT-29, pp. 439-441, May 1983.

[112] P. Viswanath and D. N. C. Tse, " Sum capacity of the vector Gaussian broadcast channel and uplink-downlink duality', *IEEE Tran. Inform. Theory*, vol. 49, N0. 8, pp. 1912-1921, Aug. 2003.

[113] G. H. Golub, *Matrix Computation*, The Johns Hopkins University Press, 1996.

[114] K. K. Wong, R. D. Murch, and K. B. Letaief, " A joint channel diagonalization for multi-user MIMO antnna systems," *IEEE Tran. Wireless commun.*, vol. 2, pp. 240-249, Mar. 2003.

[115] Z. G. Pan, K. K. Wong, and T. S. Ng, " MIMO Antenna system for multi-user multi-stream orthogonal space division multiplexing," *Proc. IEEE ICC'2003*, pp. 3220-3224, 2003.

VITA

Heewon Kang received the B.S. degree in electrical engineering from Seoul National University, Korea in 1991. He received his M.S. degree in electrical engineering from University of Southern California, Los Angeles in 1994. From 1995 to 2001, he worked for Samsung Electronics, Korea, where he was involved on the development of commercial systems for the code division multiple access (CDMA) voice service, and trial systems for the CDMA high speed data service. He has studied for his Ph. D. degree in electrical and computer engineering at Georgia Institute of Technology, Atlanta since August 2001. His current research interests include the performance analysis of the diversity techniques and multiple antenna systems, and the design of MIMO systems in a mobile-to-mobile environment.